INTEGRATION AND EVALUATION OF A 180-KW TURBOPROP ENGINE WITH A TURBOELECTRIC GROUND TEST RIG

By

JOSHUA MELVIN

Bachelor of Science in Aerospace Engineering

Bachelor of Science in Mechanical Engineering

Oklahoma State University

Stillwater, Oklahoma

2021

Submitted to the Faculty of the
Graduate College of the
Oklahoma State University
in partial fulfillment of
the requirements for
the Degree of
MASTER OF SCIENCE
May, 2023

INTEGRATION AND EVALUATION OF A

180-KW TURBOPROP ENGINE WITH A

TURBOELECTRIC GROUND TEST RIG

Thesis Approved:

Dr. Kurt Rouser

Thesis Adviser

Dr. Wei Zhao

Dr. Ryan Paul

Name: JOSHUA MELVIN

Date of Degree: MAY, 2023

Title of Study: INTEGRATION AND EVALUATION OF A 180-KW TURBOPROP ENGINE WITH A TURBOELECTRIC GROUND TEST RIG

Major Field: MECHANICAL AND AEROSPACE ENGINEERING

Abstract: This paper presents the integration of a PBS Aerospace 180-kW turboprop engine with a Cessna 172, four seat, 1,090-kg (2,400-lbf) max takeoff weight aircraft for use as a turboelectric ground test rig. The quickly growing segment of hybrid propulsion aircraft, commonly used in the urban air mobility sector, are pressing regulatory bodies to develop new certification requirements for these unique aircraft. Small-scale turboelectric systems used in unmanned aerial systems are well documented, but large-scale manned systems are comparatively rare. Therefore, it is critical to develop a large-scale turboelectric ground test rig to study turboelectric system integration phenomena to inform new certification standards from regulatory bodies. To conduct large-scale turboelectric research designing an engine mount, generator mount, a power transfer system, and a propeller spacer are required. The goal of this study was to design, fabricate, install, and test an engine mount, generator mount, propeller spacer and power transfer system for a turboelectric aircraft ground test rig. The methodology included computer aided design, finite element analysis, static component tests and fully integrated tests to acquire data to validate analysis. Electric power demand of the electric propulsors were set as 20 to 30-kW using a 50-kW generator, this power rating drove the design of the belting system. Turboelectric architecture is a parallel partial hybrid system with power being delivered to a 1.8-m three blade propeller while a portion of the engine power is siphoned to the generator. The generator drives two electric motors with 1.3-m two blade propellers mounted to the wing leading edges while also maintaining battery charge. A static torque test of over 1,300-N·m, peak engine torque is 800-N·m, was conducted on the engine mount before engine integration to verify its integrity. Observations from testing the full turboelectric system installation, without generator load, indicate the engine successfully operated at all power levels with the engine mount delivering expected structural strength. Another observation from testing shows that the propeller spacer performed well within expected parameters without erratic propeller dynamics. Results from testing the full turboelectric system installation, without generator load, indicate the engine mount withstood all engine loads within expected torsional deflections from the static torque test of around 2 degrees of twisting.

TABLE OF CONTENTS

LIST OF TABLES

LIST OF FIGURES

Figure Page

Figure Page

Figure Page

CHAPTER I

INTRODUCTION

The rapidly growing segment of hybrid propulsion aircraft is driving governmental bodies to revise certifications standards for aircraft, and in some cases creating new certifications standards specifically for hybrid propulsion aircraft (FAA, 2022). Even when considering the best battery technology batteries can only deliver around a 50^{th} of the energy density of liquid fuels (Manuel A. Rendon, 2021). High energy density is desired for longer range or endurance, this allows for more power across time for less weight, which is what batteries lack. However, batteries can deliver better power density than liquid fuels. Power density is the ability to deliver large amounts of power in a very short time, because of this, batteries can be desired for high intensity operations such as takeoff, dashing, and climbing. Thus, many developing electrified aircraft use a hybrid propulsion systems, these systems typically use a gas turbine, though some may employ a piston engine, to drive generators that in turn drive electric propulsors, power aircraft systems, and replenish battery reserves after intensive flight operations such as takeoff. This paper focuses on the application of gas turbines for hybrid gas-electric systems, commonly known as turboelectric. Therefore, emerging turboelectric aircraft systems require safe integration of the structural and supporting elements of the turboelectric propulsion system. Some architectures of hybrid propulsions systems are shown in figure 1 and will be discussed in detail in the background section of this paper.

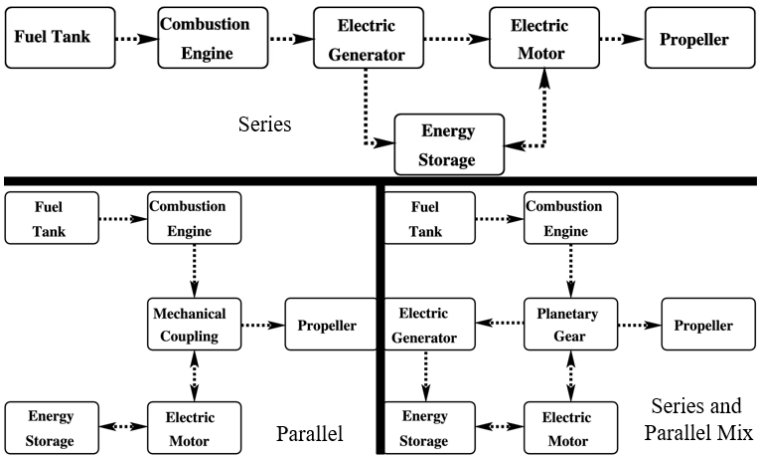

Figure 1. Hybrid Propulsion Power Trains (Manuel A. Rendon, 2021).

A solution has been developed to construct a turboelectric ground test rig to safely evaluate large scale turboelectric integration solutions. To accurately simulate a typical aircraft's structure and layout a Cessna 172 was selected to build the turboelectric system upon. Other considerations range from structural limitations, such as specific structural load paths, to pilot seating to electrical wire organization. The selected aircraft for this project, the Cessna 172, is an N model with over 13,700 flight hours, over a year and half in the air. The gas generator was selected as a PBS Aerospace TP100 Turboprop. This turboprop generators a maximum of 180-kW, for five minutes, meant for takeoff rolls, and a continuous rated power of 160-kW. This turboprop will be replacing the stock engine of the C172, a Lycoming O-320. The O-320 is a horizontally opposed, naturally aspirated, carbureted, four-cylinder piston engine with a maximum power of 120-kW. The turboprop is also significantly lighter than the piston engine, about 62-kg (136-lbf) dry (PBS Aerospace, 2014) while the piston engine weighs 130-kg (283-lbf) dry (Cessna Aircraft Company, 1985), while producing significantly more power. The propeller chosen for the turboprop is a three blade, 1.8-m, constant speed Hartzell propeller. The stock propeller is a 1.9-m two blade fixed pitch McCauley propeller. The new propeller, while smaller in diameter, is much more advanced due to having a variable blade pitch that automatically changes according to engine RPM. This pitch is controlled by propeller dome pressure charge and oil pressure supplied

from the turboprop. The turboprop and constant speed propeller will be integrated into the Cessna 172 by use of a custom designed engine mount. The supporting accessories for the engine will also be incorporated into the airframe and these include the fuel delivery system, oil system, electrical systems, and engine controlling provisions.

Figure 2. Turboelectric Ground Test Rig.

To facilitate this study components must be safely designed and installed, the final system must be evaluated to determine how the components react, and finally the results will require analysis and comparison to the design phase. These objectives are laid out below:

1. Design and analysis of engine mount, generator mount, and a propeller spacer.
2. Component level structural analysis of the engine mount.
3. Fully integrated turboelectric structural analysis without power transfer from generator belting system through use of accelerometers and gyroscopes.

CHAPTER II

BACKGROUND

Urban Air Mobility

Urban air mobility (UAM) is a newly growing segment of aviation. UAM is currently aimed at less than five passengers, though it is typically one or two at maximum. This segment of aviation is desired to alleviate ground vehicle congestion by moving services into the air of an urban area such as major cities. These services could include package delivery or public services like policing or ambulance services, and taxi services (Manuel A. Rendon, 2021). UAM vehicles will be electrified, either fully or partially with ideal flight times lasting below an hour. However, it is quickly being realized that battery technology is currently unable to manage the power requirements of flight. This is because flight, especially with vertical takeoff and landing (VTOL) aircraft such as typical UAM vehicles, requires enormous amounts of power. Current battery technology can only deliver about 50 times less energy density than liquid fuels can deliver (Manuel A. Rendon, 2021). Battery systems also retain their weight, unlike liquid fuels that are burned off during transit, this is large hindrance indeed. These encumbrances are leading many prototypes to seek a hybrid electric propulsion system. A hybrid propulsion system contains elements of both an electric aircraft and an internal combustion powered aircraft. Typically, these systems use an internal combustion engine to produce mechanical power, this mechanical power is then used to drive a generating system to produce electricity, and finally this electricity is used to drive electric motors with propellers generating the propulsive force. The internal combustion engine may or may not have its own

propeller to generate thrust, the setups for hybrid propulsion systems will be discussed in the following paragraphs. The type of internal combustion engines used in hybrid propulsion system are either a piston engine or a gas turbine. There are positives and negatives regarding both engine choices; piston engines can be fuel efficient but lose power output radically with altitude while gas turbine engines can consume a significant amount of fuel but maintains power output decently well with altitude gains. Piston engines can generate significant amount of vibrations while gas turbines spin smoothly, but gas turbines are sensitive to foreign object damage (FOD). This paper focuses on the application of a gas turbine for a hybrid propulsion system, a turboelectric system. UAM aircraft are becoming common enough that regulatory bodies, such as the Federal Aviation Administration (FAA, 2022) or European Union Aviation Safety Agency (Diaz, 2022), are developing specific new certification standards for these aircraft. Therefore, there is a critical need for a turboelectric ground test rig to conduct and study potential turboelectric integration issues and methods.

Turboelectric Theory

Turboelectric systems can have different setups, these setups revolve around how the power generated by the gas turbine is injected into the airflow of the aircraft. Some systems may elect to share the mechanical power from the engine with its own propeller and the electric system. There are two main categories of hybrid systems, those being series and parallel, and a minor third. A series system, shown below in figure 3, has the engine directly feeding the electric generator and nothing else.

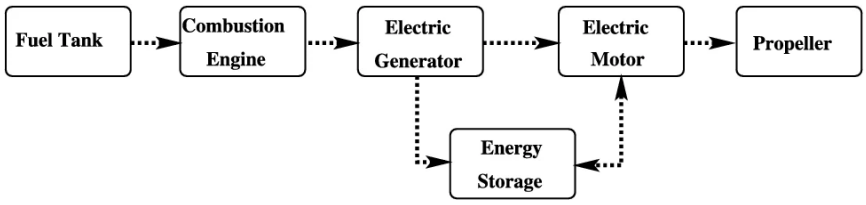

Figure 3. Series Turboelectric System Diagram (Manuel A. Rendon, 2021).

The electricity then powers the propulsors and maintains battery charge levels. It is possible for the electric motor to be driven off only battery power with the combustion engine being shut off. A parallel system, shown below in figure 4 has the engine feeding some sort of mechanical coupling that accepts both mechanical power from the combustion engine and mechanical power from the electric motor. In a parallel system it is possible to drive the propeller with either the electric motor or the combustion engine or even both.

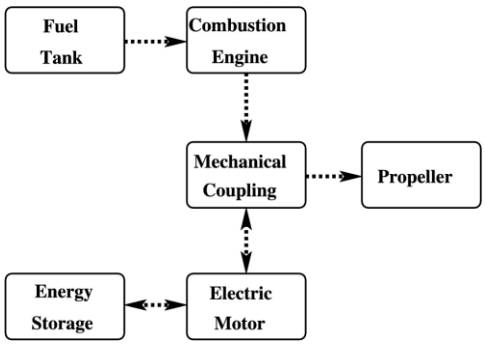

Figure 4. Parallel Turboelectric System Diagram (Manuel A. Rendon, 2021).

Lastly, the third, and least common, hybrid architecture is a mixture of series and hybrid. This mixture of series and parallel setups allows for dynamic switching of mechanical power between propulsors or generator or direct to an electric motor. A diagram of this system is shown below in figure 5.

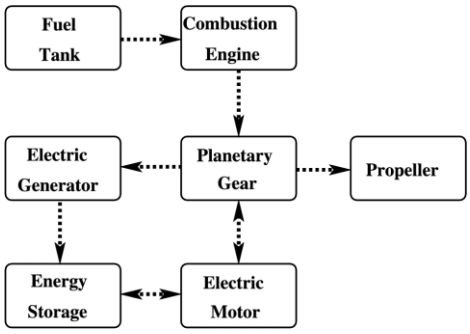

Figure 5. Series and Parallel Turboelectric Diagram (Manuel A. Rendon, 2021).

As shown in this diagram the complexity of this setup is significant and can add a considerable amount of weight to the aircraft, this is not desired for a UAM aircraft where weight is a premium. The power splitting system does not have to be a planetary gearing system as the figure shows, it can be any number of systems.

When considering turboelectric systems there are more subdivisions of architecture. NASA has developed numerous electrified aircraft concepts for larger scale transports (Jansen, 2017). Below in figure 6 is a diagram of turboelectric based architectures.

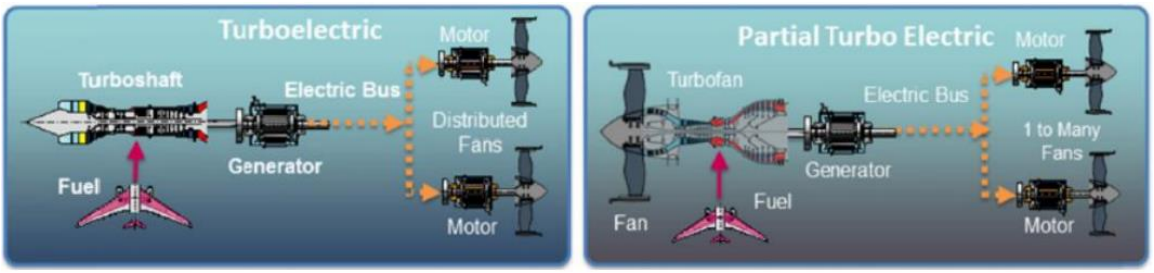

Figure 6. Turboelectric Architectures (Jansen, 2017).

Much like the basic hybrid propulsion discussed earlier, turboelectric system classification depends on how the mechanical power from the gas turbine is injected into the airstream. A full turboelectric system has the gas turbine powering only the generator. The generator then powers the electric motors and fans, or propellers, exclusively. A partial turboelectric system changes the gas turbine slightly, where instead of powering only a generator some of the mechanical power from the gas turbine drives its own fan or propeller while the rest is then fed into the generator. A final turboelectric architecture is given below in figure 7.

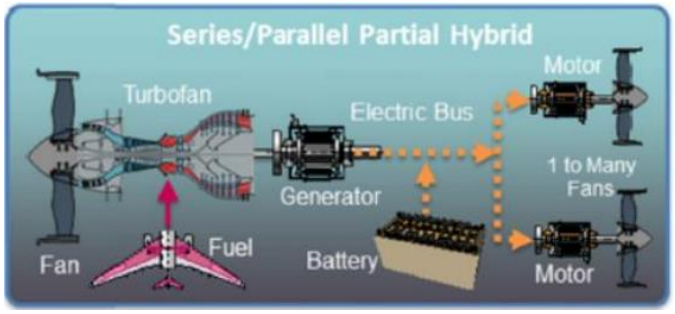

Figure 7. Series and Parallel Partial Hybrid Turboelectric Architecture (Jansen, 2017).

A series or parallel partial hybrid turboelectric system is identical to a full or partial turboelectric system but with a battery present. For series partial hybrid turboelectric systems, the battery is between the generator and propulsors acting as energy storage. For a parallel partial hybrid system the battery is present in the loop much like the previous system, though the entire system has the same features of a standard parallel system. The battery is present to augment the electrical system during intense power draws such as takeoff or dashing. A partial hybrid turboelectric system also has built in redundancy, if the gas turbine fails the battery can power the propulsion system for a short time. In a parallel partial hybrid turboelectric system if the electric system fails then the gas turbine can power the aircraft for a time. A parallel partial hybrid turboelectric system is the full classification of this project's architecture, this is because the PBS Aerospace TP100 powers its own propeller while the generator siphons off power from the propeller shaft to power electric motors and charge batteries.

Proposed Setup

This project, using the parallel partial hybrid turboelectric as discussed before, can be seen below in figure 8. The PBS Aerospace TP100 turboprop is mounted to the aircraft, the Cessna 172. A constant speed three blade propeller is mounted to the turboprop via propeller spacer. A belt driven pulley system is also attached to the turboprop output shaft, this belt system drives the electric generator that feeds the parallel electric system.

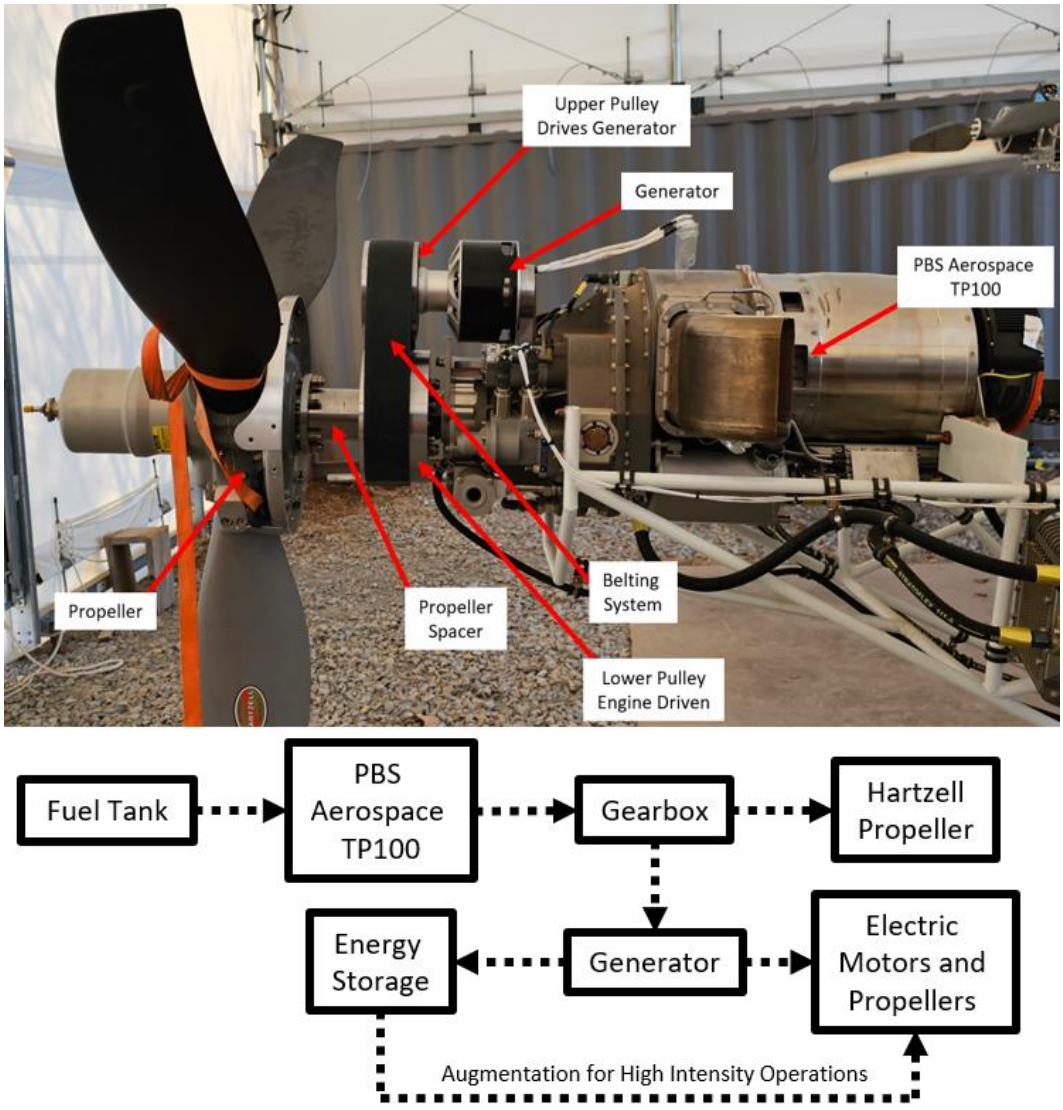

Figure 8. Turboelectric Experimental Setup and Block Diagram.

Chosen Aircraft

The aircraft chosen for this project is the Cessna 172, this aircraft is a N model with a first flight worthy registration of February 28th, 1978. The Cessna 172 is a four seat general aviation aircraft. The Cessna 172 N model has a maximum takeoff weight of 2,400 pounds (Cessna Aircraft Company, 1985). The 172 has a conventional tail configuration for its fin and horizontal stabilizers with the rudder and elevators being attached to these respective components. The wings are high mounted with a strut bracing. The wings are also of a standard rectangular design

with a small, but present, taper outboard of the flaps. The ailerons are attached via three hinges at the trailing edge of the outboard section of wing, where the taper is present. The flaps are installed on the inboard section of the wing where there is no wing taper. An airworthy Cessna 172 is shown below in figure 9. If the reader wishes to learn more about the aircraft and its controls more information can be found in the appendix.

Figure 9. Cessna 172 Under Maintenance, S Model.

Chosen Powerplant

The powerplant selected for this project is a PBS Aerospace TP100 turboprop. The turboprop contains a gas generator, this gas generator generates the mechanical power that drives the propeller through a gearbox. The turboprop generates mechanical power by ingesting air, compressing the air through stations 2 and 3, mixing the air with fuel and burning the mixture to increase temperature through stations 3 and 4, expands the high energy flow through a turbine located between stations 4 and 5. The turbine extracts a portion of the energy from the flow that is then used to drive the compressor to keep the cycle sustained. A pictorial of an idealized turboprop is shown below in figure 10 with station numbers defined.

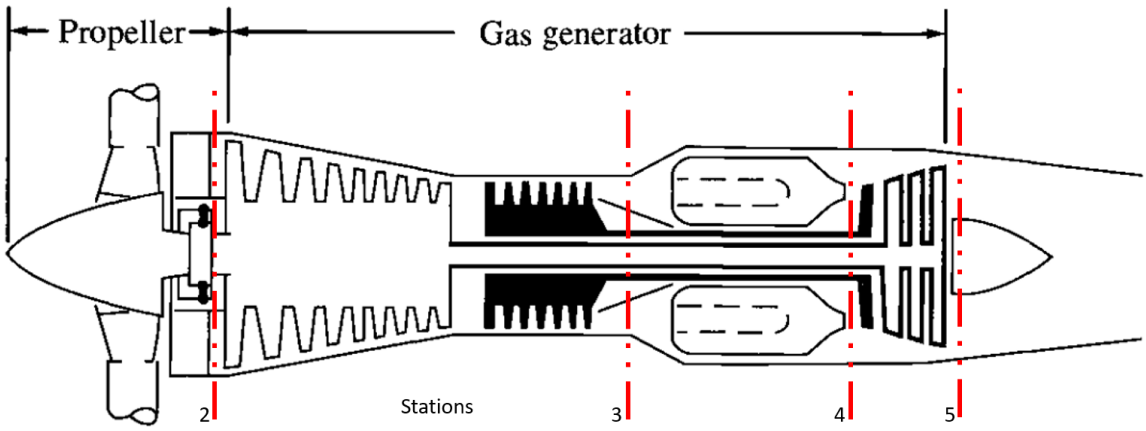

Figure 10. Schematic of Turboprop with Station Numbers (Jack D. Mattingly, 2016).

After the flow exits the core it passes through a final turbine, the free turbine, that extracts a majority of the energy remaining in the flow. The free turbine then drives the gearbox that reduces the revolutions per unit time to an acceptable speed for a propeller, if not than portions of the propeller blade will become supersonic dropping the thrust produced and efficiency of the propeller. Once the rotational speed is appropriate it is output to a propeller flange, this flange is where the propeller is mounted to. After the free turbine the flow is routed outside of the engine as exhaust. Below in figure 11 is a cutaway schematic of the PBS Aerospace TP100.

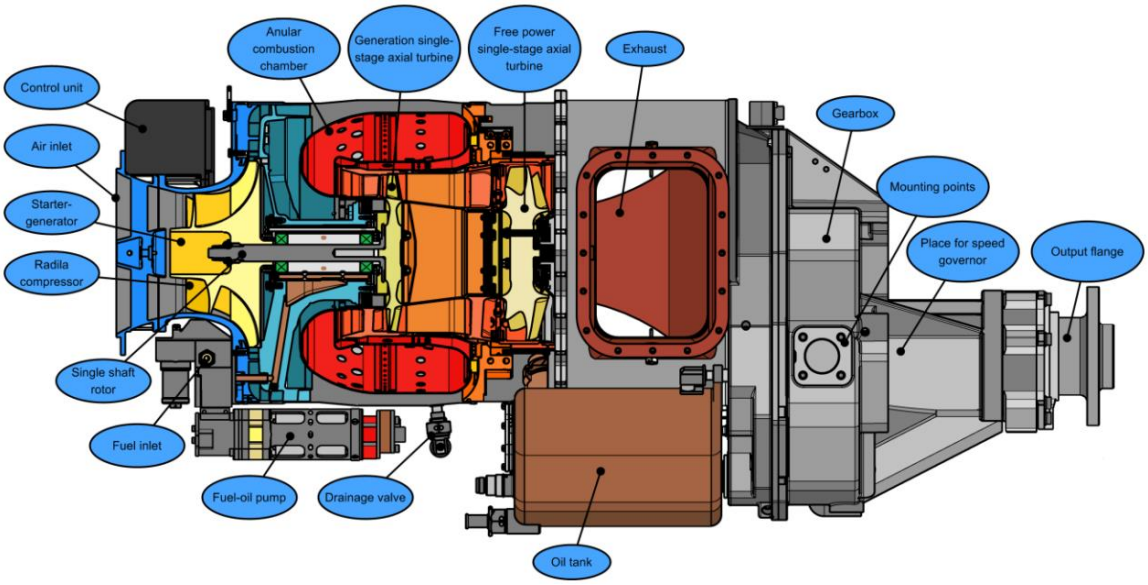

Figure 11. PBS Aerospace TP100 Cutaway Schematic (PBS Aerospace , 2015).

An important observation from this engine cutaway of the PBS Aerospace TP100 is that air is ingested at the back of the engine, opposite the propeller. Aft inlets on turboprops are common, this is because routing sufficient airflow through the root of the propeller blades and into the engine can be difficult. Moving the inlet to the back of the engine also allows for space for particle separators in inlets, which act like a filter, allowing particulates to drop out of the flow. Another interesting note is that the annular combustion chamber is a reverse flow type. A reverse flow combustion chamber allows for axial space saving by routing flow around the chamber for cooling. The flow is then turned in the opposite direction, back to the inlet, where it is mixed with fuel and burned. Finally, the flow is turned once more, back to the turbines, where it is expanded through the turbines for power extraction. There can be considerable amounts of pressure loss associated with turning the flow so many times, but this design allows for the engine to be shorter. Instead of the primary turbine being immediately aft of the combustion chamber it is, instead, nested within the combustion chamber footprint significantly shortening the length of the turboprop. Nesting the primary turbine within the footprint of the combustion chamber also yields positive results on power shaft dynamics by allowing for a shorter power shaft.

The Propeller

The propeller is constant speed, meaning the propeller blade pitch can dynamically change according to propeller rotational speed and engine power level to place it in its optimal configuration according to airspeed and propeller rotational speed. This is achieved by the engine controlling the oil pressure being fed into the propeller through the propeller flange. Within the propeller assembly there is a diaphragm, on one side of the diaphragm could be a spring, depending on the manufacturer and model, and an air charge. The air charge is calibrated to a certain pressure to ensure proper functioning of the propeller at varying temperatures. On the other side of the diaphragm, engine side, is where the engine oil is present. The magnitude of the oil pressure will increase or decrease the propeller blade angle by moving the diaphragm. The diaphragm movement manipulates cams or gears, manufacturers have their preferences, that rotate the propeller blade shanks within the hub and therefore changing the pitch of the blade. Below in figure 12 is a cutaway diagram of the propeller hub used in this application.

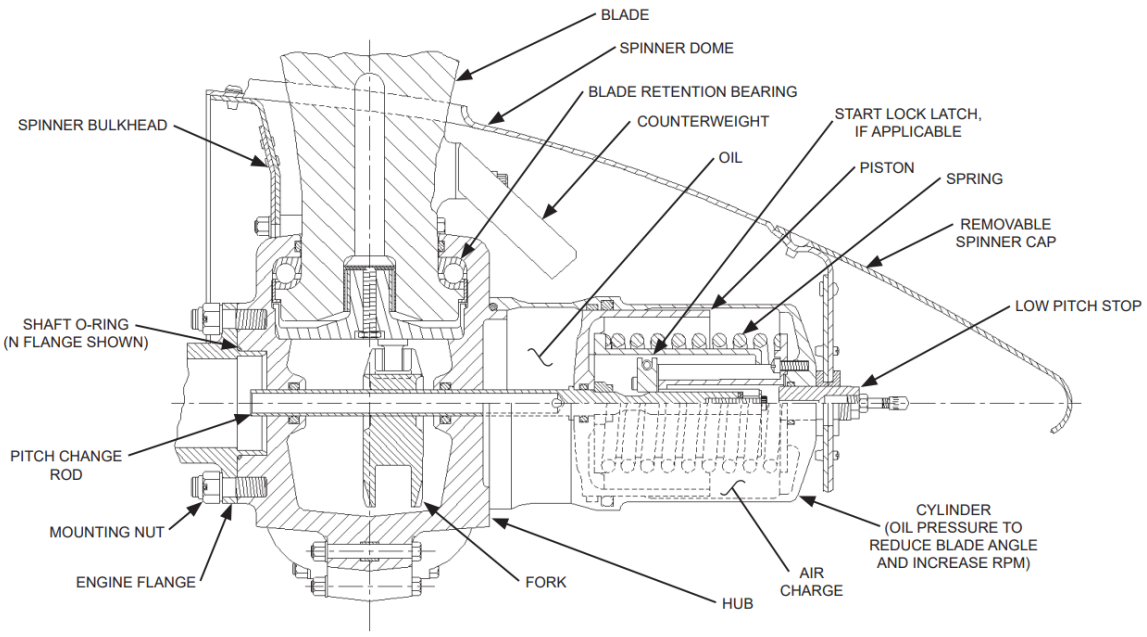

Figure 12. Hartzell -5 Turbine Propeller Used in this Project (Hartzell Propeller, 2022).

Propellers were the first form of aircraft propulsion and were driven by piston engines, not much has changed though the way the power is generated has been refined many times. These refinements include higher displacement piston engines, forced induction, higher performance fuels, and finally the introduction of turbomachinery. With the introduction of "jet engines" aircraft performance skyrocketed, literally. Gas turbine engines were soon adapted to drive a propeller, the gas turbine could generate massive amounts of power quickly outpacing even the most exotic piston engine designs. A bonus of turboprops is that they have considerably better high-altitude performance, shown below in figure 13 is a plot of power generated versus altitude for a piston engine and a turboprop for a selected power of 100-hp.

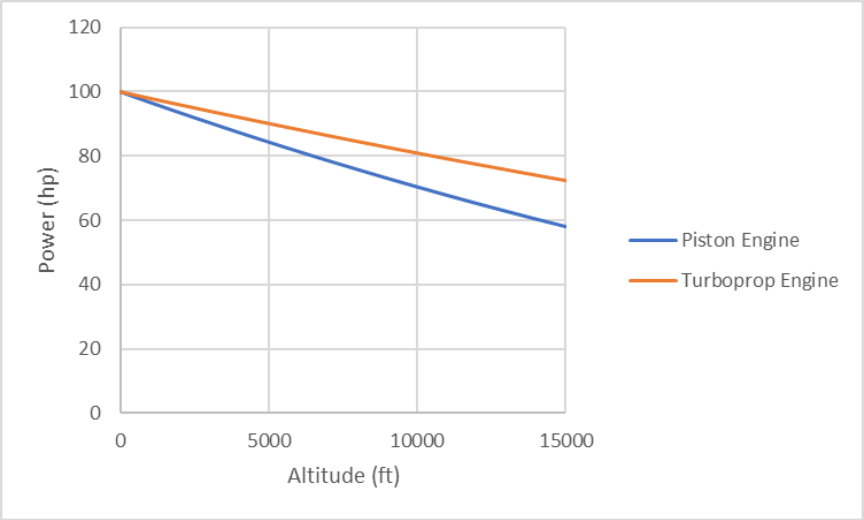

Figure 13. Piston and Turboprop Engine Power Outputs at Altitude

The correlation equation to derive piston engine power at altitude is shown below in equation 1.

$$\frac{P}{P_0} = 1.132\frac{\rho}{\rho_0} - 0.132 \text{ (Anderson, 1998)} \quad (1)$$

Where P is power at altitude, P_0 is power at sea level, ρ is air density at altitude, and ρ_0 is the air density at sea level. This correlation was derived from Torenbeck and obtained from (Anderson, 1998). The correlation for turboprop engines is given below in equation 2.

$$\frac{P}{P_0} = \left(\frac{\rho}{\rho_0}\right)^n, n = 0.7 \text{ (Anderson, 1998)} \quad (2)$$

This correlation was also obtained from (Anderson, 1998). As it can be seen in figure 13 the power generated of a turboprop is significantly higher than a piston engine at any given altitude. The power at altitude advantage of turboprops is why many electrified systems typically employ gas turbines. The power generated is fed directly into the propeller. The propeller must efficiently transfer this power into its stream tube. To do this the propeller must generate maximum thrust, minimize drag, and prevent blade stalling. Below is a figure of a propeller blade airfoil segment.

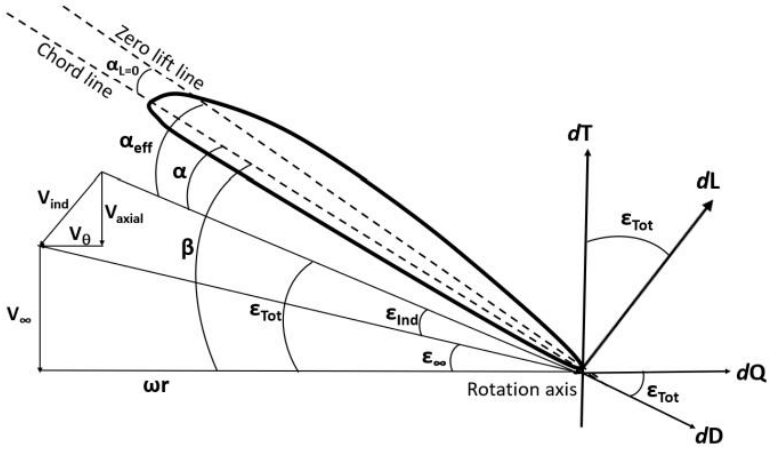

Figure 14. Propeller Airfoil Blade Angles and Vectors (Muwanika Jdiobe, 2022).

As figure 14 shows, propeller rotational speed and forward speed drive the angles of attack for the airfoil along the blade. Some important variables are V_∞, ωr, and β. V_∞ denotes the forward velocity of the propeller, ωr denotes the rotational velocity of the propeller, and β is the total angle of attack. V_∞ and ωr profoundly affect the angle of attack β and therefore stalling properties of the propeller. V_∞ and ωr also are within the function of advance ratio which is discussed below. Also note that the angle of attack will change along the blade span due to increasing rotational velocity with increasing blade radius. Propellers typically have a built-in twist of the blades, this twist changes along the blade span to account for angle of attack change

along the blade span. An important note about propeller pitch, it is not an angle. Propeller pitch is a measure of distance traversed by the propeller per rotation, this is the same for pitch in a bolt or screw. An important figure of merit for propeller is the Advance Ratio which correlates propeller forward speed to the propeller's rotational speed. Advance ratio is shown in equation 3.

$$J = \frac{V}{nD} \tag{3}$$

Where J is the advance ratio, n is the rotational speed, V is the forward velocity, and D is the diameter for the propeller. The coefficient of thrust is shown in equation 4.

$$C_T = \frac{T}{\rho n^2 D^4} \tag{4}$$

Where C_T is the coefficient of thrust, ρ is the air density, and T is propeller thrust. The coefficient of power is shown next in equation 5.

$$C_P = \frac{P}{\rho n^3 D^5} \tag{5}$$

Where C_P is the coefficient of power and P is propeller power. Lastly, the coefficient of torque is shown in figure 6 below.

$$C_Q = \frac{Q}{\rho n^2 D^5} \tag{6}$$

Where C_Q is the coefficient of torque and Q is propeller torque. Above in equations 3 through 6 are some figures of merit for a propeller. As previously stated, advance ratio relates the propeller's forward speed against its rotational speed. The higher the advance ratio the faster the propeller is moving forward compared to its rotational speed, and vice versa for lower values. As can be seen this value relates to the local angles of attack along the blade, if too aggressive then the blade may stall. Another figure of merit is the thrust coefficient, which relates the thrust

produced to the air coming into the propeller. The power coefficient is like the thrust coefficient, though in terms of power and not force. Lastly, the coefficient of torque is like the coefficients of thrust and power but it uses the propeller's torque.

Structural Requirements

Structural components of this turboelectric system will experience considerable loading conditions from the turboprop and generating system. The engine mount will house all these items and must be off sufficient strength and rigidity. Since this is a ground test rig, never to fly, weight is not of a consideration. Therefore, engine mount safety was critical which led to considerable overdesign of the engine mount to ensure sufficient strength no matter the conditions. Primary loadings for the engine mount are the engine torque and thrust output. However, the engine manufacturer defines emergency loading conditions for the engine mount, these can be found below in figure 15 along with a flight envelope.

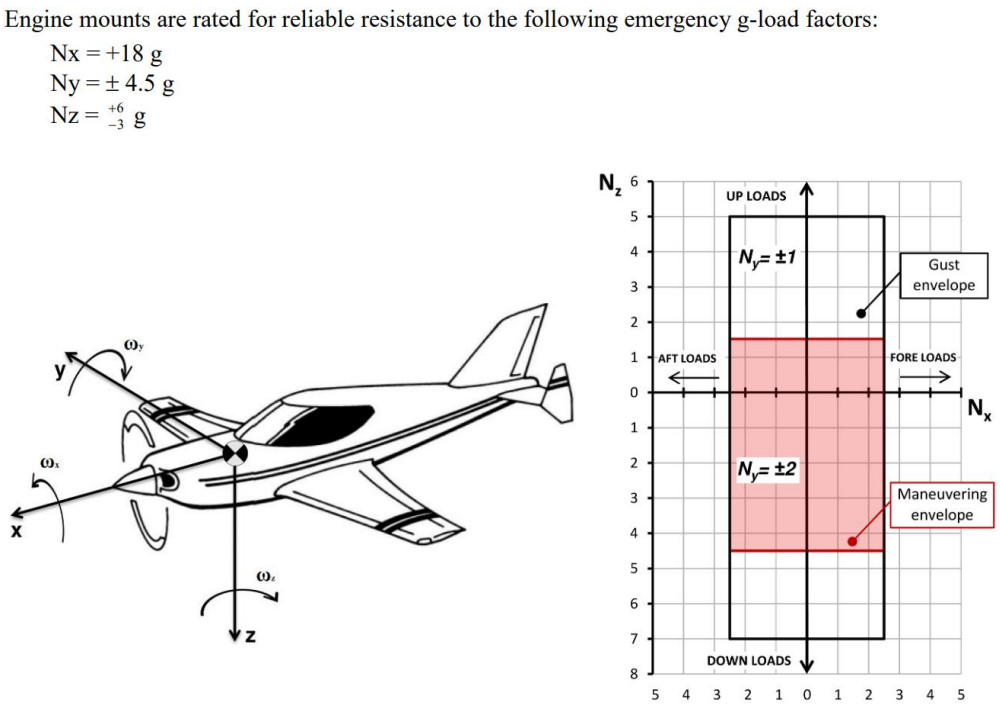

Figure 15. Aircraft Coordinates, Emergency Loads, and Flight Envelope (PBS Aerospace, 2014).

The emergency loads are quite large, such as the 18-g forward axial load, likely to capture accelerative loading conditions during a takeoff roll. g is used as one earth gravity. The final portion of consideration is the natural frequencies of the structural components. Within the FEA software a natural frequency analysis was conducted to determine the estimated natural frequencies. The primary focus is usually the first mode, however multiple modes were computed to ensure that none of the modes would danger the components. An example of an aviation turboprop engine mounting system is shown below in figure 16.

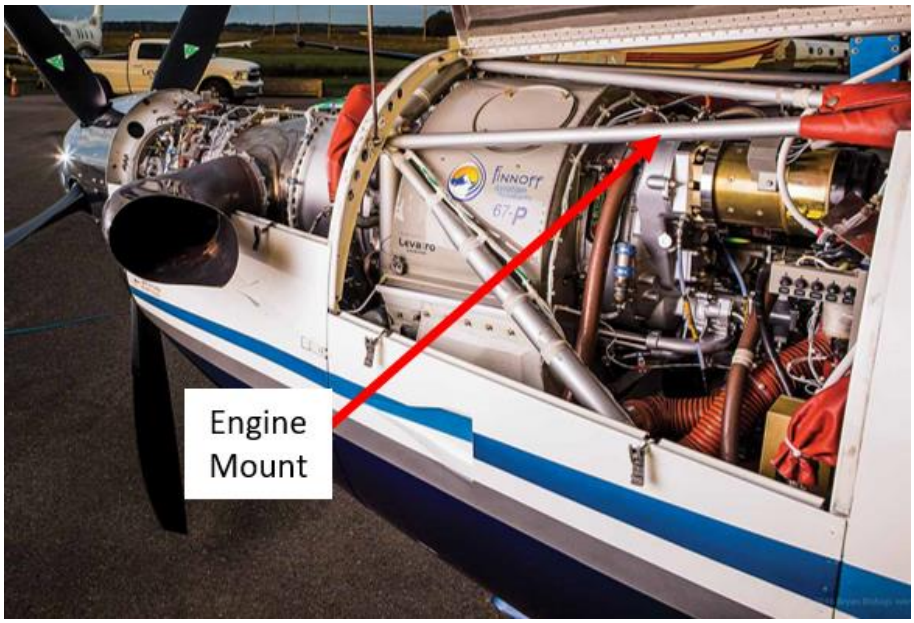

Figure 16. Typical Aviation Turboprop Engine Mount (Mark, 2019).

Generator Theory

The generator for this project is a brushless electric motor. Typical electric motors have brushes that are attached to the center rotating element. As the motor spins the brushes continuously rub against the shaft, these brushes transfer electric power to the many turns of wiring on the shaft. These powered coils generate a significant magnetic force that pushes against permanent magnets in the motor casing, causing the center element to rotate. However, brushless motors omit these brushes, hence the name. Instead, these brushless motors have a solid permanent magnetic in

place of the coil windings in the center shaft. The coils are moved to the motor casing and are charged in a certain pattern, this pushes against the center magnetic shaft causing it to rotate. As can be seen the friction of a brushless motor is much less than that of a typical electric motor. For this application the electric motor is being driven instead of driving. The causes the motor to generate a charge, this charge is used to do work and achieves the turboelectric desires. The generator is driven by a pulley and this pulley is driven by a belting system. Diagrams of brushed and brushless motors are shown below in figure 17.

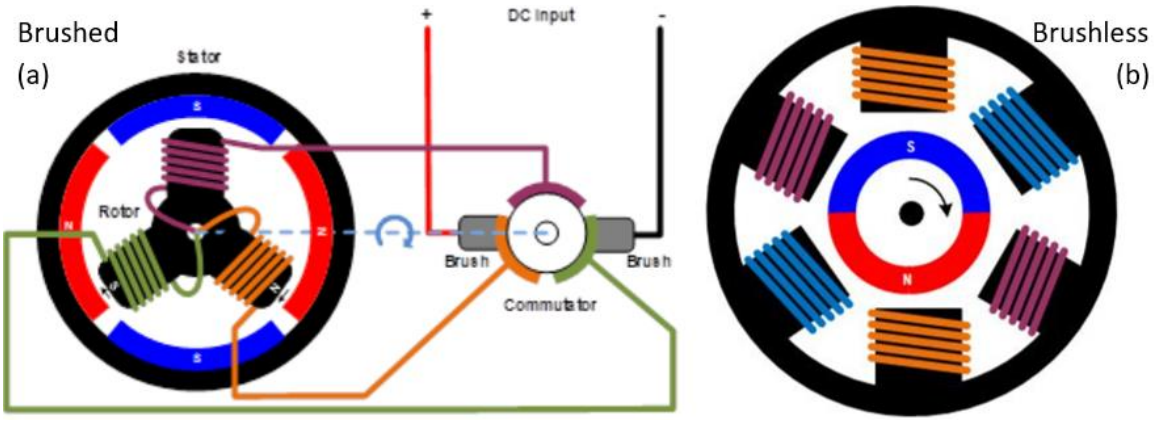

Figure 17. Brushed Electric Motor (a) and Brushless Electric Motor (b) (Millett, 2022).

Power Transfer Requirements

To generate electric power to fulfill the turboelectric aspect of this project the generator must be driven with an appropriate level of power. This will be done by transferring power from the engine output shaft to the generator. To achieve a power transfer a belting system is developed to drive the generator through use of pulleys. Power generated by the generator is directly correlated to the amount of power input to the generator. This correlation is shown below in equation 7.

$$P = IV = \tau\omega \tag{7}$$

Where P is power, I is current, V is voltage, τ is torque, and ω is rotational speed. It is important to note that the generator will not turn 100% of the mechanical power into electrical power, there

are losses associated with this. Therefore, an overestimation of mechanical power transfer is needed to ensure that adequate amounts of electrical power is obtained. As can be seen the more power from the generator that is desired requires a greater torque transfer or RPM. This is achieved using a belting system. Belting has been a cornerstone of machines since their inception, in fact the pulleys used in belting system are one of the six simple machines. Belting relies on the mechanical advantage of pulleys and the force transmission of friction. In essence torque is transferred from one pulley to the other, once a rotation is introduced this torque becomes a power transfer, while still retaining the torque transfer. This is the premise used to transfer adequate power to the generator. A desired power output at a certain voltage is set. By the generator properties an RPM that the generator requires is determined, this is the goal RPM that the belting system must drive the generator pulley at. With the turboprop outputting a constant RPM a speed ratio is obtained, for this application a higher speed at the generator is required. This leads to the generator pulley having a smaller diameter than that of the turboprop pulley. With power and RPM known belt selection may begin. There were many belt types considered, all with varying pros and cons, the final belt type selected is the Micro V-Belt type with numerous ribs. Several different belt design guide manuals were considered and used in the selection process, these manuals can be found in the references section of this paper. These manuals are provided by belt manufacturers to assist customers in choosing the correct belt. These manuals apply safety factors for belt applications and environment, a detail that is thoroughly appreciated. This is known as Design Power and is shown below in equation 8. It is noted that the following equations, 8 through 12, were obtained from the belt design manuals which are found in the references section.

$$P_D = P_M F_S \tag{8}$$

Where P_D is the design power, P_M is the supplied power, and F_S is the service factors associated with environmental and usage applications. The service factors are supplied by the

manufacturer's manual. Stepping through the manuals a power transfer required is determined, this power transfer is the base power required with the safety factors discussed earlier. With this known then pulley sizes were determined as well as pulley center to center distance being considered. With these variables known a selection of a belt subtype and length can be made. Belt length is computed by equation 9 below:

$$L = 2C + 1.57(D + d) + \frac{(D - d)^2}{4C} \tag{9}$$

Where L is length of belt required, C is the center-to-center distance of the pulleys, D is the diameter of the larger pulley, and d is the diameter of the smaller pulley. With length of belt known a subtype may be selected. For example, if Narrow Wedge type belts are being considered then the subtypes that may be chosen are the 3V, 5V, and 8V belts. With increasing numbers, the belt size grows, these subtypes are essentially larger belts for heavier duty applications. With a belt subtype selected then the number of belts required for the power transfer may be determined. Each belt is rated for a certain amount of power at a given RPM and arc of contact around the pulleys. Ideally one belt should be sufficient to transfer all required power, however this is rarely the case. Some exceptionally high-power applications may require a great many belts. The equation used to determine the number of belts required is shown below in equation 10:

$$N = \frac{P_D}{P_{STD} C_{ARC} C_{BL}} \tag{10}$$

Where N is the number of belts required to transfer the power, P_{STD} is the standard power transmission of the belt under the given conditions of RPM and pulley diameters which is given by the belt manufacturer. C_{ARC} is a modifier for arc contact of the pulley that the belt is in contact with, this data is provided by the belt manufacturer with 180 degrees of arc contact being optimum. Lastly C_{BL} is a modifier relating to belt length, the longer the belt is the higher this modifier is. These modifiers have a maximum value of one, so it is desired to keep these values as

high as possible. Once the number of belts required is known design changes may be considered. For this project the initial belt requirements for a 3V Narrow V-Belt were 16 belts, far too many for the size and dimensioning requirements of the turboelectric system. From this example belt design and the generator mount design were closely woven together. Different belt types and subtypes can transfer different amounts of power, so several belts may be considered to reduce system complexity. With these variables known some computations for belt tension loads can be completed. These equations are shown below in equations 11 and 12.

$$T_1 = \frac{P_D}{C_{ARC}V} \tag{11}$$

$$T_2 = \frac{(1.25 - C_{ARC})P_D}{C_{ARC}V} \tag{12}$$

Where T_1 is the tight side tension, T_2 slack side tension, and V is the belt speed. It is also noted again that equations 8 through 12 were obtained from belt design guide manuals for belt selection. These loads will be used to determine reactionary forces the generator mount must resist. These involve tight and slack side belt tensions, tight side is before the belt transfers power to the generator pulley while slack side is after the belt passes around the pulley. These tension loads and torque amounts were used to analyze the generator mount to ensure safety of the complete installed turboelectric system. Lastly, a final selection of a belt must be made. This requires the subtype and total length of belt required. Once these are known then a belt may be selected from a supplier.

Previous Work

Manuel A. Rendón et al. conducted a significant study survey over current and potential future systems for hybrid propulsion for UAM aircraft. This study involved battery technology, aircraft configurations, and even environmental considerations. The team concluded that full electric systems are severely hampered by battery technology stating that battery energy density is

currently around 50 times less than that of liquid fuels and may not become feasible for a considerable amount of time. Meanwhile hybrid systems, such as turboelectric, are highly recommended for their high-power outputs, efficiencies, and potential use of green fuels. However, the team did not address any practical implications of system installation, such as structural requirements, though thermal issues of the electrical systems were covered (Manuel A. Rendon, 2021). D. A. Swanson et al. developed software and used it to optimize aircraft engine mount design. This model worked to provide a mounting system that was stiff enough to provide adequate strength for the engine suspension but soft enough to isolate vibrations from the engine to the airframe. This model considers the engine and its power and torque as well as elastomeric mounts for engine suspension. However, the paper does not consider potential effects of turboelectric system components and how they might affect engine suspension (D. A. Swanson, 1993). Smruti Sahoo et al. developed an expansive model for the assessment of hybrid electric aircraft designs. This model covered all major components of a hybrid aircraft including the powerplant, generator, propulsors, batteries, cooling systems, and even aircraft structure requirements. The authors did an excellent job of considering may difference aspects and developing appropriate models for them, even an intricate cooling system for the components proposed. The authors then moved to analyze some proposed aircraft using their model, one even had power takeoff (PTO) of up to 500-kW. However, the paper never covered structural integration requirements of the powerplant and generating system, or even how PTO was accomplished. The structural analysis was limited to wing analysis (Smruti Sahoo, 2022). Raj Ghelani et al. developed a unique model in which the low pressure spool of a gas turbine engine was boosted by using a electric motor to inject more power into the engine for the megawatt class of aircraft. This model was able to demonstrate a reduction of 4.2% in fuel burn over conventional propulsion over a range of 740-km (400-nm). This paper does an excellent job of explaining all the intricacies involved in a hybrid system of this design even to the point of proposing a redesigned gas turbine and conducting complete mission analyses on these systems.

While this paper highlights the effects of a hybrid system on aircraft design no structural components or analyses are given, such as how the electric motor is integrated into the low pressure spool of the gas turbine (Raj Ghelani, 2022). Joshua Johnsen et al. integrated a 7-kW turboelectric system into an unmanned aircraft with a flight test. The paper clearly defines turboelectric systems with their pros and cons. The paper then moves to part sizing with clear rationale as to why each component was selected. However, while the paper does cover the mounting system of the turboelectric system it is not in any appreciable detail without any structural analysis. Lastly, the paper considers the application of a 7-kW system into an unmanned system, the work of this paper considers the application of a 180-kW system into a manned system (Joshua Johnsen, 2021).

CHAPTER III

METHODOLOGY

Building the Turboelectric Ground Test Rig

To support the experiment the aircraft that the test rig will be installed in must first be built. The first step was to acquire an aircraft. As stated earlier the selected aircraft was a Cessna 172, with is being delivered on the back of a trailer with the aircraft entirely disassembled, shown in figure 18.

Figure 18. Received Cessna 172.

Assembling the aircraft was the first major workload. This required installing the horizontal stabilizers, fin, wings, wing struts, ailerons, flaps, elevators, rudder, and interior. This was done by consulting the aircraft's manuals and purchasing required hardware such as nuts and bolts. After all the external components were installed the control surfaces needed to be wired up, while not necessary for the project it was desired to have functional aircraft controls. By having control

surfaces fully operational they may be locked, this prevents the control surfaces from oscillating in the wind and propeller wakes. To achieve this control cables

had to be stretched from the controls to their corresponding control surface and tensioned. Once this was finished the interior was assembled such as the seating for the pilot and copilot. The finished aircraft is shown in figure 19.

Figure 19. Assembled Cessna 172.

It was soon realized that the aircraft was without a braking system, when the propulsion system is at full power a considerable amount of thrust is generated. While the aircraft itself is anchored it is desired to have a backup in case of anchor failure, so the brake system was rebuilt. New wheels and tires were purchased for the main landing gear along with new brake discs and brake calipers. The brake master cylinders in the aircraft were rebuilt with new hardware and seals and are shown in figure 20.

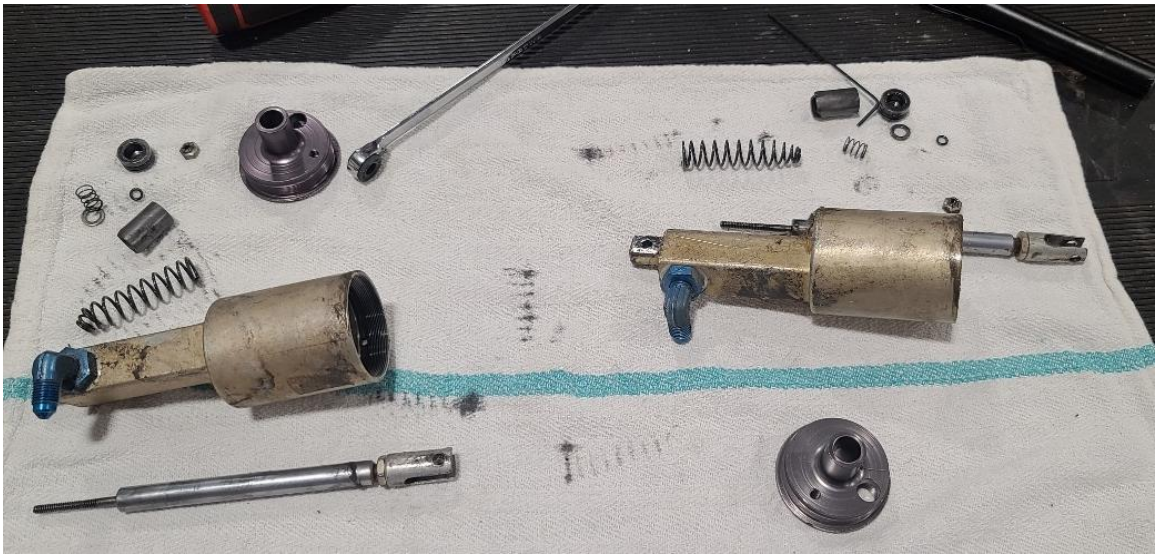

Figure 20. Disassembled Brake Master Cylinders.

The system was fully reassembled with new hose where needed, filled with hydraulic fluid, and purged of air to ensure proper brake operation, the new brake components are shown below in figure 21, these include the new torque plate, calipers, and wheels.

Figure 21. New Brake Components.

There is an independent brake system for each main wheel, this also serves to steer the aircraft during ground operation. While the brake system may not be strong enough to hold the aircraft at full power it will allow for steering and slowing while the propulsion system is deactivated, preventing the aircraft from colliding with something.

The next critical component installation is the engine. This requires the engine mount to be installed and secured to the airframe. When the mount was installed a quick torque study was done. This was accomplished by attaching an arm to the front of the engine mount and hanging an increasing amount of weight to it. This was to simulate the torque load the engine mount would have to resist from the turboprop. The torque test successfully validated the strength and rigidity of the engine mount. Once this was done the turboprop was hung from a crane and bolted to the engine mount. A fuel system was developed to feed the turboprop with Jet-A. Originally the fuel tanks built into the wings were going to be used, this would give a gravity boost to ensure optimal fuel pressure delivered to the engine. Unfortunately, it was discovered that the aircraft was missing its fuel cells, no doubt salvaged long ago. To ensure that the proposed fuel delivery system would be able to deliver fuel at the required pressure and flow rates a rudimentary pipe flow analysis was conducted. This analysis would determine the pressure drop across all hosing, all fittings, all components, and elevation changes. Equation 13 below is static pressure equation.

$$\Delta P_z = \rho_F g z \tag{13}$$

Where ΔP_z is the pressure drop according to elevation change, ρ_F is the density of the fuel, g is gravity, and z is the elevation change. Fuel is drawn through the tank from the top, but then drops down to be inline with the bottom of the tank, this negates the pressure rise required to withdraw fuel from the tank. Pipe flow analysis was then conducted on the hosing with Reynolds number, equation 14, being first computed.

$$Re = \frac{VD_H}{\nu} \tag{14}$$

Where Re is the Reynolds number, V is the velocity of the fuel in the hose, D_H is the interior diameter of the hose, and ν is the kinematic viscosity of Jet-A. Surface roughness of the hose was approximated by using values for robber on the high side. This was done as the hosing is made of synthetic rubbers and to develop an overestimation of the pressure drop through the hose to ensure that the pump would be able to deliver the fuel. The flow as found to be turbulent, so the Haaland friction factor equation was used and is shown below in equation 15.

$$\frac{1}{\sqrt{f}} = -1.8 \log\left[\left(\frac{\epsilon/D_H}{3.7}\right)^{1.11} + \frac{6.9}{Re}\right] \tag{15}$$

Where f is the friction factor, and ε is surface roughness. With this friction factor known the pressure drop through the hosing can be determined using the equation below, number 16.

$$\Delta P_H = f\frac{l_H}{D_H}\frac{\rho V^2}{2} \tag{16}$$

Where ΔP_H is the pressure drop through the hose, l_H is the length of the hose, and ρ is the density of Jet-A. According to the engine specifications fuel must be delivered to the engine at a minimum of 5-kPa, the aircraft fuel system must deliver fuel at least this pressure otherwise the engine may stall. As discussed before the standard fuel system of the aircraft was not usable due to missing fuel tanks, so a custom fuel delivery system was developed. To maintain simplicity of the analysis the flow analysis was conducted only at maximum fuel requirements of the engine. This fuel requirement was obtained from the engine manual and is given as 120-L/hr [PP-48]. Hosing material is known so surface roughness could be approximated. Hose interior diameter was also known. The kinematic viscosity of Jet-A was obtained. Next, pressure drops associated with the filter, manual shutoff valve, fittings, and electromagnetic valve were recorded from

manufacturer data. Finally, all these pressure drops were summed and compared to the pressure the fuel pump can deliver at the maximum flow rate, the pump curve is shown below in figure 22.

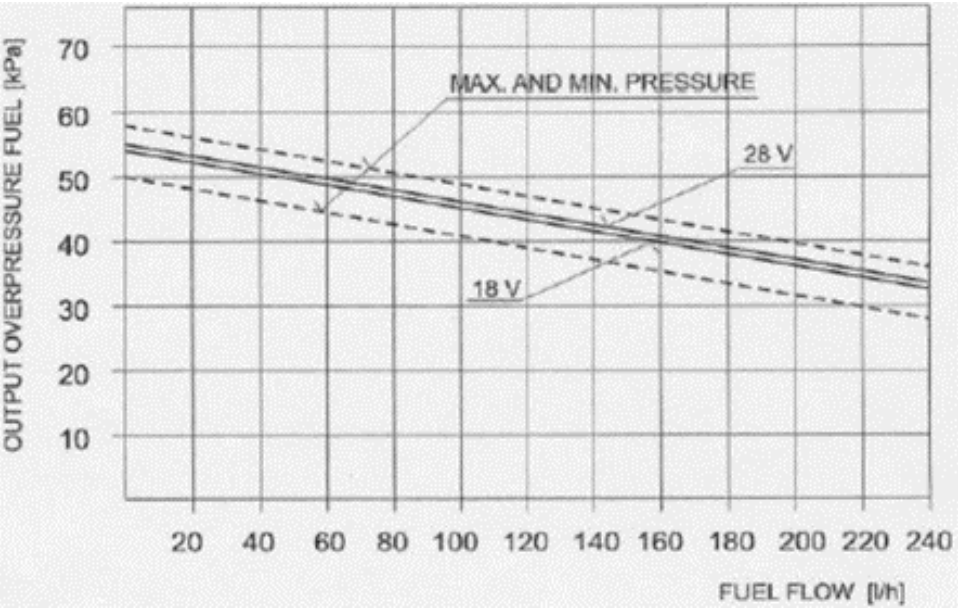

Figure 22. Pump Curve of Provided Fuel Pump (PBS Aerospace, 2014).

Once this analysis confirmed that the fuel pump had sufficient pressure delivery the system was installed on the aircraft. An 18-gallon aluminum fuel tank was purchased and mounted to the floor panels just aft of the pilot, this ensured the shortest distance that fuel lines would have to travel. Next fuel lines of various lengths were fabricated to connect all the fuel system components, these lines were made from aviation grade flexible hosing ensuring high quality lines. The components are as follows: fuel tank, fuel filter, fuel pump, manual shutoff valve, and electromagnetic fuel valve. The fuel tank simply holds the fuel in a safe manner. The fuel filter removes rough particulates, it has a 40-micron mesh filter. The fuel pump was supplied by the turboprop manufacturer and provides enough head pressure to ensure fuel delivery. The manual fuel shutoff valve is controlled by the pilot and is used to cut fuel supply in event of emergency. And lastly the electromagnetic fuel valve is controlled by the engine to fuel metering. Part of the fuel system is shown below in figure 23.

Figure 23. Partial Fuel Delivery System.

After the fuel system was successfully installed an oil system was built, which was comparatively simple. It is only two lines and an oil cooler. The oil cooler has a built in thermostat which will open at a determined oil temperature to let oil pass through the cooler. The oil routed out of the engine's gearbox, very hot, and into the oil cooler assembly. Then the oil is routed back into the engine at the oil tank. The oil cooler was mounted off to the side of the engine mount so that it will experience propeller wash to help effectively cool the oil. The oil cooling loop is shown in figure 24.

Figure 24. Oil Cooling Loop.

Lastly the electric and engine controls were installed. This required a significant amount of wire of varying gauge size to be measured, crimped or soldered, and installed. The first components to be installed was the main bus and activation circuit. A relay was used to supply the engine control unit (ECU) with power from the battery. This relay is activated by use of a master switch and circuit breaker. Once the switch is activated and the circuit breaker has continuity, current from the battery passes through a fuse, through the relay, and into the ECU and the main bus, the battery circuit is shown below in figure 25.

Figure 25. Battery Circuit.

The bus provides power to circuit breakers for the fuel pump, propeller feathering unit, and propeller reduced speed circuits. Power then moves from these circuit breakers to switches for the fuel pump, propeller feathering unit, and propeller reduced speed. These propeller controls will be discussed later with the engine controls. After these circuits were completed the engine controls were installed. This included a significantly populated wire harness to be built that plugs into the ECU and is shown in figure 26.

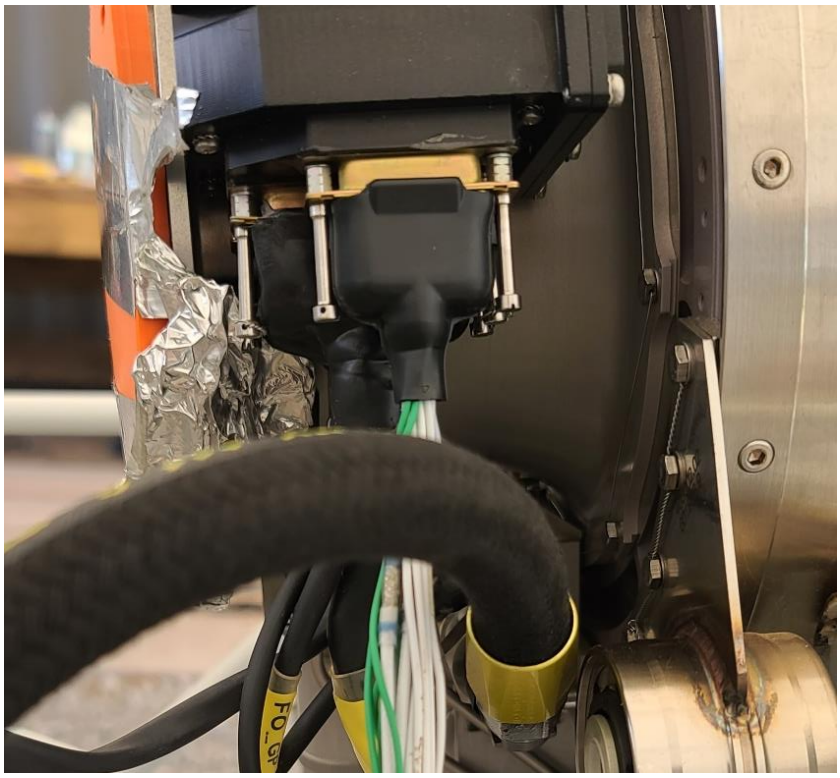

Figure 26. ECU its Wiring Harness.

This harness is populated by elements for the ignition source, electromagnetic fuel valve, engine control lever, engine monitoring through controlled area network (CAN), and engine kill switch. The ignition source is powered from the ECU and generates a large voltage that is pumped into a spark plug that is in the burner liner, this arcing from the plug ignites the fuel. The electromagnetic fuel valve is installed on the fuel line, as mentioned earlier, and controls fuel metering to the engine from the fuel delivery system. The engine control lever is in the cockpit and is manipulated by the pilot. Depending on the location of the lever in relation to the body a certain voltage is output by the control lever to the ECU. This voltage dictates an operation for the engine such as an engine power percentage, start, stop, cold start, and hot start. Along with this engine control lever the propeller controls are also present on the dashboard. The propeller feather switch will immediately feather propeller, that is force the blade's chord in line with the air flow, minimizing drag and preventing propeller windmilling. This is done in emergencies such

as engine failure. When the propeller reduced speed switch is engaged the propeller blades are manipulated to increase aerodynamic loading, this drops the engine RPM by a few percentage. While this is not a considerable amount it is enough to stave off overspeed conditions. The engine CAN lines transfer packets of data containing critical engine data such as turbine RPMs, exhaust gas temperature, and engine torque. There are many more, but these are some of the more critical examples. This data is passed through a CAN module that is hooked into a computer through USB. The turboprop manufacturer provided software that reads this data and displays it in a window for the user. This computer is installed in the interior of the aircraft and is how the pilot monitors the engine. The last switch is the engine kill switch. When engaged the engine will cease function and will not start again. The dashboard with electric and engine controls is shown below in figure 27.

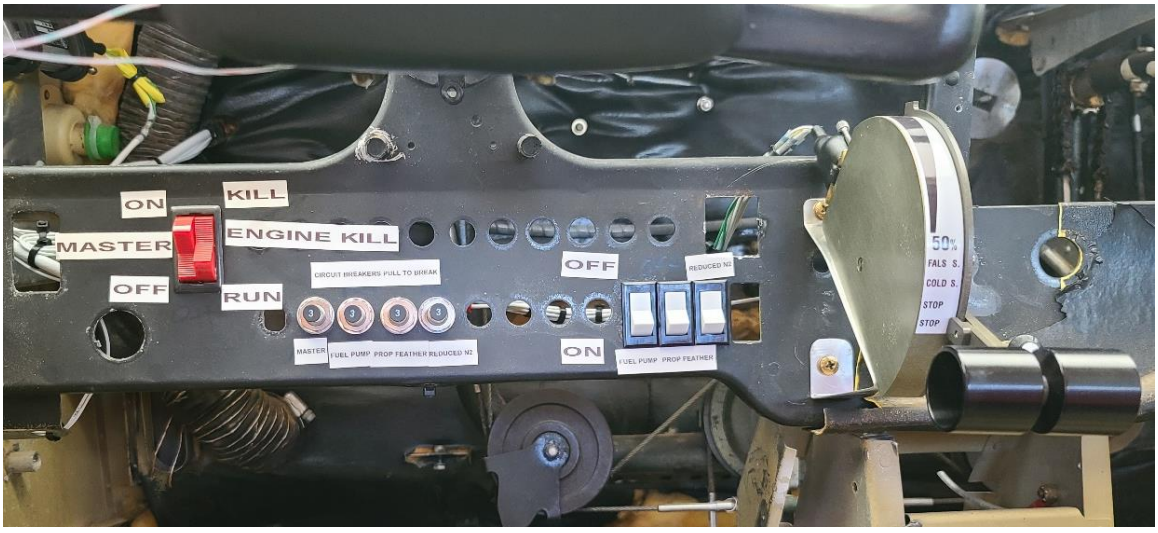

Figure 27. Electric and Engine Controls.

With all the components installed onto the aircraft the weight on the nose wheel was significant, considering that the nose strut was nonfunctional potential aircraft stability issues when running the engine could be experienced. To prevent any risks to safety the nose strut was rebuilt, the disassembled nose strut is shown below in figure 28.

Figure 28. Disassembled Nose Strut.

As can be seen the damage to the nose strut was severe. All surfaces were cleaned of rust and verified for secure mounting of the orifice tube. Once everything was cleaned the strut was reassembled with a rebuild kit for all sealing components such as O-Rings and the wiper. Next the strut was filled with hydraulic fluid and charged to the appropriate pressure with compressed air. The rebuilt nose strut is shown in figure 29.

Figure 29. Reassembled and charged nose strut.

Once more this paper details the processes required to design a custom turboprop engine mount, propeller spacer, and a generator mount for safe operating conditions in a turboelectric ground test rig. These components will endure considerable loading conditions and must not fail. Secondly, the engine mount will be tested at the component level to ensure safety. Lastly, the full system will be experimentally tested without any generator load to verify all components operate correctly in unison. This experimental evaluation will ensure numerous integration issues and considerations are addressed. These addressed issues will be used to inform new certification

standards for regulatory bodies. Experimental results will also be used to validate initial design theories for the components designed for this project, such as the engine mount.

Engine Mount

All structural design work was done through Solidworks and Solidworks Simulation. Models were developed using dimensioning and loading requirements of the specific system. The parts must fit and mesh with existing engine components, such as RPM sensors, without making physical contact with them or affecting their operation. The parts must be strong enough to withstand all potential loading conditions imposed upon them and rigid enough to minimize any deflections that may affect the fit and function of the assembled system.

The engine mount design started with considering the dimensioning of the engine mounting blocks and the aircraft's firewall bolt layout. Trussing elements were stretched from the locations to make mechanical contact with each other. The layout of these elements was desired to absorb loading conditions in an optimal way, such as the horizontal elements for thrust and angle elements from outboard to inboard to absorb torque loads. Figure 30 is an overall view of the engine mount model. As can be seen the engine mount is, in essence, a simple cantilever beam with a mass at the end. The four large plates are the location where the turboprop will be bolted to. The forces the turboprop generates must be transferred from the mounting plates, through the trussing, and finally to the aircraft's firewall.

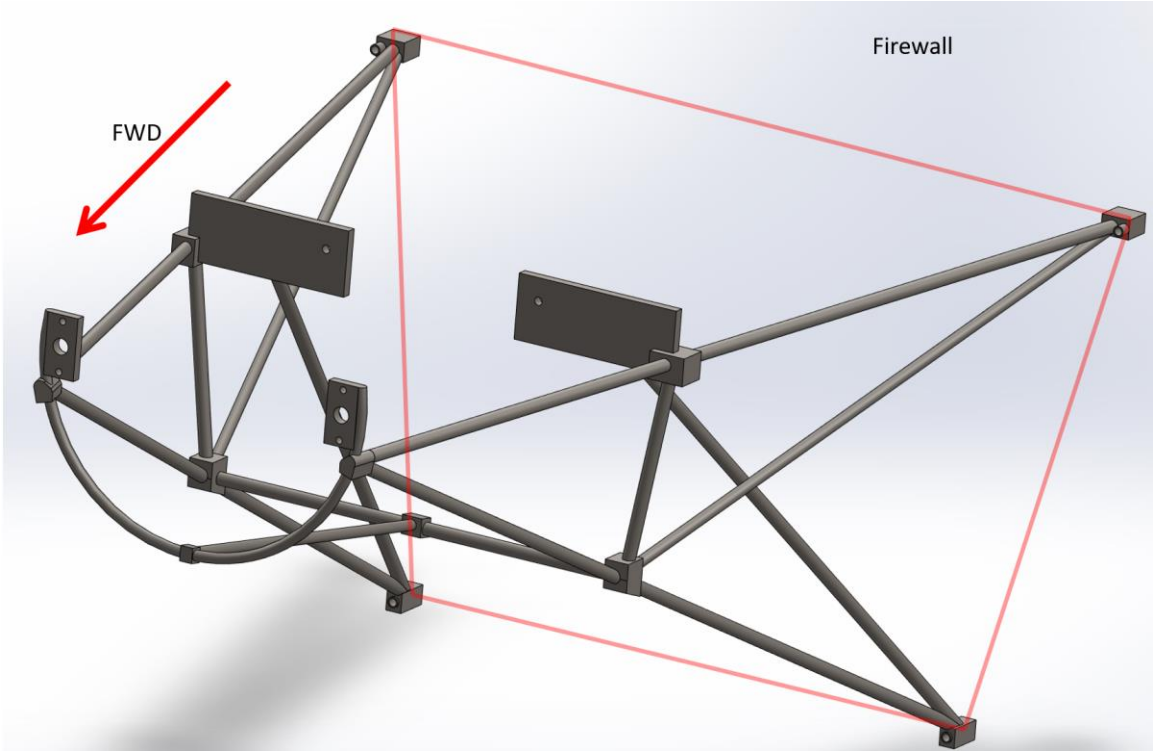

Figure 30. Engine Mount Overview.

The final material was selected to be a steel chrome molybdenum, grade 4130. This grade of steel is commonly used in aviation engine mount systems. Initially many different engine mounts were benchmarked, everything from piston engine mounts to turboprop mounts to increase familiarity with the design project. PBS Aerospace provided installation examples of their engine from some of their customers, this assisted with the general layout of the engine mount trussing. After many refinements the final dimensions of the trussing are a 0.75-in outer diameter with a 0.060-in wall thickness. Most of the refinements dealt with the trussing elements, adding elements as needed to absorb the loading conditions optimally. More reinforcement was added to the front end underneath the engine, these additional elements were added with the intention to increase the rigidity of the mount to decrease deflection and increase resonance frequencies. It is important to note the block elements on the engine mount, these were added to simulate the welded joints to ensure proper load transfer in the simulation. Lastly, the angular pieces to the aft end of the

mount were added to increase inertia of the engine mount. The increased inertia in the engine mount allowed for more torque absorption and easier load transfer to the airframe. An interesting note about the aircraft, the firewall itself is not structural but instead the stringers and ribs within the fuselage that interface with it. The engine mount bolts to the aircraft long stringers, these stringers are a C-Channel type design.

After the model dimensions were finalized, the model was imported into SOLIDWORKS Simulation. The simulation selected was a static simulation, this requires boundary conditions and loads to be applied to the model. Then a mesh must be generated, and finally the simulation may be executed. Figure 31 below depicts the fixtures applied to the model.

Figure 31. Engine Mount Fixture Points.

After the model was fixtured, the loadings were defined, these loads were discussed in the background section. The loads shown in Figure 32 are the ones that would be expected at full engine power level on the ground. A smaller model was developed to represent the turboprop itself, an engine simulacrum. This turboprop model was defined so that the center of gravity and propeller thrust line falls into their corresponding places on the actual turboprop. The following loads were applied to their corresponding locations on the engine simulacrum mode. The forward

thrust load was set to 4,000-N, the engine weight, pointed downward, was set to 1,000-N. This is a potentially large value but was selected to ensure that the weight of all accessories and propeller was adequately captured and represented in the model. The accessories and propeller will manipulate the center of gravity, but since its location cannot be known the liberal application of loads and safety factors will be relied on. The final load applied to the engine mount is the engine torque output. The engine torque was applied in the opposite direction of rotation of the propeller with a value of 1,000-N·m. Figure 32 shows these loads and their application.

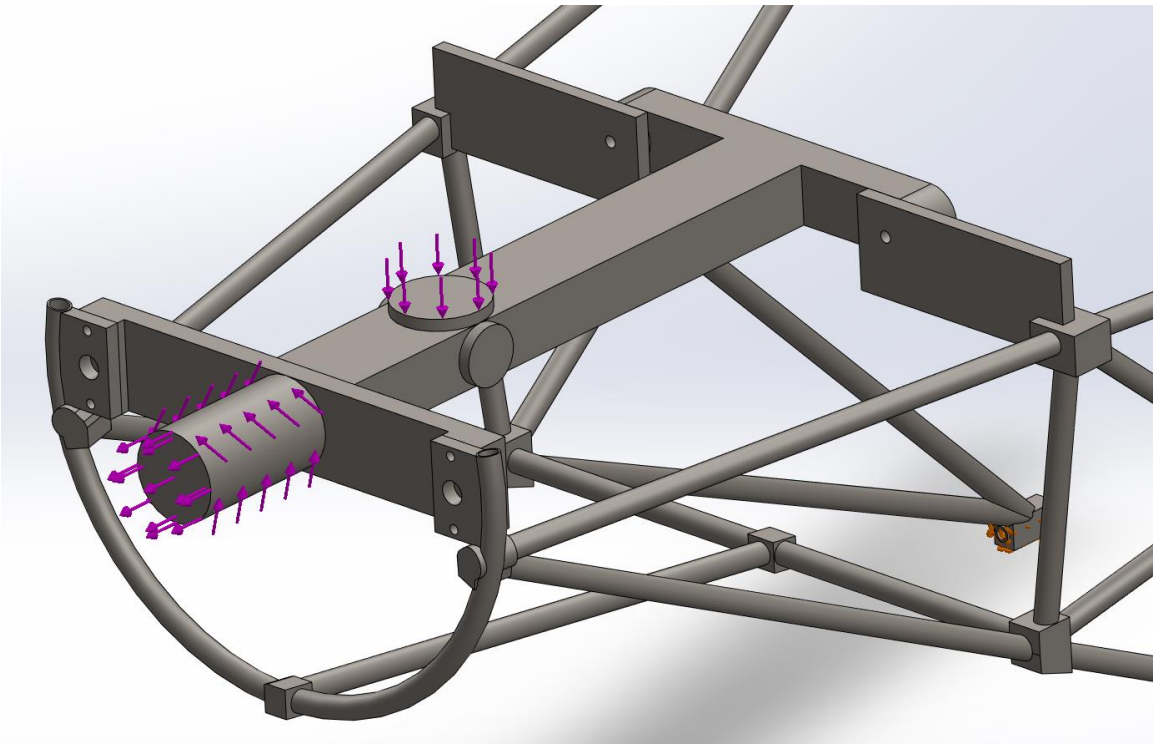

Figure 32. Engine Mount Loadings.

With the 3D CAD model imported into the Simulation tab, the loads and boundary conditions from above applied and next a mesh may be generated. A simple triangular grid mesh was generated with an element size of 4.2 mm and a tolerance of 0.21 mm. This led to a total of 326,446 elements. The mesh is shown below in figure 33.

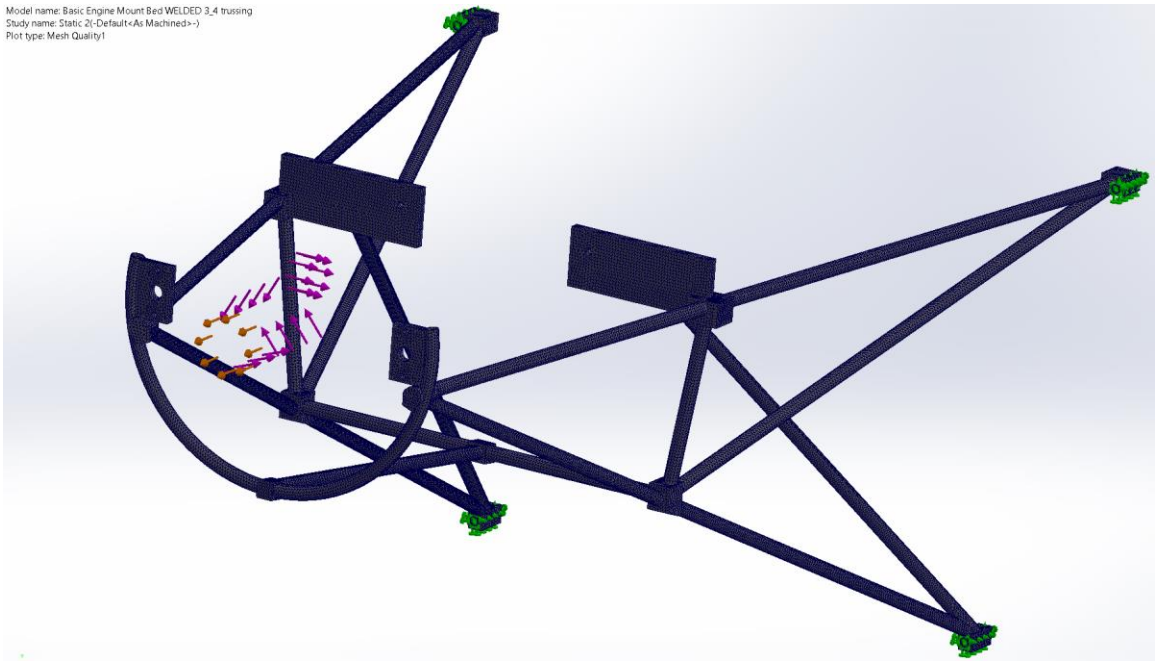

Figure 33. Engine Mount Mesh.

The mesh is fine, this was needed to ensure all the model's geometry was captured and adequate simulation accuracy is achieved. Another item of note are the large protrusions of material at all trussing and mounting plate intersections. These were applied as an approximation of the weldments that would be added in the fabricated mount.

Once the mesh was completed the simulation was initiated. After results were obtained the stress variation plot was studied to determine any high stress areas. Then a custom plot was defined, this plot was a Factor of Safety plot, based off Von Mises Stress. Base color was set to default blue with any cell with a factor of safety less than 1.5 instead colored red. The model was refined until red was no longer visible in the factor of safety plot. This signifies a complete and safe model.

To finish the engine mount design a frequency analysis was conducted. This frequency analysis was used to inform the team of any potential resonance conditions to ensure safety of the system. The same model was used but the simulation type was changed from static to frequency. All load, fixture, and mesh settings were kept the same. As frequency analyses were conducted, they were

used to inform design revisions until an adequate final model was arrived at. The approach of this FEA analysis was also used on the propeller spacer and generator mount.

Once the engine mount design was finalized, manufactured, and installed a static torque test was conducted. This was done to ensure that the engine mount would be strong enough to resist the torque loading of the engine itself. To simulate engine, torque a moment arm was attached to the engine mount, this arm spanned outboard on the port side. At the end of this moment a chain was attached with a weight scale at the end of the chain. The weights of these items were also accounted for. Then, weight was added to the chain in increments of 89-N (20-lbf) by use of weight plates. Total weight applied to the moment arm was around of 1,330-N (300-lbf), this correlated to a maximum torque value of around 1,360-N·m (1,000-ft·lbf) with a moment arm of 1.04-m (41-in). The turboprop itself has a maximum torque output of 800-N·m (600-ft·lbf), therefore the engine mount was over-proofed to ensure safety. Below in figure 34 shows how this weight test was conducted. To measure the angle of twist on the engine mount and firewall a digital protractor was used, the angles were recorded for every weight increment at the firewall and the front of the engine mount. The difference was taken to isolate only the twisting in the engine mount.

Figure 34. Engine Mount Static Torque Check.

To further validate the FEA model and identical torque test was applied to the model. This torque test had the same magnitude of torque applied to the same location as the static torque test. An important note is that this is not pure torque, as the moment arm and model have two fixture points on the engine mount. It more closely resembles a force coupling though not precisely as the magnitudes of the forces applied to the mounting plates will not be identical. The FEA model for the torque test is shown below in figure 35.

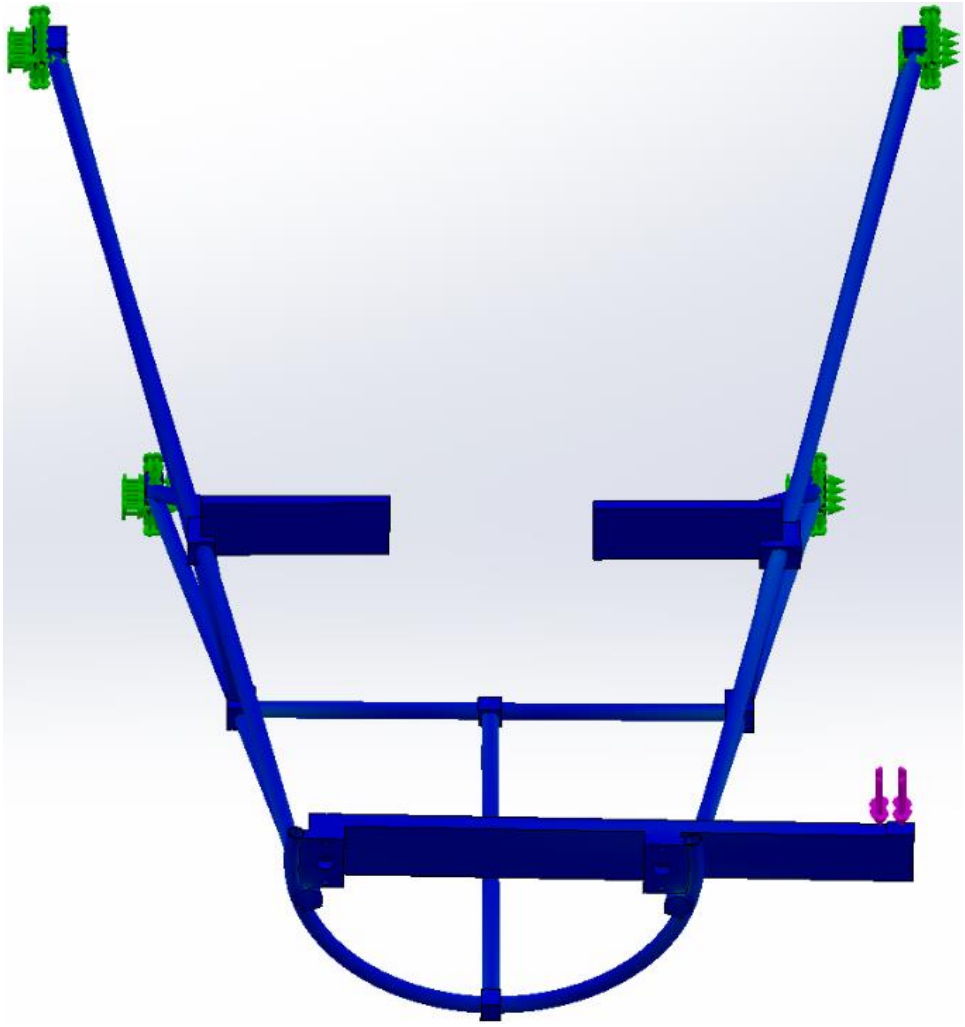

Figure 35. FEA Static Torque Test Model.

The last analysis conducted on the engine mount model was a buckling analysis. Buckling analysis is a dedicated tool in the Solidworks Simulation package and is used to compare buckling factors of safeties to internal stress factors of safeties. If the model's buckling factor of safety is lower than that of the internal stress factor of safety the model will experience buckling conditions before material failure. The model was fixtured as usual with total engine installation weight being estimated at 1,500-N, torque set to 800-N·m, and thrust was set to the peak Hartzell propeller thrust from figure 39 of 2,700-N.

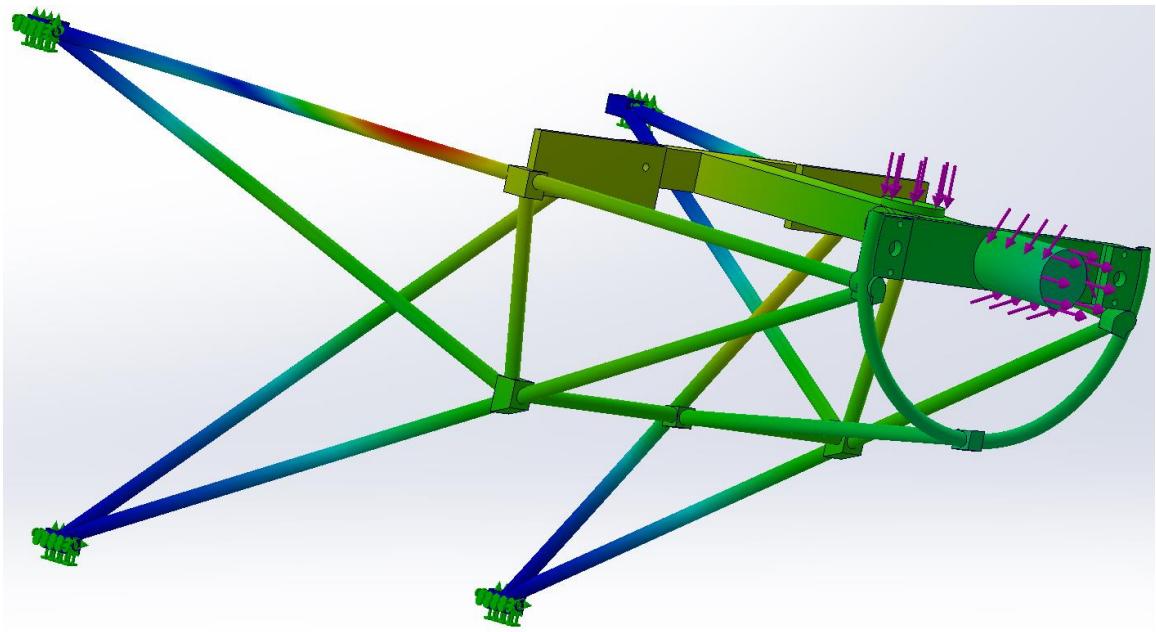

Figure 36. Example of Engine Mount Buckling Analysis, Red Denotes Buckled Element.

Propeller Spacer

As the components of the turboelectric system came together it was quickly realized that there would not be enough room for a generator to be mounted at the optimal location due to the propeller. The blades of the propeller have a large chord that sweeps aft. This aft sweep extends aft of the propeller hub and wraps around the engine gearbox itself. If a generator was mounted the propeller blades would physically impact the generator. The physical impedance means that the propeller must be moved forward, a propeller spacer, or extension, was needed. This spacer was designed to give nearly six and half inches of extra space between the propeller and the engine, this extra space ensures there is room for the generator and its drive system. Like the engine mount this propeller spacer must resist all potential loading conditions with minimal deflection at sufficient FoS. The loading conditions for this spacer were like that of the engine mount as the propeller generates the thrust and consumes the torque from the engine. The emergency loadings were approached slightly differently, instead of using the weight of the turboprop the weight of the propeller was used. This was obtained from the specification sheet

provided by the manufacturer for the propeller and weights 38-kg (84-lbf). The dimensions of the flanges on the spacer were predetermined from the propeller flange type used by the engine and propeller manufacturers, these dimensions are given below in figure 37.

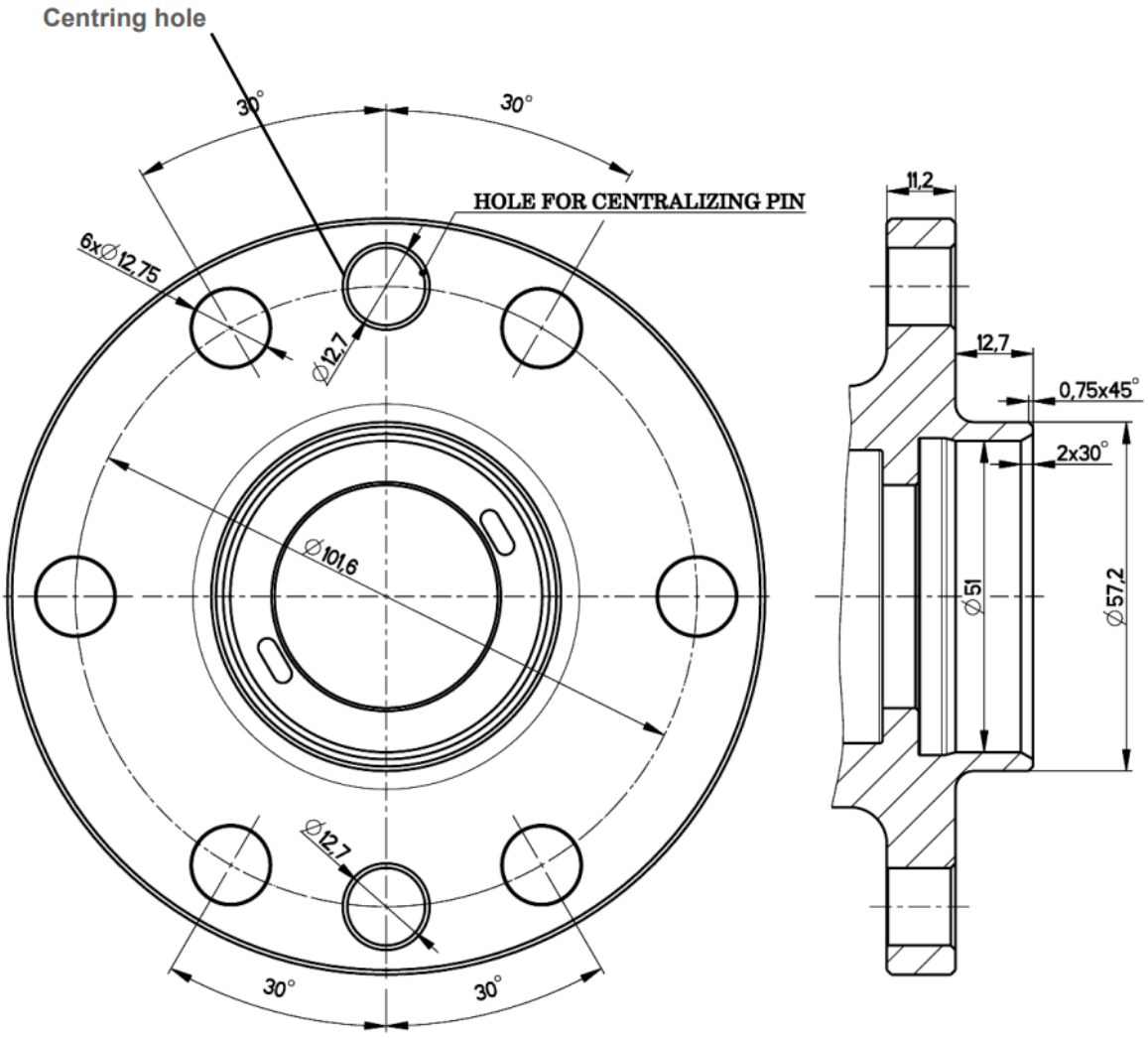

Figure 37. Propeller Mounting Flange, ARP 502 Standard (PBS Aerospace , 2017).

The aft end of the spacer, the portion that bolts to the engine, was designed to mimic the propeller itself. Even the exact same mounting studs, dowels, nuts, and washers were purchased that the propeller manufacturer uses. The forward end, where the propeller is mounted, was designed to mimic the engine flange precisely. This ensures the propeller can be mounted seamlessly. The last

items of consideration are sealing features within the spacer. Since the propeller is constant speed oil pressure must reach the propeller dome. This requires that the spacer be hollow and provide sealing surfaces for O-Rings. For the aft section of the spacer an O-Ring groove was provided to seal it against the engine. For the forward section a neck down protrusion was provided so that the propeller may seal against it, just like the neck on the engine flange. The material chosen for this spacer was stainless steel 316. This grade of steel provides adequate strength for the loading conditions and maintains a respectable resistance to corrosion, both environmental and bi-metallic. An example of a propeller spacer can be found below in figure 38.

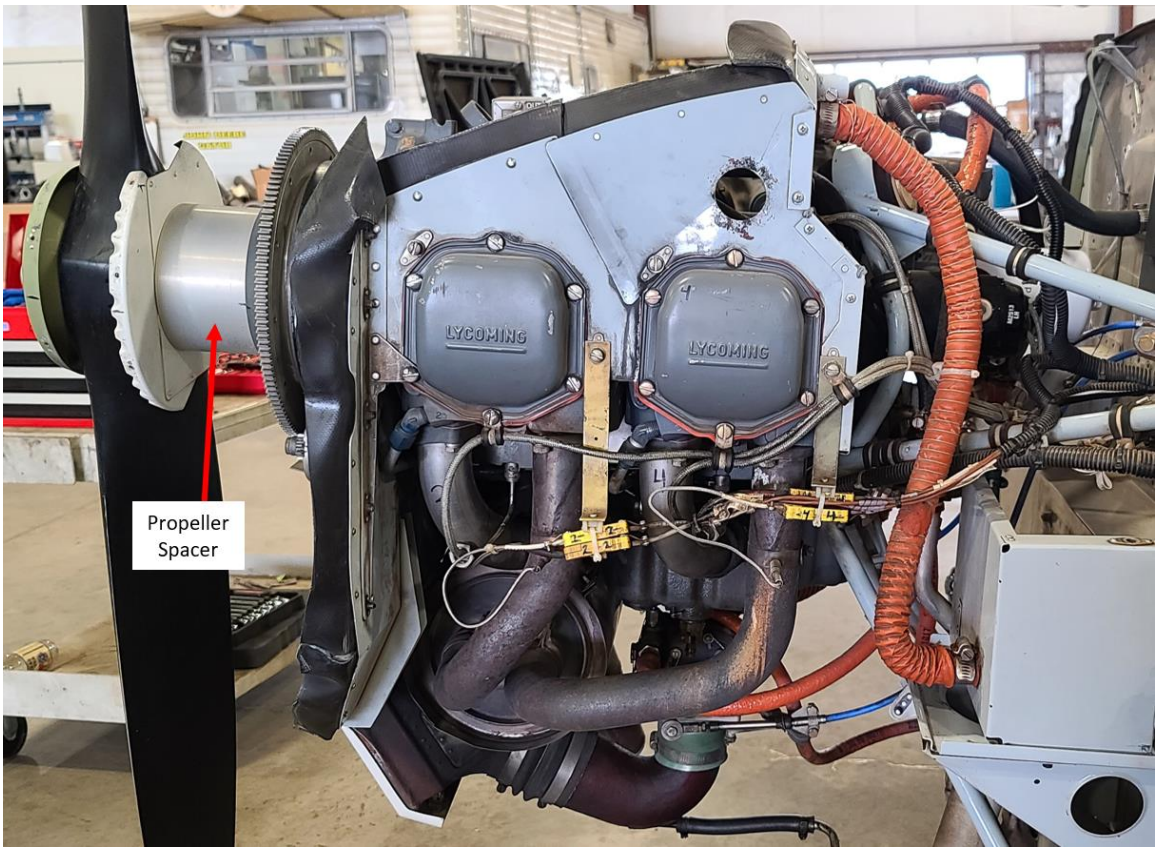

Figure 38. Propeller Spacer, Stock Cessna 172.

The design space for the propeller spacer was quite limited due to the flange requirements and the need to keep it at a reasonable length. If the spacer is too long then it may deflect more radically

leading to instabilities, if too short then the generator and power transfer system may experience installation issues. It was deemed that about 152-mm (6-in) would give sufficient space for the generating and power transfer systems. The diameter of the web between the two flanges was kept well below 102-mm as this is the dimension of the mounting studs. If the diameter is too great, then the mounting hardware for the propeller studs would unable to be installed correctly. However, the center diameter must be large enough to maintain proper strength and resistance to loading conditions. Interior diameter was set so that the engine flange would be able to be installed with ease while providing appropriate sizing for the propeller flange sealing. Provisions for the mounting studs and dowels were given to allow for press fits of these components. These press fits were given as it is critical the studs and dowels do not move from their positions, if they do then propeller dislocation, or even dismount, becomes possible. Finally, the O-Ring grove was provided in the design with its sizing obtained from standard O-Ring compression requirements.

Like the engine mount the propeller spacer was designed to resist considerable loadings that the engine and propeller generate. These are torque and thrust loads, gyroscopic loads were initially considered but were quickly dismissed as this is a ground test rig. The aircraft will never leave the ground and will always be supported by all landing gear elements negating effects of gyroscopic forces. The thrust loading was obtained from the turboprop manufacturer, a plot with several different propeller brands with thrust generated when installed on the TP100 was provided and shown below in figure 39.

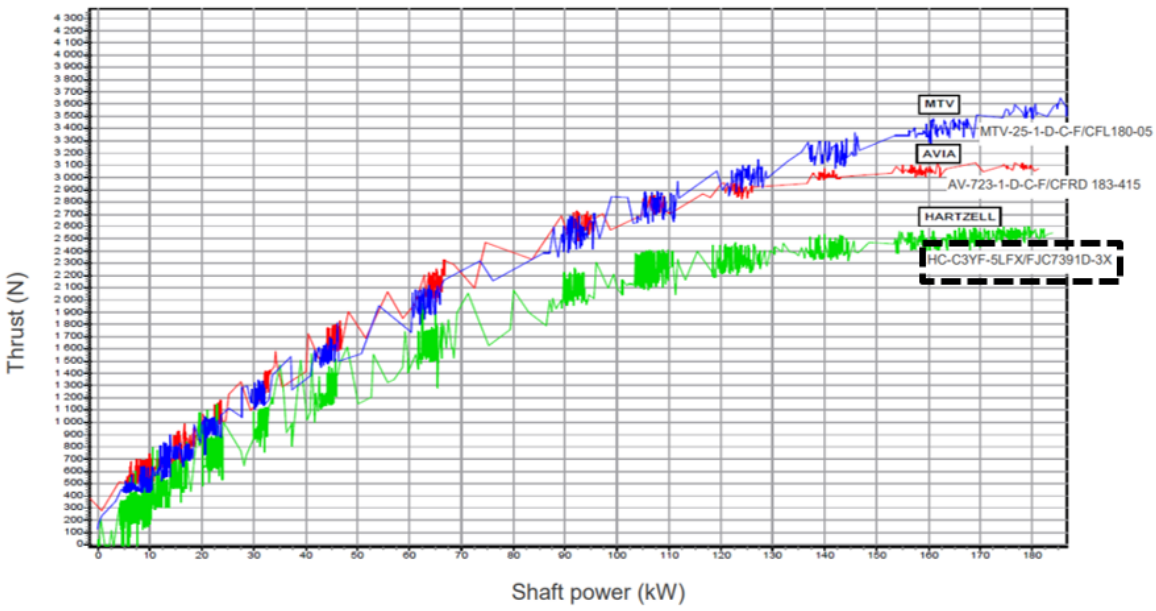

Figure 39. Propeller Thrust Values from Manufacturer (PBS Aerospace , 2017).

The propeller that generates the maximum amount of thrust is from the brand MTV at around 3,700-N. However, the propeller obtained for this project is a Hartzell HC-C3YF-5LFX, which produces around 2,600-N. To ensure safety the maximum thrust of 3,700-N was used with this further being rounded to 4,000-N. Using equation 7 torque applied to the propeller was computed at maximum power, this computed to around 800-N·m and was further rounded to 1,000-N·m to ensure complete system safety. The spacer was fully analyzed using FEA in Solidworks using these loading conditions. These loads were applied to the propeller interface point, the forward flange, and the model was fully fixtured at the aft flange where the studs and dowels reside. Mesh independent studies were conducted to ensure that the solution was independent of the mesh, no radical changes to the solutions were experienced. This indicates that the model is mesh independent and that the solutions are reliable. Emergency loads were also studied, these were discussed in the engine mount section. However, the weight of the propeller was used instead of the weight of the engine. This leads to no difference in the structural strength of the spacer, even when considering lateral loads such as downward or to the left. This is attributed to the rigidity

derived from the large values of moments of inertia of the webbing in the spacer. The FoS selected for this spacer was 1.5, an industry standard. The propeller spacer model is shown in figure 40. A resonance frequency analysis was conducted to determine the shaft critical speed of this propeller spacer to ensure that the spacer would not become unstable during use. Lastly, a buckling analysis was conducted on the propeller to ensure the part would not buckle under any expected loading conditions.

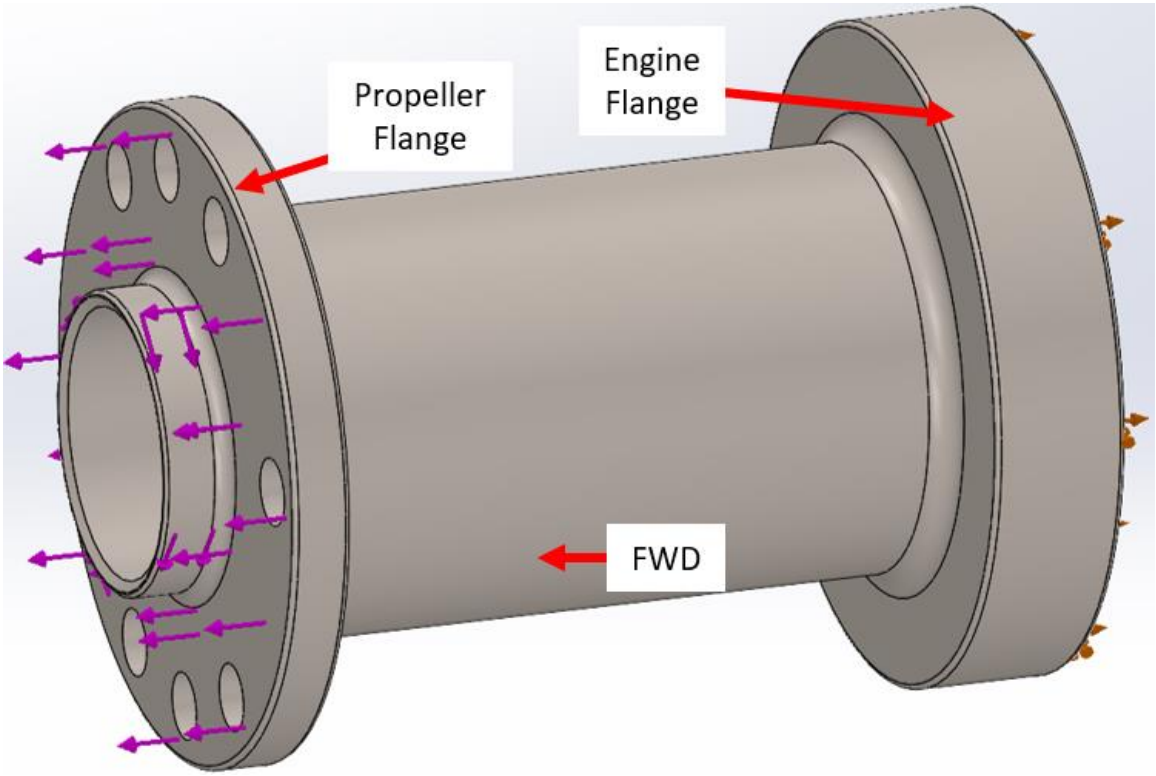

Figure 40. Propeller Spacer with Loadings.

Unfortunately, after the spacer was manufactured and received some slight modification was required due to unique part dimensions. During the modification process the spacer was destroyed beyond repair. A new part was ordered but first some modifications were made to the design to ensure easier installation and uninstallation of the spacer, these changes included a reduced center diameter, slightly smaller neck down for the propeller seal, and lastly a slightly increased stud

hole diameter on the propeller flange. The center web was decreased slightly as with the first spacer it was difficult to properly install the nuts and washers onto the propeller studs. The neck down for the propeller seal was slightly decreased because with the first spacer it seems just slightly too long and prevented proper installation. Lastly, the stud holes for the propeller studs were slightly increased, it was found that with the first spacer the threads of the studs would hook into these holes preventing simpler installation and uninstallation.

Generator Mount

Another custom piece of engineering work was the generator mount. This mount constrains the generator while it is generating electrical power for the electrical propulsion system. This mount must resist the torque being transferred from the engine to the generator as well as the tension forces the belting system is under. Due to the considerable amounts of power needed for transfer, 30-kW, emergency loadings were not considered for this part. This will be discussed later as part of the concluding remarks for certification standards. The loadings associated with this power transfer were enormous. The driving design requirement was the dynamic tension loads from the belt, together the sum tension force pulling downward on the generator was just shy of 2,220-N of force. The generator only has one mounting point, at its back and with the pulley mount at the front of the generator the bending moment became large. This drove the bracketry design to become significantly thick to withstand this loading with minimal deflection. Deflection was desired to be kept to a minimum as it would affect belt tension under load leading to a potential for belt slippage. Generator weight and torque was still considered, though they had little effect compared to the tension forces of the belt. Lastly the generator mount had to translate vertically, this is because it had to be close enough for a belt to be installed and spread apart enough to properly tension the belt. Initially there were two potential design choices, mount the generator to the engine mount or to the engine itself. Mounting to the engine mount was quickly eliminated. This had many reasons, the chief of which related to engine displacement. The turboprop is

mounted to the engine mount with bolts, however the portions of the engine that mounts to the engine mount are isolated by rubber inserts. This means the rubber is free to compress and stretch according to engine conditions. This leads to unpredictable behavior of the engine in relation to the mount, if the generator was mounted to the engine mount, then this would lead to a very dynamic loading and unloading of the belt. The loading and unloading of the belt, at the minimum, would decrease the life of the belt and at worse introduce belt slippage and intermittent power transfer. The generator mounting location was selected to be on the engine near where the manufacturer would install their own alternator system. With this location the generator would move with the engine ensure proper belt tension no matter what. Though this alternator outputs significantly less power than the generator used here, 1 to 2-kW versus the 30-kW goal of the generator. A typical aviation alternator mounting system can be found below in figure 41.

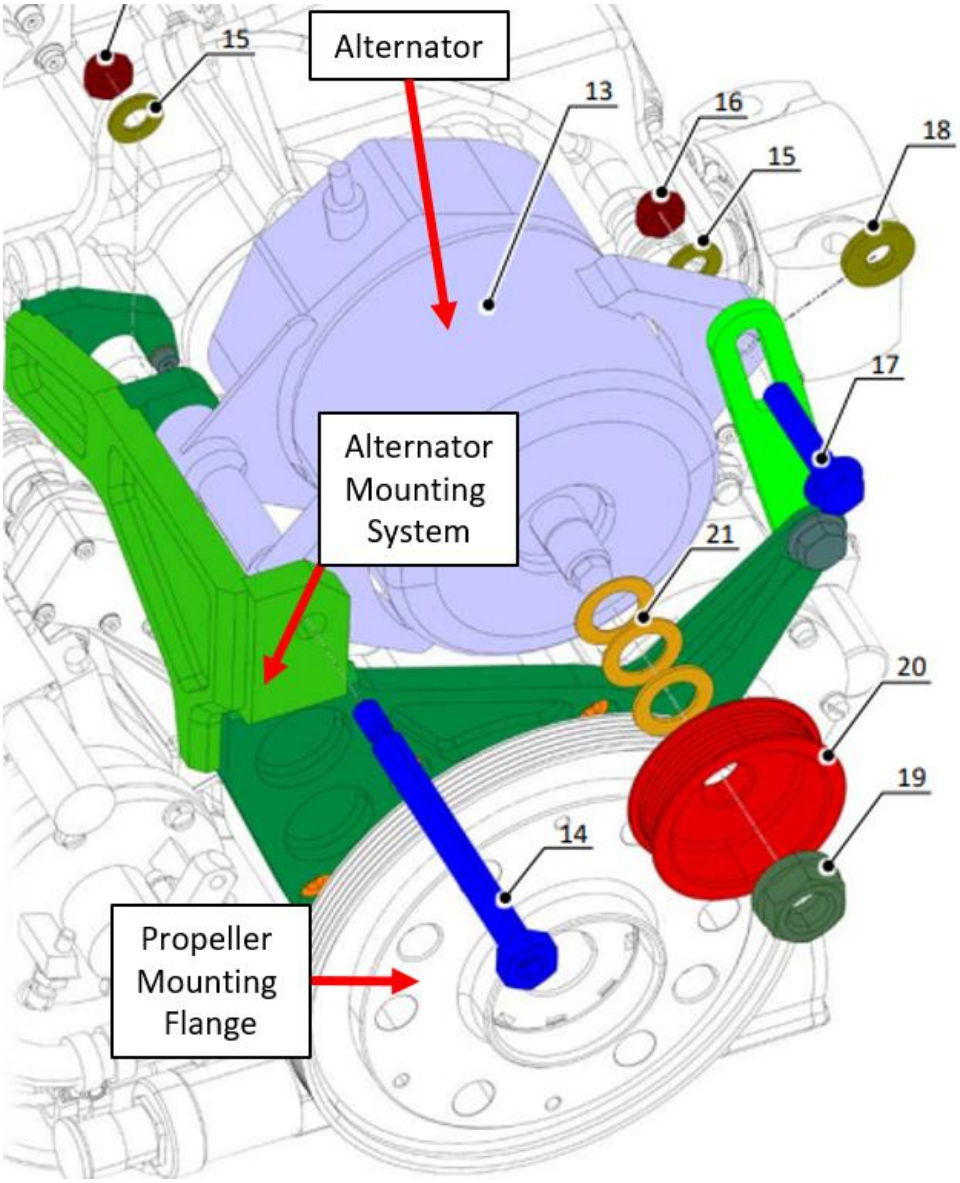

Figure 41. Typical Aviation Alternator Mounting System, PBS Aerospace TP100 (PBS Aerospace , 2017).

With the location of the generator chosen a mount needed to be developed, this mount must consider all engine components in the area to ensure that nothing would be impeded. For example, to the left and right of the generator are the RPM and torque sensors of the gearbox, below to the left and right are the propeller control devices, and lastly immediately aft of the generator is the gearbox wall. All these components must be considered so that generator, pulley,

and mounting system do not make physical impact with these components. Thankfully, PBS Aerospace provided a 3D model of the engine, using this model a dimensions for the engine and its components at the generator location was obtained. Many different mounting systems were considered, even ones similar to the one depicted in figure 41 above. However, many mounting systems were quickly eliminated because of how the generator itself is mounted. The generator only has on mounting location on its centerline at the back of it, no mounting blocks on the sides like the ones found in figure 41. The generator mounting dimensions are shown below in figure 42.

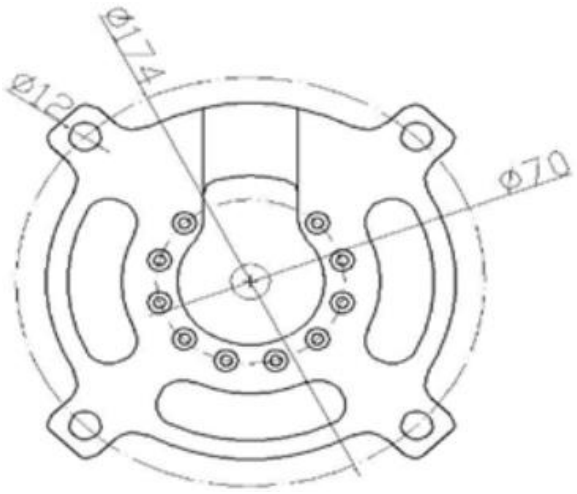

Figure 42. Generator Mounting Dimensions, in Millimeters (Off the Grid Sun, n.d.).

As seen in figure 42 the outer most four bolt holes were disregarded, these would increase the size of the mounting system greatly. Instead, the inner 10 bolt holes were used, this would maintain a small generator mount footprint. Lastly, a belt tension system had to be provided. If the drive belt is not tensioned, then no power can be transferred. With all these considerations it was desired to keep the mounting system simple, therefore a simple L-Bracket was developed that the generator would bolt to, this L-Bracket would then bolt to a vertical plate, and finally this entire assembly would bolt to the engine at the nose seal which is the exact location PBS Aerospace uses for their own alternator system. The vertical plate is slotted where the L-Bracket

bolts are installed, this slotting allows for vertical translation of the L-bracket, and therefore the generator with its pulley, to allow for the drive belt to be tensioned. Keeping in mind all the considerations illuminated above the design work for the generator mounting system began.

The generator mount design work was a departure from the propeller spacer and engine mount, instead of applying emergency loads to the mount belting loads were applied. Another load applied to the generator mount was the torque associated with power transmission and the weight of the generator itself. The torque associated with power transmission was determined through use of equation 7, and was determined to be around 360-N·m. This was obtained from the desired amount of power transferred, 30-kW, at 3,000 RPM. The RPM was determined from considering the specifications of the generator, to obtain the desired power output at the desired voltage a generator RPM of 3,000 was required. Next the belt tension loadings of the belting system must be considered using equations 11 and 12 for the tight and slack side tensions, respectively. The total tension loads were around 2,220-N, this is the sum of the slack side and tension side. A minimum FoS of 1.5 was applied to all the generator mounting systems, including fasteners. Fastener locations were analyzed to ensure the mounting methods were strong and safe enough to transfer all loadings through the structures. A rough model of the generator was developed to simulate the generator and its loading conditions. A resonance study was also conducted for the generator mount to ensure that the rotating generator would trigger a resonance response in the mounting system. Engine geometry was also deeply considered during the design of the engine mount such as the location of propeller control devices, engine sensors, drain lines, and electrical lines. It was determined that the generator would sit in the center line between engine sensors directly above the propeller flange. Lastly, a buckling analysis was conducted on the generator mount to ensure that the structure would not buckle under any of the expected loading conditions. The FEA model of the generator mount is shown below in figure 43.

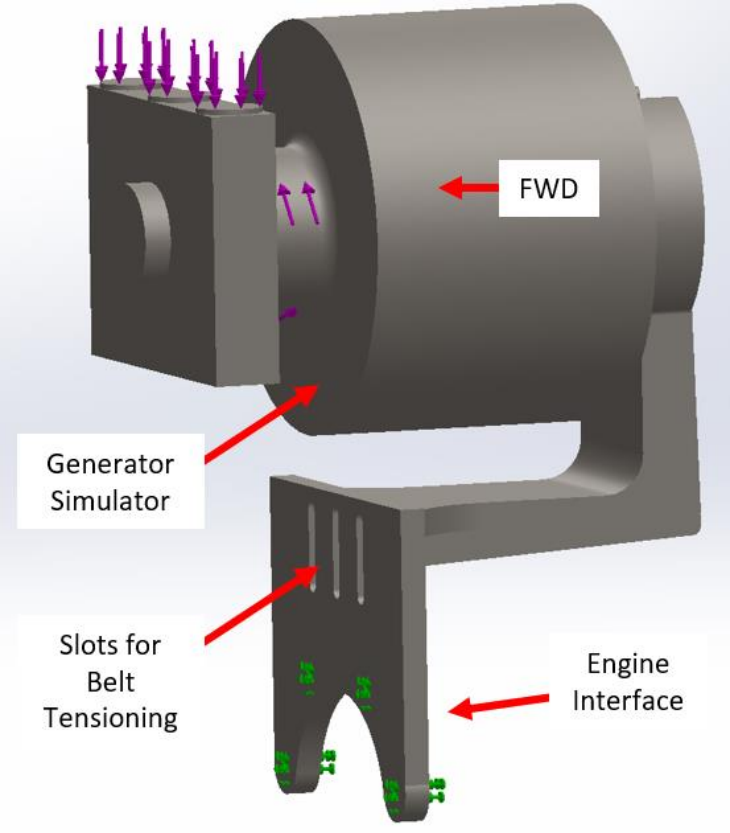

Figure 43. FEA Model of Generator Mount with Loads and Fixtures.

Belting Analysis

The belting system was designed and refined over numerous iterations. This is due to the incredibly large amounts of power needed to be transferred in a rather small volume. The amount of power being transferred for this turboelectric setup approaches power transfers of extremely large industrial equipment. Because of the smaller diameters of the pulleys on this system finding a belt strong enough became difficult. The larger belts used in larger power transfers have minimum bend radius, often this minimum radius is larger than the pulleys of this system and even can approach the radius of the propeller itself.

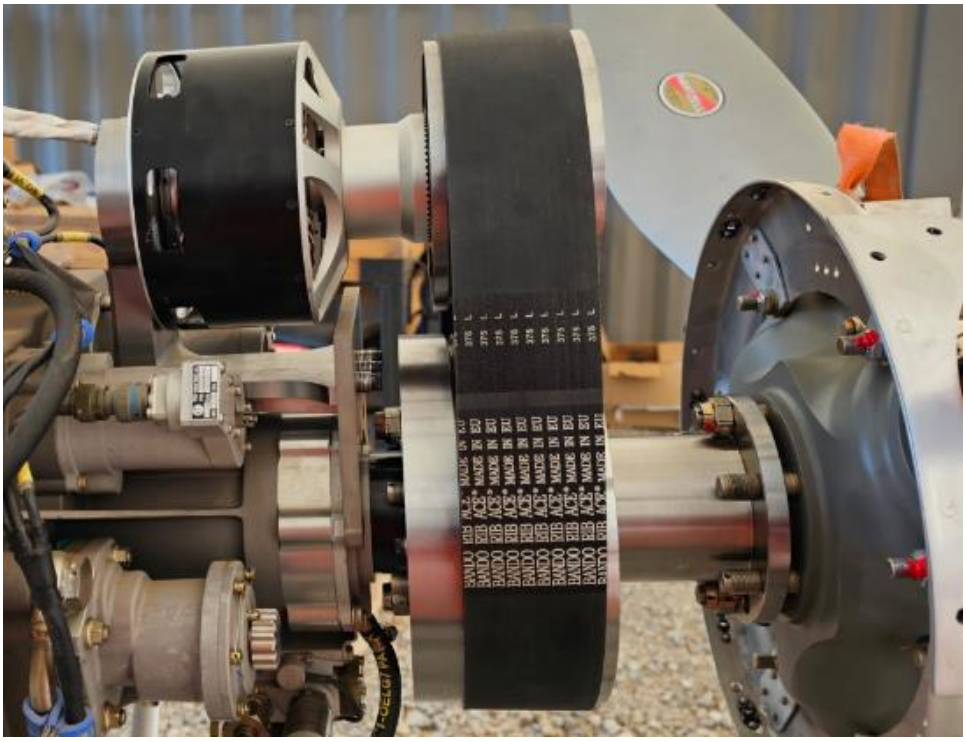

Figure 44. Generator Belting System, Slack Side Shown.

As seen in figure 44 the belt used for this application is rather large, this is because many ribs were needed to transfer all the power required. But first a design power was computed using equation 8, this was found to be 34-kW. Next the diameters of the pulleys were determined from using the known speed ratio, the engine pulley has a diameter of 203-mm and the generator pulley at 145-mm. Next total belt length could be determined by use of equation 9 and was found to be 0.95-m (37.5-in). Now the number of ribs required to transfer all the power was determined by using equation 10 and this came out to 13.76 ribs. Which was rounded to 14 ribs as a partial rib is not possible. Lastly the belt cross section had to be determined, this was done by considering minimum bend radius and maximum per rib power transfer rating. The selected cross section type is the L-Type cross section of the Micro-V belts and is shown below in figure 45.

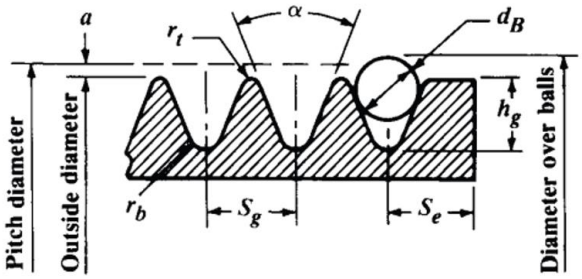

Face width = $S_g\ (N_g - 1) + 2S_e$, where N_g is number of grooves

Cross Section	Minimum Recommended Outside Diameter	α Groove Angle ±0.25 (deg)	S_g[a]	r_t +0.005, −0.000	$2a$	r_b	h_g (min)	d_B ±0.0005	S_e
L	3.00	40	0.185 ±0.002	0.015	0.058	0.015 +0.000 −0.005	0.183	0.1406	0.375 +0.075 −0.030

Figure 45. Pulley and Belt Cross Section Dimensions for L-Type Micro V-Belt (ERIK OBERG, 2012).

The computed values are the necessary values to determine the proper belt, the belt was obtained from a supplier with the name of the belt being 375L14. Now that these values are known the tension forces the belt will experience may be determined. These tensions forces are the loading conditions that the generator mount must endure, as well as the torque being transferred. Using equations 11 and 12 for tight and slack side tension, respectively, the tensions were computed to be around 1,780 and 445-N. Due to the geometry of the pulleys these forces are essentially joined together pulling the generator down with 2,220-N of force. Initially this value was around 3,560-N but was reduced to the 2,220-N value by manipulating pulley diameters and center distances. Knowing that 30-kW was the power desired to be transferred and the optimal generator speed was 3,000-RPM equation 7 was used to determine the torque imposed onto the generator. This value was determined to be about 96-N·m but was rounded to 100-N·m.

Data Acquisition

For a full system test run a more exotic method of measuring engine mount twisting is required, this is obvious because someone would never approach the spinning propeller to place and read a

digital protractor. This is where the Arduino Nano and MPU-6050s come into play. The sensor used in this study is an MPU-6050 manufactured by InvenSense Inc. The MPU-6050 6-axis motion tracking devise using the I^2C communication bus and is pictured below in figure 46.

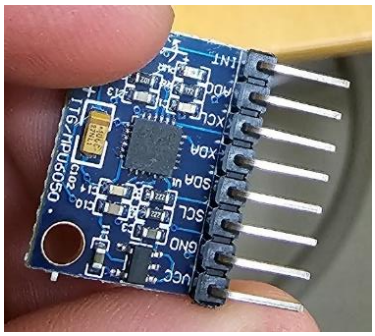

Figure 46. MPU-6050 Sensor Cluster.

The MPU-6050 sensor has a built in 3-axis gyroscope, 3-axis accelerometer, and a temperature probe. Both the accelerometer and gyroscope have a 16-bit resolution. The gyroscope outputs values in degrees per second in four ranges of ±250, ±500, ±1000, and ±2000 degrees per second. The accelerometer outputs values in g, as in multiples of one earth gravity. The accelerometer also has four ranges of ±2g, ±4g, ±8g, and ±16g (InvenSense, 2013). As ranges increases the resolution of the scale across this ranges decreases. Since the MPU-6050s will only be used to measure an almost static the default ranges of ±250 degrees per second and ±2g will be used. This will maximize the resolution of twist angles as well as act as a filter with high magnitude vibrations being uncaptured. One MPU-6050 is placed at the very front of the engine mount while the other is placed on the firewall. These sensors were mounted using foam tape, this tape helps to isolate the sensors from vibration. Below in figure 47 is a depiction of where the MPU-6050 sensors will be located.

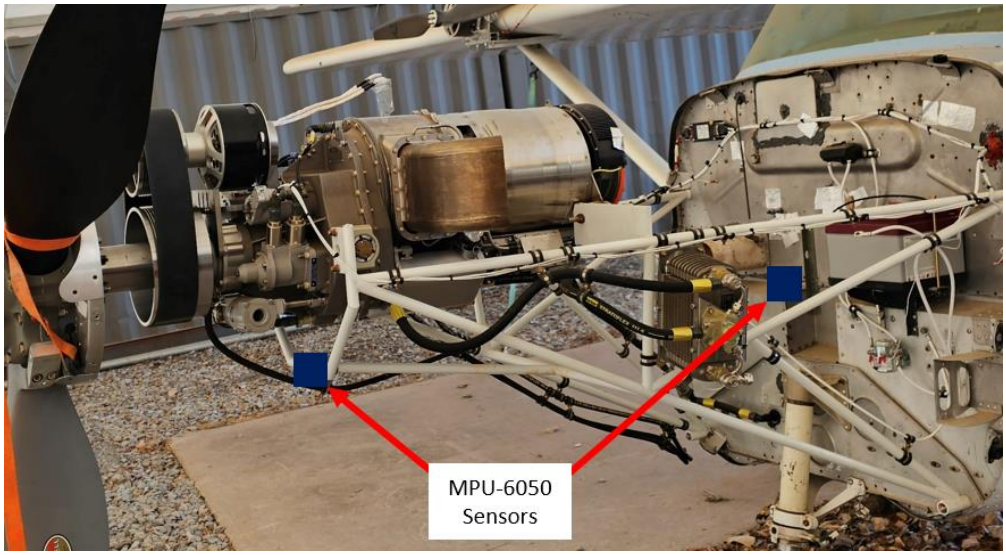

Figure 47. MPU-6050 Sensor Locations.

With these sensors the total twist in the engine mount can be determined and compared to FEA and the static torque test. These sensors will also be able to capture transient loads such as engine spool up. For these sensors to fully operate with the Arduino Nano a partially custom code was developed which is displayed below in figure 48.

```
#ifdef OUTPUT_READABLE_ACCELGYRO
    // display tab-separated accel/gyro x/y/z values
    Serial.print("a/g:\t");
    Serial.print(ax); Serial.print("\t");
    Serial.print(ay); Serial.print("\t");
    Serial.print(az); Serial.print("\t");
    Serial.print(gx); Serial.print("\t");
    Serial.print(gy); Serial.print("\t");
    Serial.println(gz);
#endif

#ifdef OUTPUT_BINARY_ACCELGYRO
    Serial.write((uint8_t)(ax >> 8)); Serial.write((uint8_t)(ax & 0xFF));
    Serial.write((uint8_t)(ay >> 8)); Serial.write((uint8_t)(ay & 0xFF));
    Serial.write((uint8_t)(az >> 8)); Serial.write((uint8_t)(az & 0xFF));
    Serial.write((uint8_t)(gx >> 8)); Serial.write((uint8_t)(gx & 0xFF));
    Serial.write((uint8_t)(gy >> 8)); Serial.write((uint8_t)(gy & 0xFF));
    Serial.write((uint8_t)(gz >> 8)); Serial.write((uint8_t)(gz & 0xFF));
#endif
```

Figure 48. Arduino Code Snippet.

A library was found on GitHub to help facilitate sensor integration. The library is titled I^2C Developer Library and is published by Jeff Rowberg. This library contains many different coding examples but most importantly contains coding to read raw data from the MPU-6050 sensor. The only modification made was the addition of a timer for use in gyroscope angle analysis.

To further reduce the effect of vibrations on the twist angle a mathematical filter is employed, this model is a complimentary filter meant to fuse measurements from both the accelerometer and the gyroscope. This filter also addresses the issue of gyroscope drift, a known issue with gyroscopic devices. Gyroscopic drift is simply compounded sensor error that is added with each iteration. A complimentary filter simply takes fractions of each sensor type and combines them into one value. The complementary filter equation is shown below in equation 17.

$$\theta = (1 - \alpha)\theta_G + \alpha\theta_A \text{ (MathWorks, n. d.)} \quad (17)$$

Where θ is the filtered angle, α is the weighted percent which is typically around 2%, θ_G is the angle measured by the gyroscope, and θ_A is the angle measured by the accelerometer. The user may choose a value for α, the greater the value the more the accelerometer data drives the filtered angle. A high α can become detrimental as more noise is injected into the filtered angle. As discussed earlier the complementary filter also helps to reduce the effects of gyroscopic drift. This is achieved from the application of accelerometer data to the filtered angle. Since the accelerometer measured gravity the application of accelerometer data to the filter angle pulls the filtered angle back to neutral.

As discussed earlier the gyroscope and accelerometer do not directly measure angles, so some mathematics are required to derive the angles from the data captured by the accelerometer and gyroscope. To properly define angles the axis directions must be defined. The sensor will be placed so that the x-axis points out through the nose, the y-axis points out to port, and the z-axis points to the sky. This correlates the pitch rotation about the y-axis, roll about the x-axis, and yaw

about the z-axis. From these definitions the roll angle is of interest as this is the same as the twist in the engine mount. Since the angle cannot be directly determined from the accelerometer some trigonometry is required and is shown below in equation 18.

$$\theta_{R,A} = \tan^{-1}\left(\frac{g_y}{\sqrt{{g_x}^2 + {g_z}^2}}\right) \tag{18}$$

Where $\theta_{R,A}$ is the roll angle from the accelerometer, g_y is the accelerometer g measurement in the y-axis, g_z is the accelerometer g measurement in the z-axis, and g_x is the accelerometer g measurement in the x-axis. Equation 18 shows the equation used to get the roll angle; it can easily be modified to work with pitch. However, it is important to note that accelerometers cannot be used to find yaw. This is because gravity is constantly downward and rotation around this cannot be detected. When considering the gyroscope, the angle can be easily derived, this is since the gyroscope measures in degrees per second. One would only need to integrate, with respect to time, the gyroscope data to obtain the angle. This leads to a very simple equation, shown below in equation 19.

$$\theta_{R,G} = \theta_{R,G_{t-1}} + \dot{\theta}_{R,G}\Delta t \tag{19}$$

Where $\theta_{R,G}$ is the roll angle from the gyroscope, $\theta_{R,G_{t-1}}$ is the previous roll angle, $\dot{\theta}_{R,G}$ is the current gyroscope data, and Δt is the time elapsed between samples. The gyroscope roll angle is simple, though it must be remembered that gyroscope drift will be present that will quickly destroy any accuracy.

Once the angles from the accelerometers and gyroscopes were derived it was discovered that the data was heavily polluted with vibrational data, which had to be removed to be usable. This was achieved by applying a code-based 2nd order low-pass Butterworth filter to the data. Cutoff frequency for the filter was obtained by conducting a Fast Fourier Transformation, FFT, to isolate the frequency at which the critical data resided. Finally, the accelerometer and gyroscopic data

can be fused together through use of the complimentary filter. Below is equation 20 which combines the complimentary filter equation, accelerometer equation, and gyroscope equation.

$$\theta_R = (1 - \alpha)\theta_{R,G} + \alpha\theta_{R,A} \tag{20}$$

To interface with the MPU-6050 an Arduino Nano is used. The Arduino Nano is a small microcontroller meant to interface with a laptop through USB. Code is written in the Arduino software on a computer and uploaded to the Arduino Nano. Once the upload is complete the Arduino Nano will execute it. The user then opens a monitor on the computer in the Arduino software. Once the data is collected it is copied from the monitor and pasted into a text file to be imported to a spreadsheet processor. The Arduino Nano is shown below in figure 49.

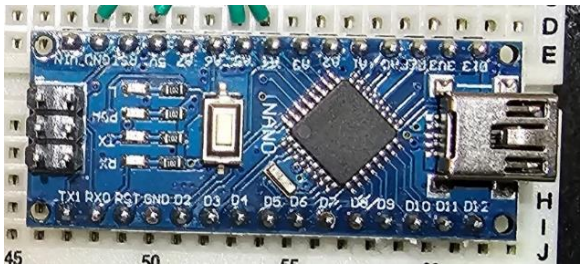

Figure 49. Arduino Nano.

To successfully pull data from the MPU-6050 with the Arduino Nano a wiring diagram must be closely followed, otherwise the microcontroller will be unable to draw data from the MPU-6050. Below in figure 50 is the wiring diagram for an Arduino Nano and MPU-6050.

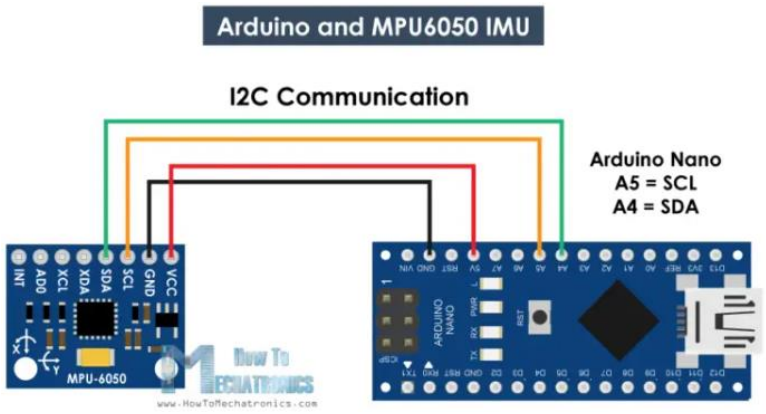

Figure 50. Arduino Nano and MPU-6050 Wiring Diagram (Dejan, n.d.).

Since it is impossible to ensure complete and total accuracy from every single MPU-6050 manufactured the sensors must be calibrated. Calibrating the sensors was done quickly and easily by simply resting the sensor on a level table while data was collected. For the gyroscopic sensor 2,000 samples were collected at rest, since the sensor is not moving the rate of change in angle orientation is zero. With this data an average for x, y, and z directions were obtained, these averages were then used as offset to bring the sensor outputs to zero. A couple more steps were required to calibrate the accelerometer. The sensor was left resting in three directions, one for each x, y, and z. Data was collected, 2,000 samples, in each orientation. Since gravity is constant and was in line with each of these orientations 1-g should be measured for each orientation. The samples were averaged and subtracted from a value of 1-g, the remainder was used as an offset to bring the measured values to 1-g for all x, y, and z orientations. Below in figure 51 is an example of the calibration data retrieved for one of the sensors.

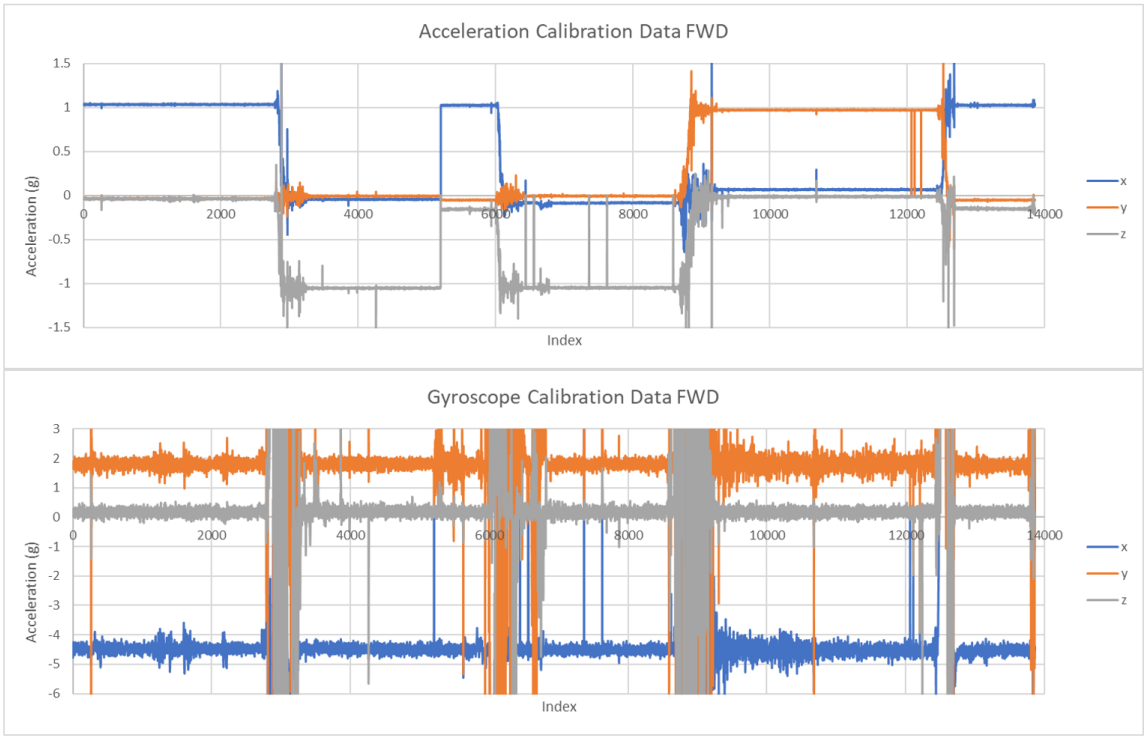

Figure 51. Example Calibration Data for MPU-6050.

Engine data collection is comparatively simple to the engine mount torsion data collection. PBS Aerospace provided desktop computer software to couple with the ECU in the TP100 to display critical engine data points while the turboprop is running. Some examples of this data include turbine RPMs, engine running hours, and chip detector status. ECU data is output to a CAN bus adapter. The CAN bus adapter converts the wiring from the ECU to a USB port that is then plugged into a computer with the provided software. The software translates the CAN data and displays it for the pilot to read. Below in figure 52 is a block diagram of the CAN bus system.

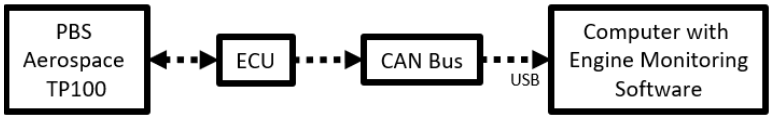

Figure 52. PBS Aerospace TP100 Data Collection.

The engine monitoring software can be configured to display different data types, for this application the software had gauges and plots added for free turbine RPM and propeller shaft torque. It is also interesting to note that if correctly configured the monitoring software can control the turboprop, but for the current work the monitoring software is limited to only monitoring the turboprop. However, this data is not recordable and usable. To solve this data recording issue a screen recording software was used to record all data as the monitoring software obtained it. This ensures that any data that is needed is reachable, though the team must transcribe some values. Below in figure 53 is a picture of the engine monitoring software.

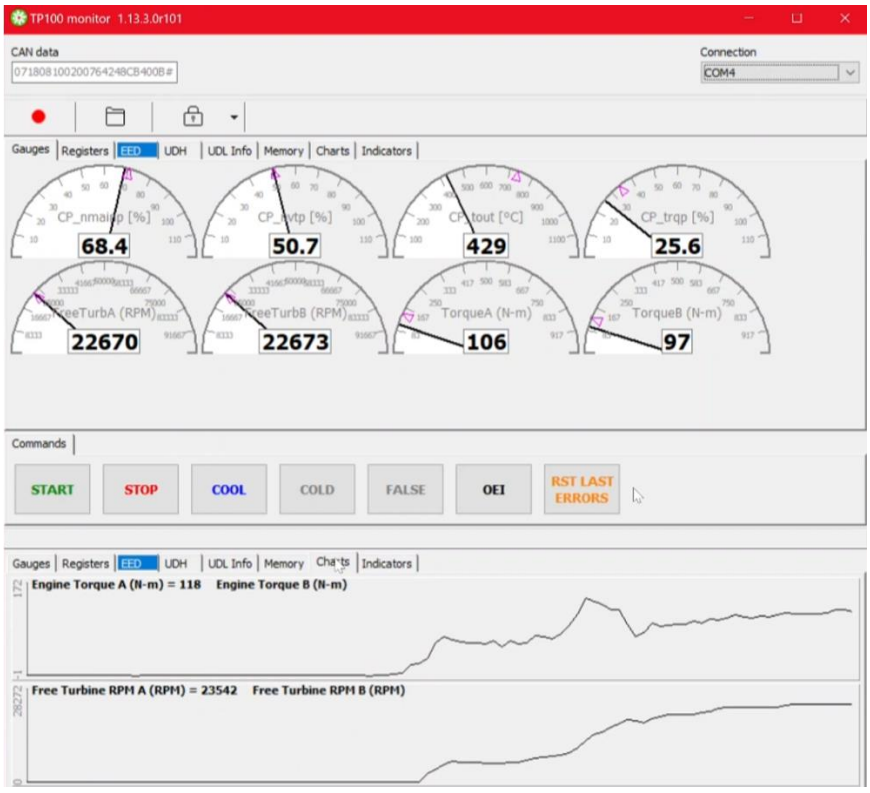

Figure 53. Engine Monitoring Software.

This engine monitoring software communicates with the turboprop through a USB port and a CAN bus. A computer is setup up in the cockpit and is plugged into the engine, this is shown below in figure 54.

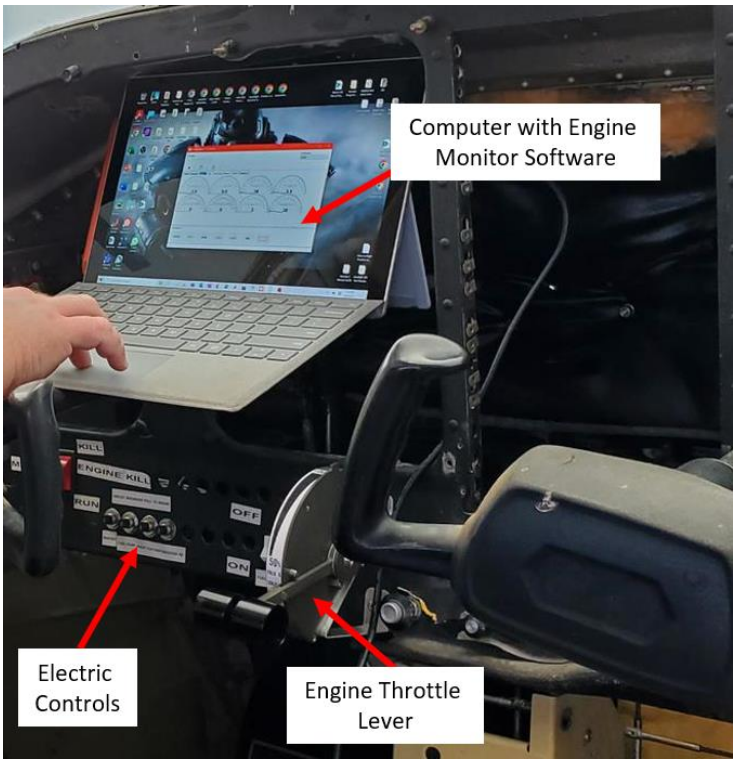

Figure 54. Engine Monitoring Software and Computer.

Once the engine run was completed the data was extracted from the Arduino and processed. This involved applying the offset values for the sensors obtained from sensor calibration. Once the data was calibrated and equations 18 and 19 used to obtain roll angle data it was discovered that it was heavily polluted with vibrational data, it was passed through an FFT function, shown below in figure 55, to obtain primary frequencies for filtering.

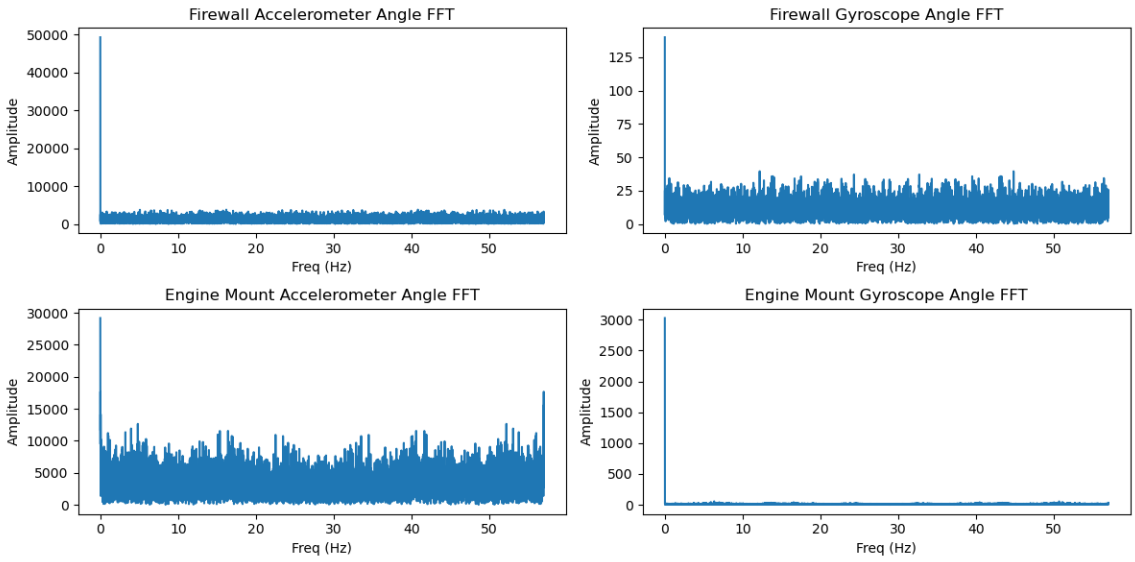

Figure 55. FFT Analysis of Dynamic Engine Mount Test.

Using the results from the FFT analysis a cutoff frequency was obtained at around 0.1-Hz. This cutoff frequency was passed into a 2nd order low-pass Butterworth filter with the results of the filtering shown below in figure 56.

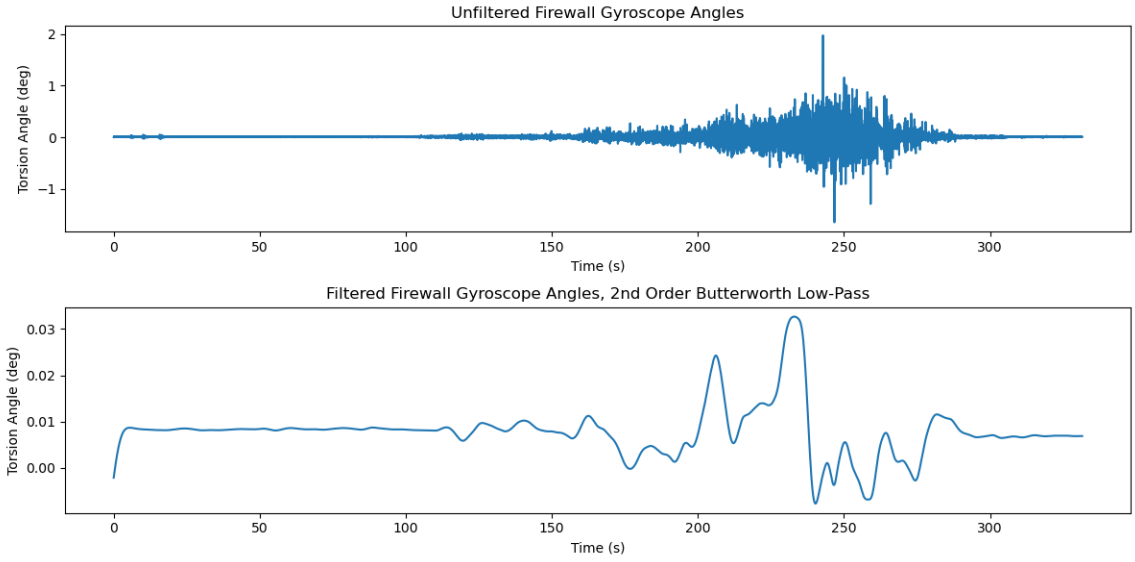

Figure 56. Filtered and Unfiltered Gyroscope Roll Angle Data.

With the Butterworth filter applied to the data it becomes clear that a trend in roll angle data is present. The developed Butterworth filter was applied to both the accelerometer and gyroscope data from the engine mount and firewall sensors. Finally, equation 20 was used to fuse the data between the accelerometers and gyroscopes. The final filtered and fused data was plotted against time to display the roll angles throughout the duration of the engine run.

Experimental Procedure

Once the aircraft was ready form the dynamic engine mount testing, that is fueled, oil, greased, and all pressures up to charge, the aircraft is rolled out of the hangar and anchored to the ground with chain. Chocks are placed at the wheels for extra safety. All data acquisition systems were initialized. The engine is started and brought to idle conditions to heat the oil. Once the oil is heated and the engine is ready for a full power sweep. The engine was first brought to 70% N1 and held for a short moment to stabilize the sensor readings. Next, the engine was brought to 80% and 90% N1 respectively. After a short period at each of these power settings the engine was lastly brought to the full power of 100% N1, where it was held for another moment. Finally, the engine was slowly brought back down to idle and shutdown with appropriate cooling procedures. This completes the dynamic engine mount testing.

CHAPTER IV

RESULTS AND DISCUSSION

Engine Mount

The final engine mount design handled all loads without experiencing a factor of safety below 1.5 in any portion of the model. As this is the standard in the industry, and the minimum for a vast many certification requirement in many FARs, it was taken as a safe model and cleared for manufacturing. The engine simulacrum was treated as a rigid body with contact criteria on the engine mounting plates. This was done to conserve computational resources. It was also done to ensure that the forces are perfectly transferred to the engine mount. The weight of the engine mount itself was also neglected. The weight of the engine mount is negligible compared to its total strength. Figure 57 displays the model's Von Mises Stress at the loads discussed above.

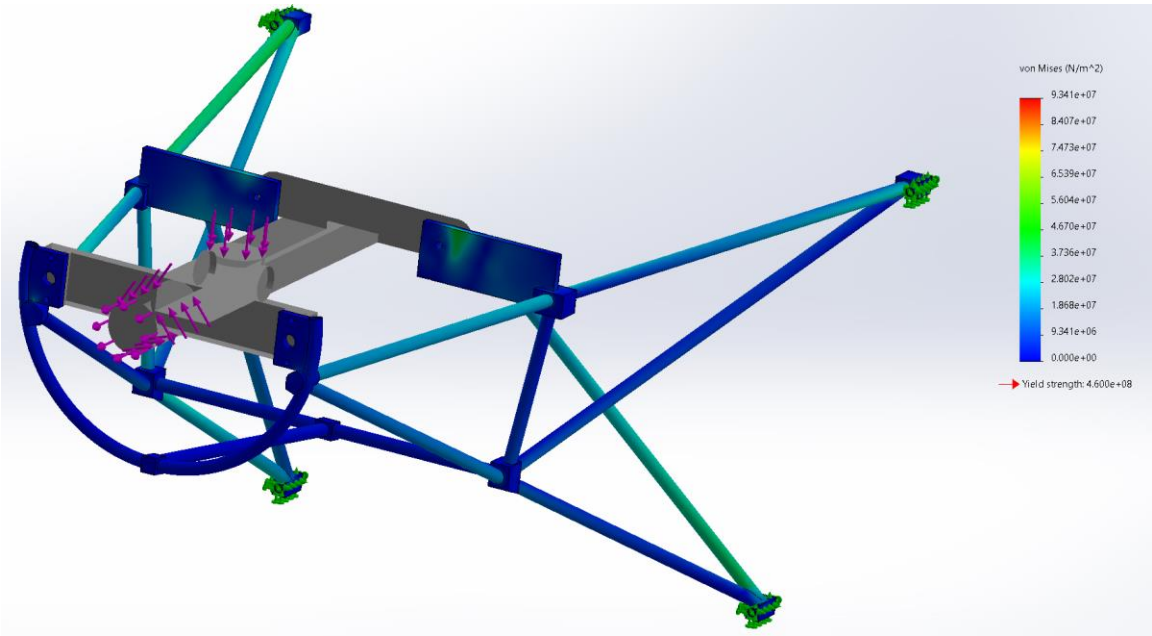

Figure 57. Engine Mount FEA Stress Distribution.

As can be seen the critical components of the structure are the trussing members at the firewall. This is logical, as they are experiencing the maximum stress in the structure, as a cantilever beam would at its root. Other critical areas are the mounting plates, this also makes sense as they are the first elements that experience the engine loads. Figure 58 depicts the factor of safety for the engine mount at these same loadings.

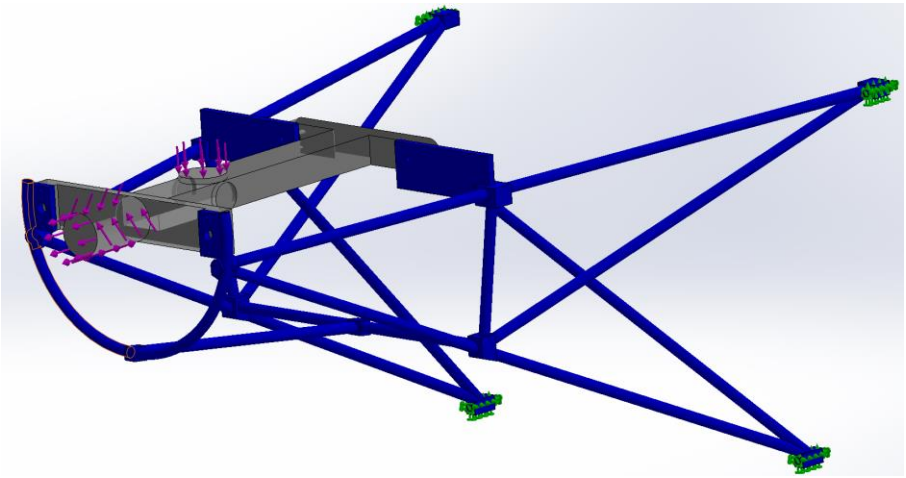

Figure 58. Engine Mount Factor of Safety Plot.

Blue is considered safe with a factor of safety above 1.5, if any of the elements in the model have a factor of safety below 1.5 they would be highlighted red instead of blue. This is computed from the Von Mises Stress distribution and the materials yield stress. Thankfully the model is solid blue, indicating a consistent factor of safety of at least above 1.5 throughout the entire model. Figure 59 is a displacement plot used to determine maximum deflection and deflection behavior.

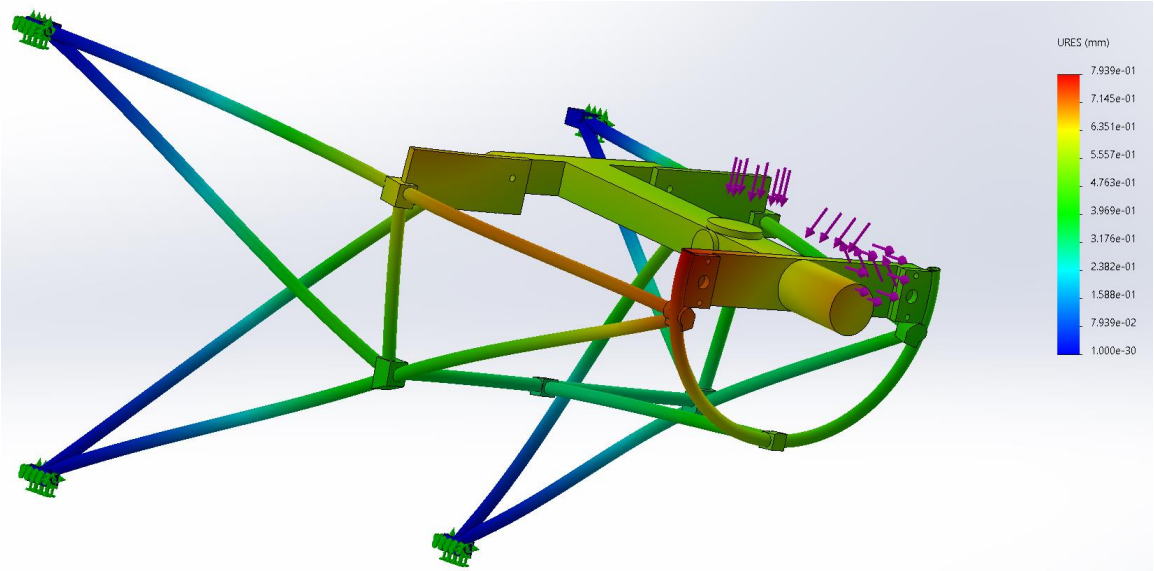

Figure 59. Displacement of the Engine Mount.

It must be noted that this is not true scale deflection but instead has a multiplication factor of 100 applied to it. This is done to highlight how the engine mount is expected to deflect under various loadings. Displacement is extremely important, if the mount is strong enough to withstand the loadings but deflects too much the fit and function of the engine might be affected, as well as the safe operation of engine accessories such as the oil cooler. In an absolute extreme situation, the propeller could even impact the ground leading to critical failure. Under standard full throttle conditions, it is expected that the engine mount will only deflect a maximum of about 5.1-mm. The maximum deflection of 5.1-mm is ideal, this indicates that the engine mount can withstand engine loadings with minimal deflection.

Figure 60 documents the use of the Solidworks Simulation to compute the natural frequencies and modes of the engine mount model. This analysis used the same loading conditions, fixtures, and mesh as the static simulations. However, the engine simulacrum was removed in favor of remote loadings, this was done to remove any potential extra mass that the software may consider. It was also done to save on computational resources as this simulation type is extremely expensive. The remote loadings were placed in the correct locations for center of gravity and propeller thrust line. The values used were the same as the ones imposed on the engine simulacrum. The remote loading type was also set as a rigid connection, the mounting plates do not move in relation to each other, but all may move in unison based off deflection amplitude. A rigid connection was chosen because once the engine is installed it will hold the mounting plates at their locations in relation to each other. After these boundary conditions were set the simulation was initiated.

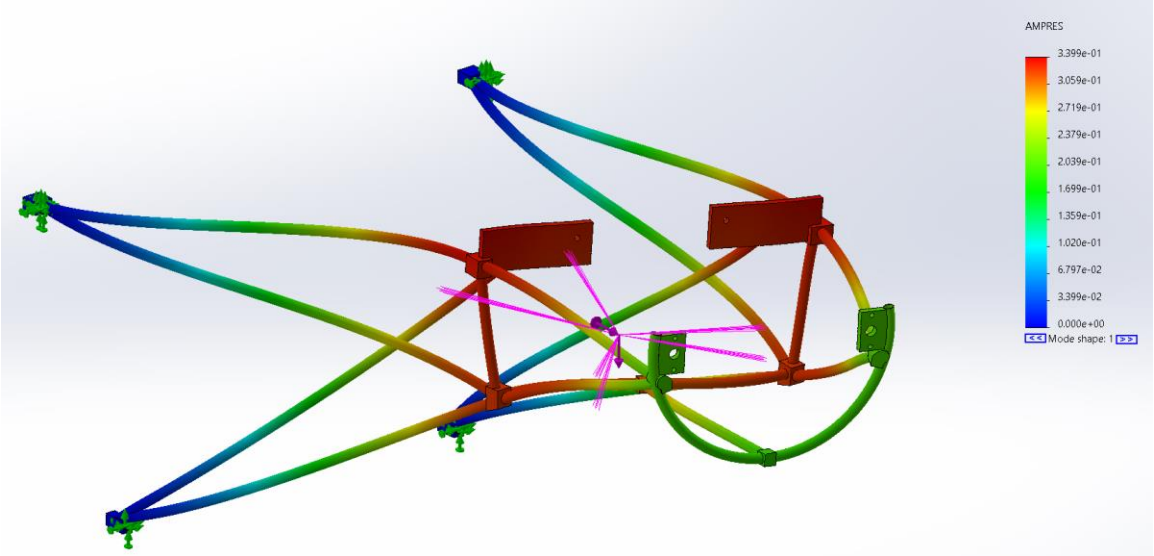

Figure 60. Mode 1 Displacement for the Engine Mount

Shown directly above in figure 60 the first mode shape seems entirely lateral, likely augmented from engine torque. This mode is triggered at 35-Hz. The propeller rotates at 2,158-RPM and the propeller selected for the integration has three blades. Therefore, the blade pass frequency is 108-Hz, with this mode being triggered at only 35-Hz this mode is of no concern.

The next mode is computed to trigger at 108-Hz, which is what the blade pass frequency is. However, as this mode looks unrealistic with many of the members somehow passing through each other. Because of this this mode is neglected. The third mode is computed at 136-Hz, since this and all the proceeding modes are far above that of the blade pass frequency they are neglected. The subsequent modes are also equally unrealistic as the one above.

It must be noted that these frequencies are for a perfectly rigid attachment, the turboprop has vibrational isolators built into it on all four bolt pickups. These will massively reduce the amount of vibration transferred to the engine mount. If the transferred vibrations are too intensive additional isolators can be added to the turboprop bolt pickups and even to the airframe firewall to further absorb the vibrations.

As the model was analyzed it was discovered that more trussing was needed, trussing layouts were changed and optimized across numerous loading conditions including emergency conditions. When the model was analyzed for natural frequencies triggered by dynamic responses it was found that its rigidity was insufficient for reasonable frequency responses. The frequency response was corrected by increasing tube outer diameter and decreasing wall thickness. By changing the tubing dimensions an increase to the overall strength of the engine mount and even a reduction to the deflection across all loadings was achieved. The increased performance of the mount is attributed to the increase in inertia gained from the increased tubing diameter.

A mesh independent study was conducted to determine if the meshing was appropriate. This study took cell counts from the hundreds of thousands to millions. As expected, computational load was increased greatly but results changed marginally. It was deemed appropriate to keep cell count down at the expense of mild inaccuracy to ensure that computational sessions would not crash. The optimized cell size is used above, therefore some slight differences between the FEA model and the real engine mount are expected. Though the magnitude is not known, especially

when the accessories are installed onto the engine mount. The final engine mount is shown below in figure 61 with some dimensions.

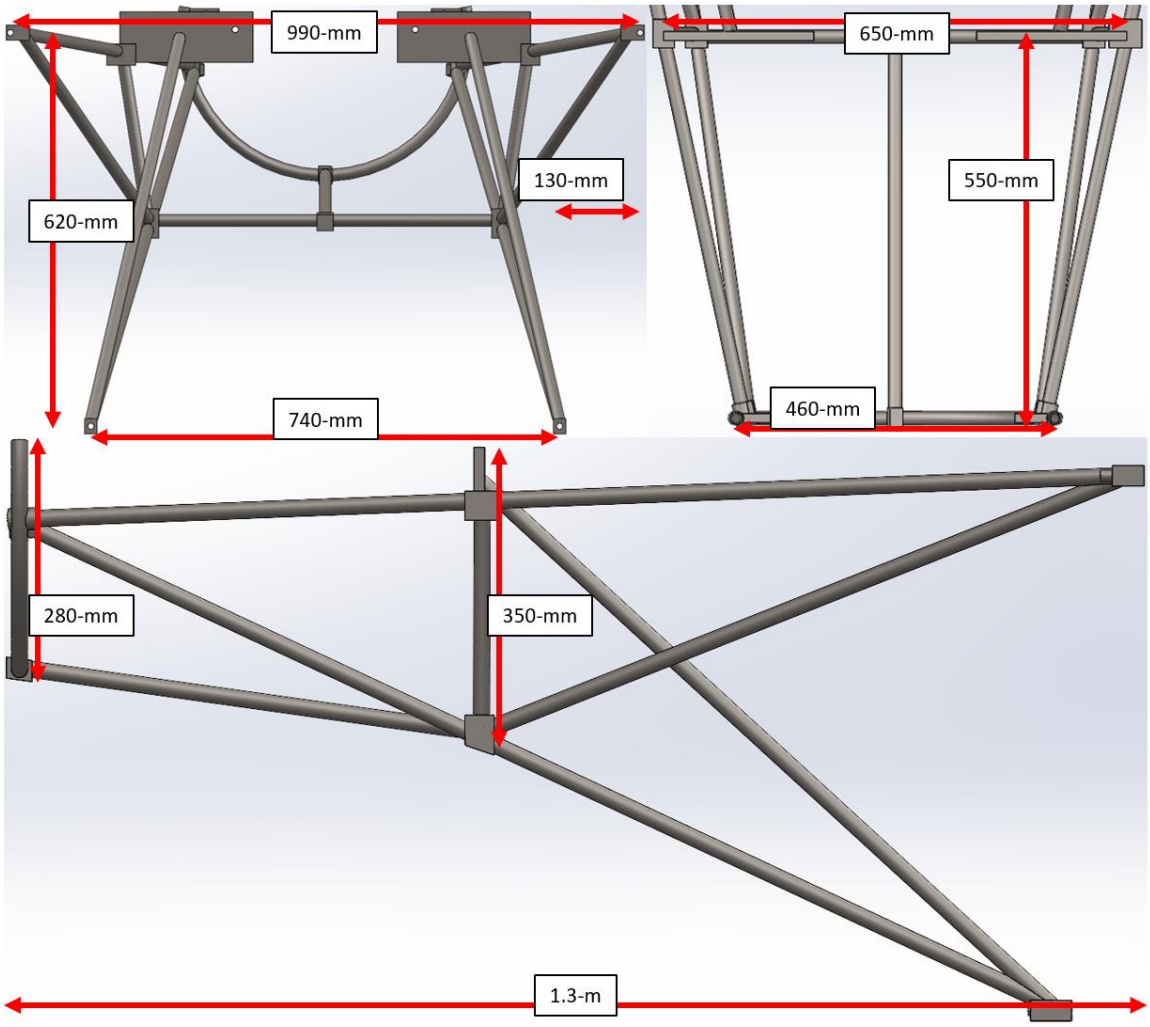

Figure 61. Final Engine Mount Design with Dimensions.

As previously mentioned, a static torque test was conducted on the engine mount once it was received from the manufacturer. The static torque test of the engine mount returned positive results, the engine mount was found to be safe within the expected operating conditions and even beyond as the mount was over-proofed for safety.

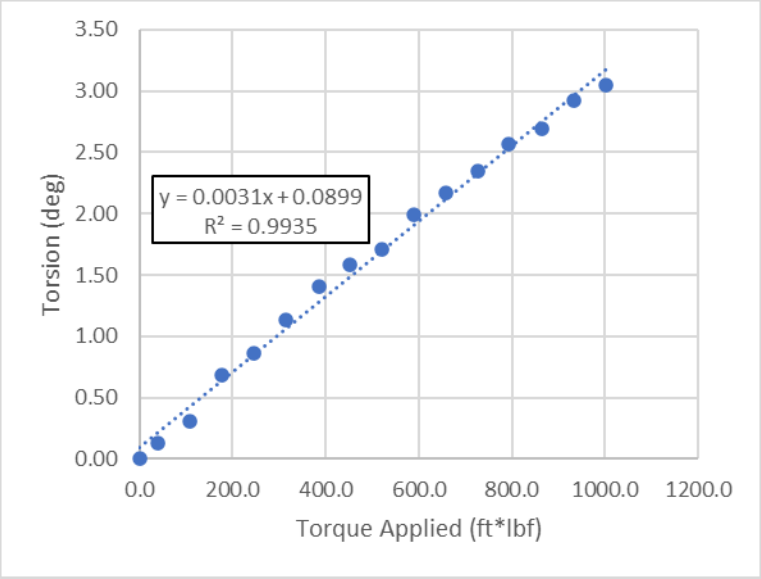

Figure 62. Twist vs. Torque of Engine Mount Under Static Torque.

Figure 62 depicts the twist of the engine mount against torque applied. The engine only produces a maximum of about 800-N·m, or about 600-ft·lbf, and only experiences a twist of 2 degrees. This is extremely ideal as the deflection of the engine mount must be at a minimum to prevent issues with the fit and function of the system. Lastly, the R^2 value of the trendline indicates a near perfect linearity showing that the engine mount is still well within the yield strength of the steel. This shows that the engine mount could handle higher loading conditions without failure. If the mount was not within the yield region, then this plot would become more parabolic showing an entrance into the ultimate stress region of the material. This would include permanent deformations of the engine mount.

Below in figure 63 are the results from the FEA static torque test plotted with the results from the actual static torque test.

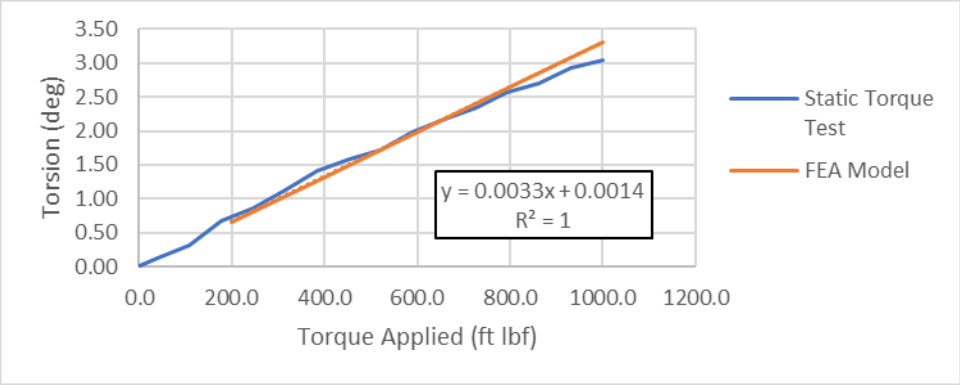

Figure 63. Torsion of Engine Mount and FEA Model Under Static Torque.

As it can be seen the FEA model predicts exceptionally close to the measurements obtained from the static torque test. However, after 600-ft·lbf of torque the FEA model seems to overpredict the torsion in the engine mount, even surpassing a quarter of a degree of difference between the model and the measurements from the static torque test. Another interesting note is that the FEA model data is perfectly linear with an R^2 of 1, this further reinforces the fact that the material in the engine mount never experiences stress more than its yield stress.

The final computational analysis conducted on the FEA model of the engine mount in its gambit of testing is a buckling analysis. This was done to ensure that the engine mount would not buckle under expected engine running conditions. Buckling is a unique failure mode; it does not depend on the internal stress of the material but instead its rigidity and resistance to deflection. A structure may buckle before it fails in terms of material yield stress, or it may fail in terms of yield stress before it buckles. A structure may also buckle in tension or compression. Due to the exotic structure of this engine mount a buckling analysis must be conducted to ensure that the structure does not buckle in any of the trussing elements before the material yield stress. Ten modes were computed to ensure adequate resolution of the analysis. Below in figure 64 is a plot from the buckling analysis.

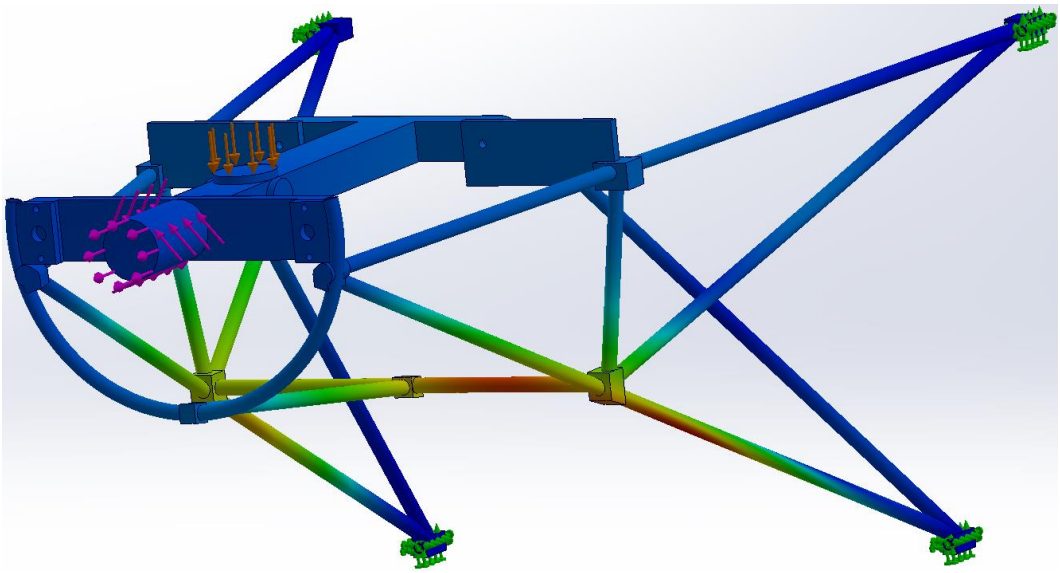

Figure 64. Engine Mount Buckling Analysis Plot, Red Denotes Buckled Member.

The darker regions denote a higher deflection and are suspect of buckling under the given conditions. This particular mode, which has a factor of safety of 16.5, buckles in the lower segments of the structure, this is intuitive as this portion of the structure must absorb the compressive loading of the weight of the engine itself as well as the effects of the torque output of the engine. Below in table 1 is a summary of all ten modes and their factors of safety.

Buckling Factors of Safety	
Mode	FoS
1	-23.4
2	-19.6
3	-18.1
4	-14.9
5	-9.79
6	-5.48
7	16.5
8	20.3
9	22.4
10	24.2

Table 1. Engine Mount Buckling Factors of Safety.

The first mode of concern is mode 7 with a FoS of 16.5, which, when compared to the same static model conditions with a stress based FoS of 3.40 signifies that the engine mount will fail

materially before it fails in buckling. Failure in material before buckling is considered safe as the engine mount was designed using material limits. Modes 1 through 6 are negative, this signifies that if the loading conditions were flipped the model would buckle at these factors of safety. None are smaller than the stress based FoS of 3.40 further signifying that the engine mount is indeed safe to use. However, these reversed loading conditions would be critical to consider if this was a flight worthy aircraft, gusting conditions could impose these flipped loading conditions on the aircraft if extreme enough.

Before the engine mount could be dynamically tested with an engine run the aircraft had to be prepared. Fuel had to be pushed through the fuel lines to evacuate most of the air and potential contaminants from assembly. The fuel pump was charged, valves opened, and tank filled, this led to considerable flow of fuel emerging from the disconnected firewall passthrough. This waste fuel was collected and disposed of. The engine was oiled, nose strut charged, battery connected, propeller dome charged, and all data acquisition systems were activated.

After all the systems were installed onto the aircraft an engine check run was conducted. These systems include the fuel, oil, electrical, and engine controls. This engine check run was designed to bring the engine to a medium power setting to ensure that the all the systems, namely engine controls, worked as they should. Initially a cold start, which uses the starter motor to move air through the engine, was used to flush air through the engine to blow out any dust that may have collected. Next a hot start was conducted. A hot start is identical to a cold start except fuel pumps are also engaged. This is meant to flush the engine fuel lines of preservatives. Starting procedures were initiated and soon the turboprop was idling smoothly, it was kept idle for a couple of minutes to ensure proper heating of the oil supply. N1, core turbine, was brought to about 70% and held there for a period while data was collected. Below in figure 65 is the data collected during the run.

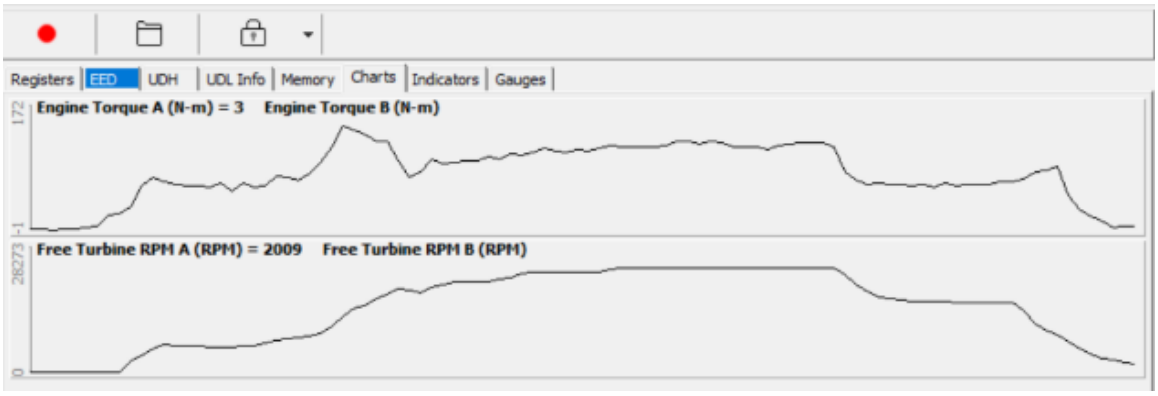

Figure 65. Engine Data from Check Run.

Data was successfully collected from the engine, with the torque and free turbine speed a power output can be determined. This power output will be useful in the turboelectric analysis portion of this project. Using equation 1, the power output from this run at 70% N1 was about 13-kW, it should be noted that the gear reduction from the free turbine to the output shaft is a factor of 20.75. This power was only fed into the propeller but will also feed the generator later. The engine check run also served other purposes. By conducting a successful check run the electrical and engine control systems were found to be working as intended. After the run all fuel and oil lines were checked for any leaks, none were found. With the engine check run being a success, the engine is fully installed and ready for further testing.

After all the supporting elements for the turboelectric system were installed, those being the propeller spacer, generator mount, and belting system, a dynamic engine mount test was conducted to validate the structural strength and response of the engine mount. It is noted that this testing was with no load on the generator as the full turboelectric system was not ready in time.

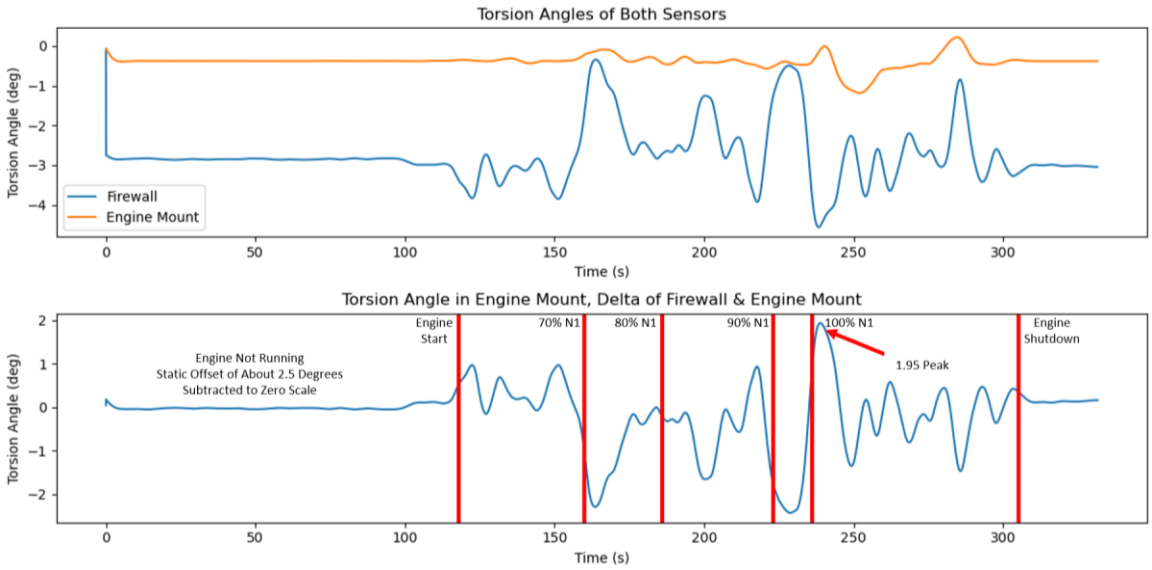

Figure 66. Engine Mount Torsion Angles During Engine Run.

Figure 66 shows the torsion angles recorded by both sensors, it is obvious that the sensors in the engine mount and firewall recorded different values indicating twist in the engine mount. To isolate the torsion angle in the engine mount itself the difference between the engine mount sensor and firewall was taking. The difference between the two sensors isolates the twisting in the engine mount relative to the airframe. After the difference was taking it was discovered that the resting difference was about 2.5 degrees, this was subtracted from the torsion angles to zero the scale. Once the scale was zeroed the peak torsion angle at full power was recorded as 1.95 degrees which agrees with the static torque test as well with the FEA model static torque test at peak engine torque. However, this is not completely agreeable as the engine was unable to reach peak power as the gauges indicate below in figure 67.

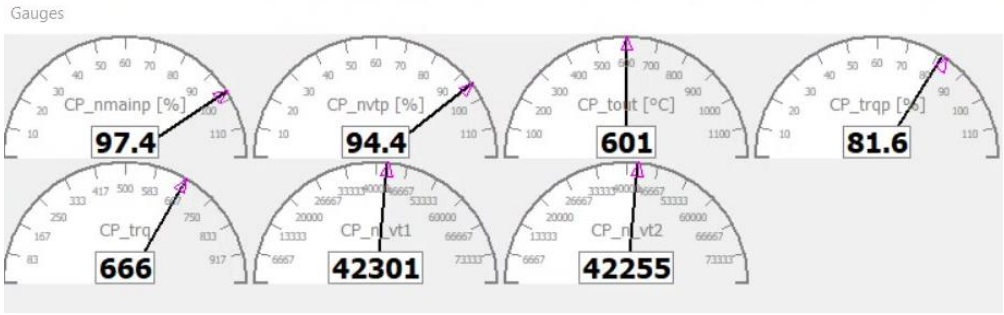

Figure 67. Peak Engine Power During Dynamic Engine Mount Testing.

Using the peak torque, peak free turbine RPM, gearbox reduction ratio, and equation 7 peak power was computed to be 142-kW. This 142-kW peak power is far from the certified peak power of 180-kW, including the peak torque of 666-N·m versus the rated peak torque of 800-N·m. The short power and torque is attributed to environmental conditions, the day of testing had some considerable wind and the and temperature may not have been at the optimum for the engine. So, when considering this deficit of torque, 666-N·m, versus the static torque tests of 800-N·m having the same deflection on the engine mount a question arises, why are they so similar? The similarity is attributed to two things, vibrations and total engine installation weight with accessories. Vibrations imposed on the engine mount from the running engine could be forcing further deflections through the momentum of the engine weight. However, the most likely reason for this difference is the total installation weight of the engine and its accessories such as the oil cooler, fluid lines, and electrical lines. The weight of the accessories would preload the structure allowing for larger deflections with lower torque while items like fluid lines or electrical lines could be assisting the structure in absorbing some loadings.

Lastly, an uncertainty analysis was conducted on the data obtained from the accelerometers and gyroscopes to ensure reasonable propagation of uncertainty when the torsional angles are computed. Below in figure 68 is a plot of the engine mount twisting with uncertainty bounds.

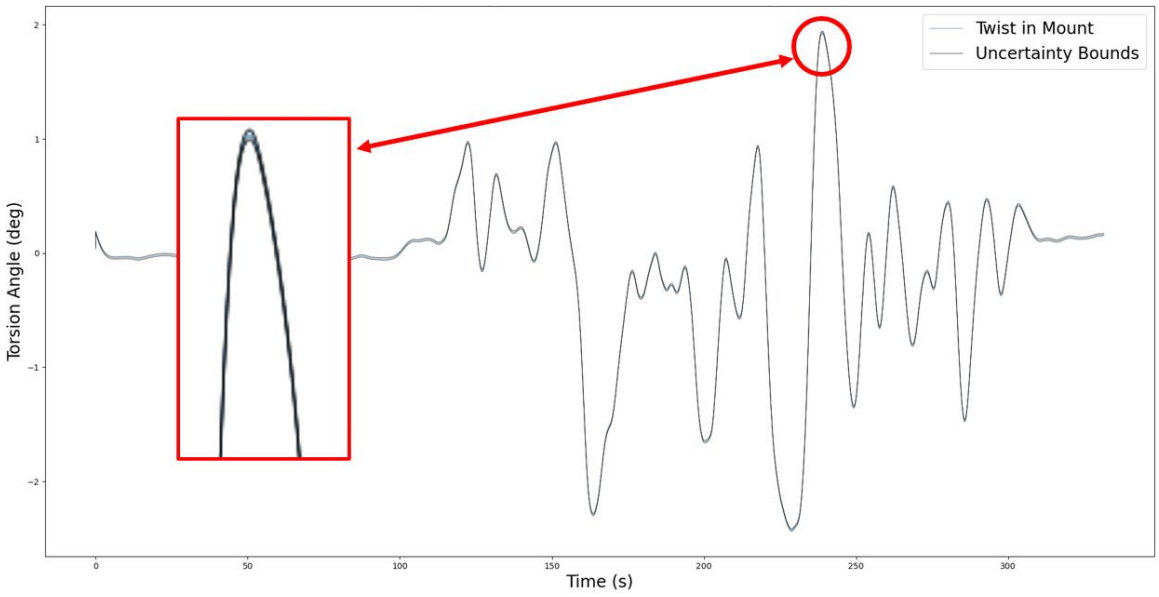

Figure 68. Uncertainty in Torsional Angles in Engine Mount.

As the plot reports the uncertainty bounds of the angle computation are exceedingly small, in fact it is only ±0.10 degrees. With such a small uncertainty more confidence can be placed with the measurement of the engine mount torsional angles. This uncertainty was derived from using the Uncertainties Library for Python developed by Eric O. Lebigot [uncertainties library]. Lastly, the standard deviation of the torsional angle data is reported as 0.697, the mean is -0.146, and the total sample size is 17,903. The small value of standard deviation, 0.697, further reinforces confidence in the measurement data.

Propeller Spacer

The propeller spacer was also modeled and analyzed in SOLIDWORKS, including a mesh independent study. The mesh independent study returned no difference in model stress results, it is concluded that the model is reliable. Even at 36,000-N and 1,200-N·m emergency loading conditions the propeller spacer absorbed the load without critical failure or at a below favorable factor of safety. Maximum deflection of the spacer at these conditions was reported at 0.056-mm. This deflection is small and is desired, if deflection grows too large the propeller thrust line may

change significantly leading to aircraft control problems. Below in figure 69 is a stress plot of the propeller spacer.

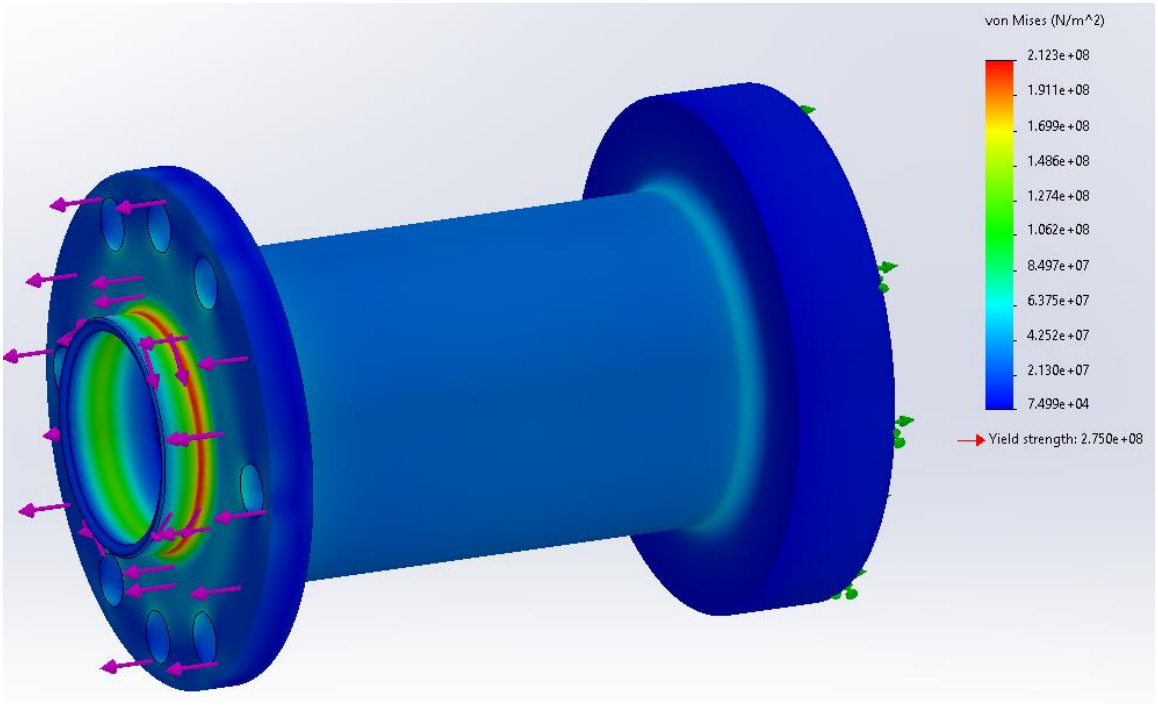

Figure 69. Von Mises Stress Distribution of the Propeller Spacer.

As it can be seen the stresses are concentrated at the neck down, for oil sealing, and is intuitive as this is how the torque loading was applied to the model. In reality this would not be the case as torque is transferred through the mounting mechanisms of the propeller. It was modelled this way to reduce model complexity. The area of concern is the space between the two mounting flanges, the web. As the stress plot indicates this area experiences an elevated stress, but it is minimal. This is desired as the web will be responsible for transferring all the thrust and torque generated to the engine. The propeller spacer is now considered safe to use up to these conditions highlighted above. Under peak engine running conditions, maximum torque of 800-N·m and 2,700-N of thrust, the minimal FoS is 2.00.

A frequency study was conducted to determine how the propeller spacer reacts to rotational velocities imposed on it. In simpler terms the shaft's critical speeds were determined. The study returned positive results that indicated the first mode of critical speed would happen around 110,000-RPM. The propeller shaft only rotates at a maximum of 2,158-RPM, the spacer is indeed safe and will never experience critical speeds in this application. A mesh independence study was also conducted on the critical speed analysis taking total element count from 960,000 to well over 12 million. No discernable difference in results was observed. This indicates that the shaft critical speed of the spacer is, in fact, around 110,000-RPM.

Lastly, a buckling analysis was conducted on the propeller spacer to ensure that buckling would not be an issue with how unlikely it would be when considering the geometry of the spacer. Below in figure 70 is a plot from the buckling analysis on the propeller spacer.

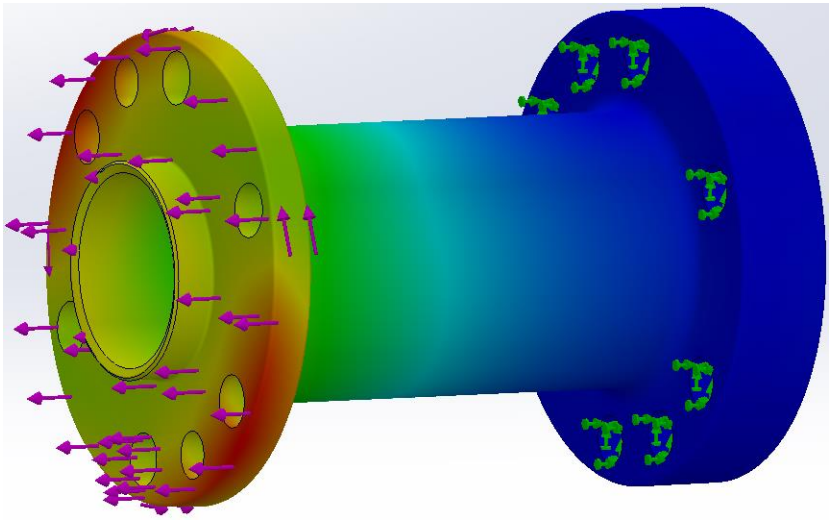

Figure 70. Propeller Spacer Buckling Analysis Plot.

As can be seen the buckling in the propeller spacer will be largely dependent on the flanges, this is intuitive as they are the thinnest portion of the part that has a significant protrusion from the center. Lastly, the 10 modes computed in the buckling analysis is shown below in table 2.

Buckling Factors of Safety	
Mode	FoS
1	-2,090
2	-2,020
3	-1,970
4	-1,950
5	-1,940
6	-1,880
7	-1,340
8	-1,050
9	1,360
10	1,400

Table 2. Propeller Spacer Buckling Factors of Safety.

As table 2 shows the minimum buckling factor of safety is only 1,360, this indicates that the model will fail in terms of stress, FoS of 2.00, far before the part will have any chance of buckling. This further reinforces the fact that the propeller spacer is indeed safe to use.

With all these analyses conducted on the propeller spacer, those being stress, frequency, and buckling, the spacer has considerably large factors of safety. These large factors of safety on the spacer ensure that it will be safe to use in the full turboelectric system even though a component level analysis of this part was unable to be performed. The final propeller spacer with some dimensions is shown below in figure 71.

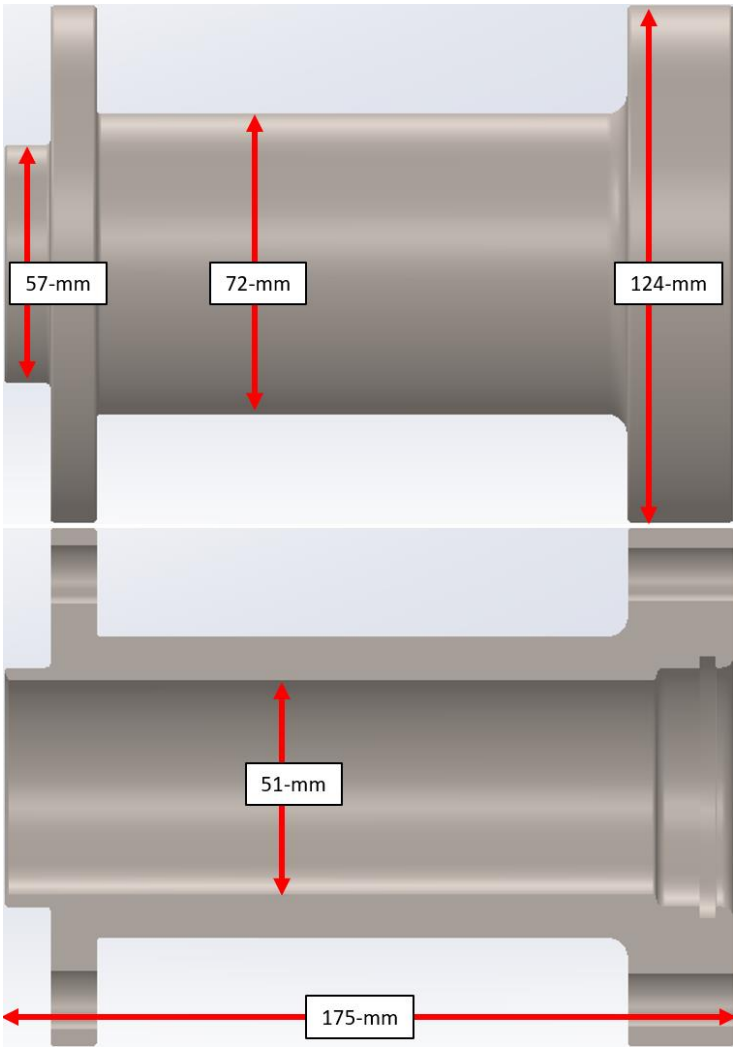

Figure 71. Final Propeller Spacer Design with Dimensions.

Generator Mount

Much like the engine mount and propeller spacer the generator mount needed to be fully analyzed through use of FEA to determine that the design was, in fact, safe to use in the experiment. As already discussed, this involved building the model with correct dimensions so that it may fit in and around the engine system. Another item of consideration was the placement of the pulleys, they must be in line. The models were designed with this in mind, and it should allow for the generator pulley to be in line with the engine pulley. However, if alignment is slightly off the

generator pulley may be shimmed to the appropriate location. The model was developed and loaded with the conditions discussed above, a stress plot is shown below in figure 72.

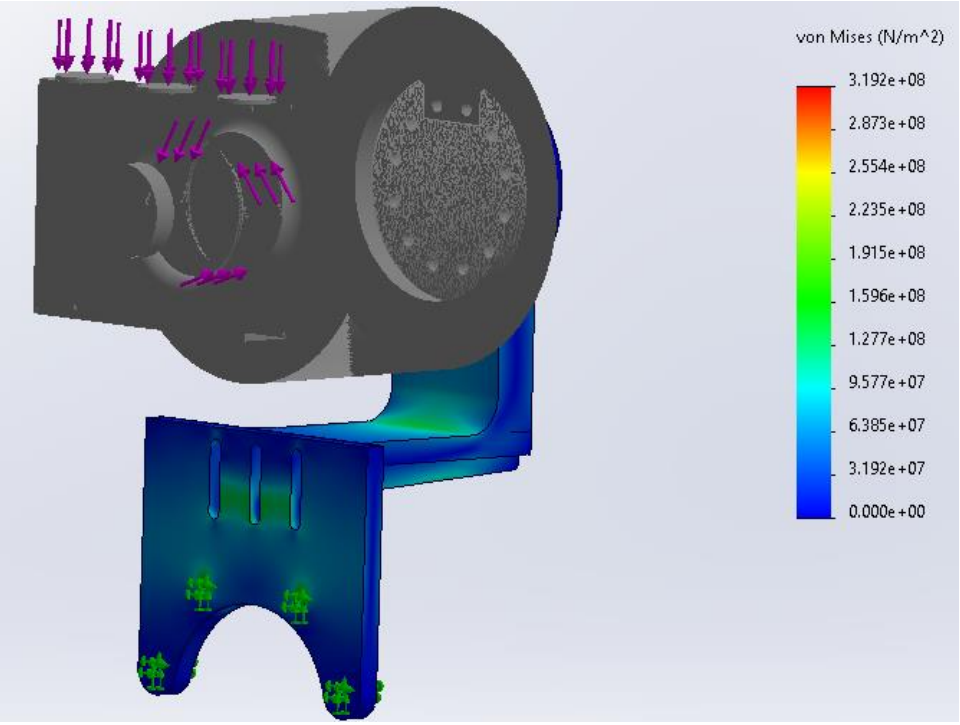

Figure 72. Generator Mount Von Mises Stress Plot.

As can be seen the model experiences very little stress, in fact this was not the driving design requirement of the model. The driving design requirement quickly became minimizing model deflection. The reasons were discussed earlier. Therefore, the generator mount must be of sufficient rigidity to prevent this, specifically in the vertical web where the generator is mounted. The web was doubled from the initial value, this led to a maximum deflection of only 2-mm. While not totally small it is insignificant enough to ensure system operation. If the deflection was desired to be further reduced a much more complex system would be required. A mesh independent study was also conducted on this model, this led to a reduction in the cell size to ensure adequation resolution and accuracy. The minimum factor of safety is recorded as 1.6, however, the actual factor of safety is likely much larger. The reason for such a low factor of

safety is that the surface contact between the generator simulacrum and the L-Bracket induces some surface cell stress concentrators. These stress concentrations will not be present in the actual part, but these issues are inherent to FEA software. Even with the surface issues of the model the minimum factor of safety does not drop below the required value of 1.5.

Next the fasteners selected to assemble this system were analyzed. This was done by simply providing extrusions where the bolts were located and fixturing them. The simulation was ran and each bolt was analyzed for peak stress. It was found that the peak stress each bolt would experience would not come close to half of the bolts' yield stress. Finally, a resonance analysis was conducted on the generator mount system. This was done to ensure that the generator mounting system would not experience any resonance events and would remain safe in the operational envelope. This also included another mesh independent study ranging from 160,000 cells to 5.25 million, though no changes in results were observed. The first mode of the model is experienced at around 6,800-RPM. With the generator only spinning at 3,000-RPM this is considered safe.

Lastly, the generator mount had a buckling analysis conducted on it to further increase confidence in the design. This was done like the engine mount and propeller spacer with running loading conditions imposed onto the model and 10 modes were computed. Below in figure 73 is a plot from the buckling analysis.

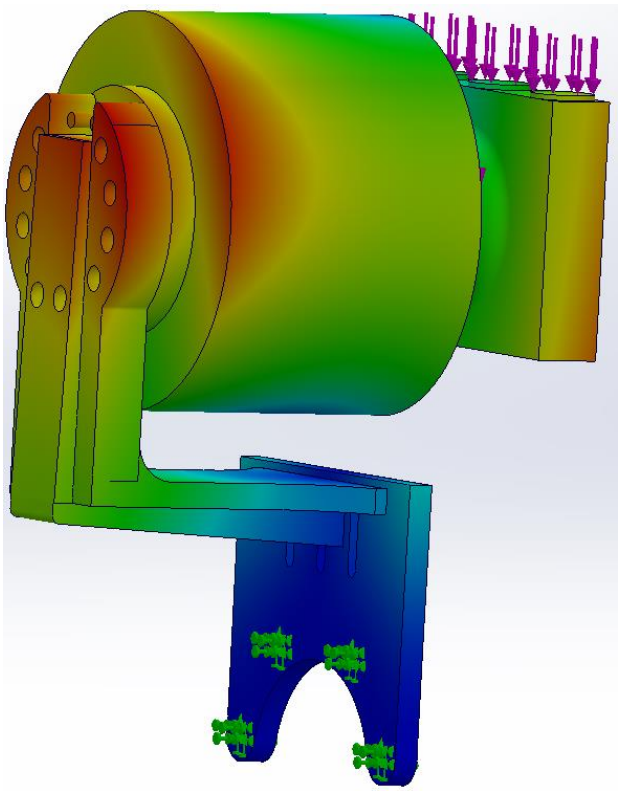

Figure 73. Generator Mount Buckling Analysis Plot, Red Denotes Buckled Element.

As can be seen the generator mount buckles in the L-Bracket, this is clear from the loading location as the loads are a significant distance from the bracket itself. With these loads far from the L-Bracket a large bending moment is generated within the bracket thus leading to a likelihood of buckling. Below in table 3 is a summary of the buckling analysis on the generator mount.

Buckling Factors of Safety	
Mode	FoS
1	-420
2	-416
3	-132
4	-56.0
5	295
6	363
7	389
8	401
9	407
10	426

Table 3. Generator Mount Buckling Factors of Safety.

As table 3 shows the buckling factors of safety are large and indicates the generator mount will fail in terms of material limits far before it fails from buckling. The large buckling factors of safety makes sense as the design of generator mount focused on minimizing the deflection the mount experienced. When considering deflection sectional rigidity is critical, rigidity depends on geometry, or the inertia, and material properties. Buckling also heavily depends on sectional rigidity as well, therefore since deflection was minimized the buckling factors of safety were indirectly maximized.

With all these analyses conducted on the generator mount, those being stress, frequency, and buckling, the generator mount has considerably large factors of safety. These large factors of safety on the generator mount ensures that the mount will be safe to use in the full turboelectric system even though a component level analysis of this part was unable to be performed. The final generator mount with some dimensions is shown below in figure 74.

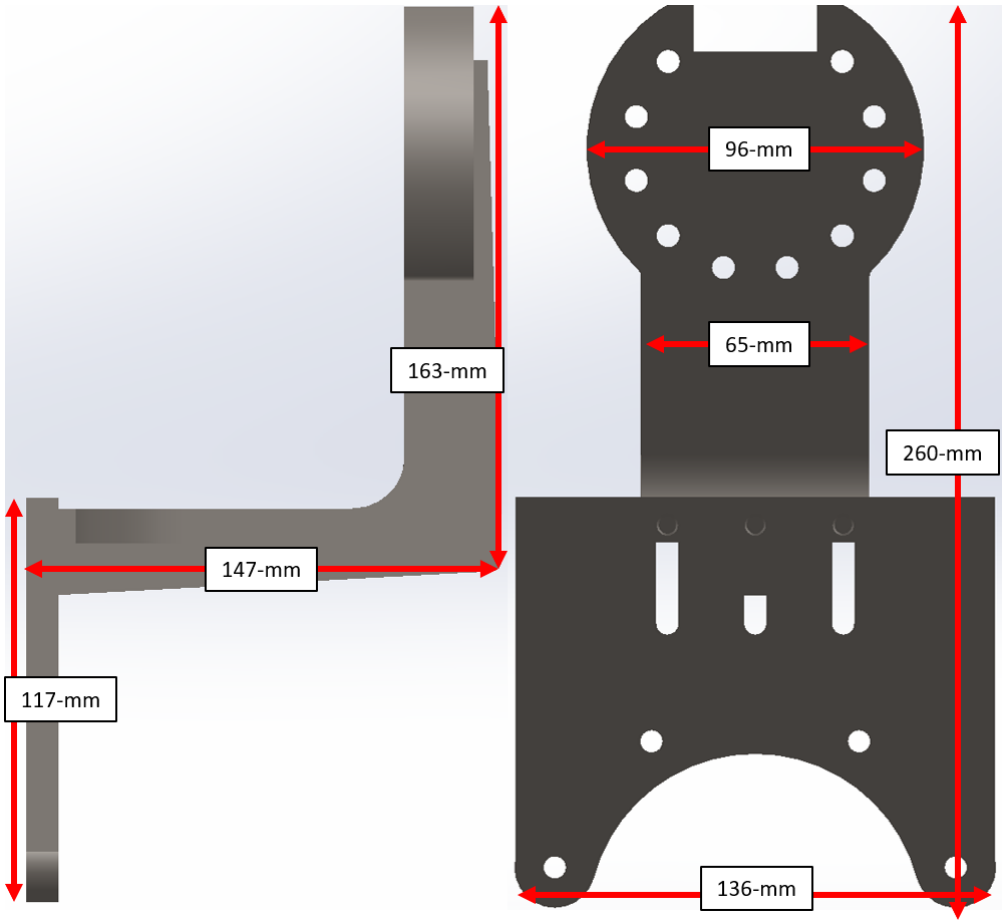

Figure 74. Final Generator Mount Design with Dimensions.

Unfortunately, since the full turboelectric system was unable to be tested due to timing restraints observations on the generator mount and belting system under load were unable to be completed. However, the generator was still being driven by the belting system, just without any load. With the free spinning generator and a tensioned belt they can still be observed to ensure proper function. With the dynamic engine mount test it was observed that the generator mount and belting system operated as intended with no belt slippage whatsoever.

CHAPTER V

CONCLUSIONS, RECOMMENDATIONS, AND FUTURE WORK

To conclude the engine mount, propeller spacer, and generator mount were successfully designed and integrated. It was found that the engine mount was safe through use of FEA analysis, a static torque test, and a successful dynamic engine mount test by running the engine. The propeller spacer and generator system operate safely and at expected conditions by using extensive FEA analyses since full component level tests of these components were outside the scope of this work. It is highly recommended that designers fully resolve a belting system and consider all potential loading conditions to safely transfer power from a turboprop to a generator through use of a belting system in a parallel partial hybrid turboelectric arrangement. The tension loadings of the belt are enormous and must be fully considered so that safe integration of turboelectric generators can be done. If more space is required between the turboprop and the propeller for components then a spacer may be designed, however this spacer must have provisions for oil transfer and oil sealing so that the propeller can fully function as intended as a vast majority of turboprop propeller assemblies have dynamic propeller control through use of engine oil pressure. For engine mount design it is recommended to consider placement of trussing elements in relation to maintenance provisions such as filter access. Trussing elements should be laid out to optimally transfer loadings, like torque and thrust, as this will maintain simplicity and minimize weight.

It is noted that the generator system should have emergency loads considered, namely the weight of the generator under sudden accelerative loads, likely the same used by the engine mount to

ensure secure mounting no matter loading conditions. If the generator mount were to be redesigned using current knowledge two things might be considered; the first being an auto tensioning system to ensure optimal belt tension, the second being a slightly difference L-Bracket to vertical plate mounting system. The current method of fastening the L-Bracket to the vertical plate are by use of 3 fasteners in a row, a new proposed method would be to stagger the fasteners to achieve a more even clamping force. It has been noted that when the belt is tensioned on the generator pulley the L-Bracket pivots slightly at the vertical plate interface, a staggered fastener application would solve this potential issue. As for any propeller spacer design alterations there are none, all were deployed for the second spacer after the first was destroyed. Finally, for the engine mount there are many different potential redesign elements. The first redesign option for the engine mount would be dedicated provisions for a inlet system for the turboprop, this would require designing the inlet and engine mount in tandem to ensure proper fit and function. A second redesign option for the engine mount would be dedicated mounting provisions for engine accessories such as mounting pads for the ignition source, oil cooler, and electric disconnect. All the mounting provisions would also be grounded, as well as grounding provisions for the engine mount itself, these grounding provisions would ensure everything would have proper grounding. Lastly, the last engine mount redesign option would be a radical change in the aft engine mounting blocks. When the engine mount was originally designed not all tech data was acquired, within this tech data were specifications for the after mounting blocks. These aft mounting blocks are nonstructural and meant only to keep the engine level, these mounting blocks also axially grow and shrink radically from heat. Originally these mounting blocks were assumed to be structural, however the engine mount was also designed to ensure that the front mounting blocks could absorb all loading conditions as a safety feature. The redesign of the aft mounting mechanism would include a new U-Bracket that the engine mounting blocks would rest in, this would allow for easy thermal expansion considerations and maintain engine levelness.

The engine mount must have sufficient strength to hold all these components together with minimum deflection. It is also recommended to consider all engine accessories, including the generating system, during the design phase of the engine mount. Placement of these accessories and their weights should be injected into the engine mount design analysis to ensure proper mount strength and rigidity of the full installation. The current work only considers the turboprop itself, since at the time none of the accessories were known, and thus is a source of potential underestimation in structural strength. In regard to the power transfer system belting should be sufficient up to the power used in this work. However, for power transfers greater than 30-kW it is recommended to invest in a gear driven system as power per rib or belt can become limiting as the number or size of belts grow greatly. Chain driven systems may also be considered but these may become heavier than a simple gear system.

Further work will involve slightly greater power transfers into the electric propulsion system, this would be used to test the limits of the belting system. The belting system is also only designed to transfer around 30-kW of power, if the system pulls more the belt may fail. This can be leveraged as a safety feature to ensure that larger amounts of power are not pulled from the generator thus protecting the entire system in emergency events. Another future experiment may involve massively increasing the voltage of the electric system. This would decrease the amount of current required for the same power, equation 7, thus decreasing electrically generated heat and electrical wire requirements. However, higher voltages lead to a higher risk of arcing. A last potential is to adapt the power transfer system into a gear driven system. A gear driven system would allow for greater power transfers and allow for power transfer components to be fully enclosed. However, there are several design challenges associated with a gear driven system such as sufficient lubrication, structural strength of the gears, shafts, and casing.

Other future projects associated with this turboelectric ground test rig are numerous, such as an inlet system, cowling, and a fully integrated engine monitoring system. An inlet system for the

turboprop would involve numerous aerodynamic and practical considerations. Airflow must be routed to the engine with minimal total pressure losses and as little circulation in the flow as possible, if either is too great then engine performance can be severely hampered. Another option for the inlet system would be a particle separator, this separator would be used to ensure clean air is delivered to the turboprop by dropping out any solid particulates. A cowling for the turboprop would fully enclose the entire engine system, including the generating system. This enclosure would make the aircraft much cleaner and increase some performance aspects if done correctly. However, enclosing all the components could lead to increased temperatures on these components, if hot enough they could fail. Therefore, a cowling design would have to consider thermal limitations of components and ensure proper cooling flow is delivered to all of components. Lastly, the fully integrated engine monitoring system would require a considerable effort to install. An example of an engine monitoring system is shown below in figure 75.

Figure 75. Engine Monitoring System (PBS Aerospace , 2014).

As shown in figure 75 an engine monitoring software can be complicated, this system integrates all engine monitoring elements such as the CAN data that is displayed on the computer in addition to external, as in not connected to the turboprop ECU, sensor for oil temperature, oil

pressure, fuel pressure, fuel flow rate, battery voltage and battery drain or charge. Requirements for all these measurements would be sensors and wiring. To fully install the engine monitoring system some minor airframe modifications would be needed, primarily a custom built dash board to accommodate this system.

A proposed test matrix is given below in figure 76 for a full turboelectric system test.

	Engine Throttle	20%	40%	60%	80%
ESC Throttle					
0-50%		1	1	3	3
0-100%		1	1	3	3
0-50% *2x*		1	1	3	3
0-100% *2x*		1	1	3	3
50-0%		2	2	4	4
100-0%		2	2	4	4
50-0% *2x*		2	2	4	4
100-0% *2x*		2	2	4	4

Figure 76. Proposed Full Turboelectric System Test Matrix.

As the test matrix indicates the systems are initially started at low power settings and are brought up in power slowly. By doing this it ensures that the systems are not immediately taxed, and enough time is available to shut down in case of emergency. As engine power is increased electric power is also increased, this increases the loading on the generator and generator mounting system. While the generator is loaded and unloaded engine mount deflection is expected to slightly change as the power transfer places torque in different locations relative to the engine mount, this will be captured by the MPU-6050s. Rapid electric power demand reduction is also included in the testing matrix to determine how the system responds to unloaded conditions. Once all testing is complete all data will be extracted and analyzed to determine system response to various conditions.

REFERENCES

1. Anderson, J. D. (1998). *Aircraft Performance and Design* . McGraw-Hill Education .
2. Bando. (n.d.). *V-Belt Design Manual.* Bando.
3. Cessna Aircraft Company. (1985, March 20). Service Manual, Model 172 Series, 1977 Thru 1986. Cessna Aircraft Company.
4. D. A. Swanson, H. T. (1993). Optimization of Aircraft Engine Suspension Systems. *Journal of Aircraft* .
5. Dejan. (n.d.). *Arduino and MPU6050 Accelerometer and Gyroscope Tutorial*. Retrieved from How to Mechatronics : https://howtomechatronics.com/tutorials/arduino/arduino-and-mpu6050-accelerometer-and-gyroscope-tutorial/
6. Diaz, P. (2022). *EASA Publishes the First Regulations on Urban Air Mobility in the World.* Retrieved from Aviacionline: https://www.aviacionline.com/2022/06/document-easa-publishes-the-first-regulations-on-urban-air-mobility-in-the-world/
7. ERIK OBERG, F. D. (2012). *Machinery's Handbook 29th Edition* . Industrial Press.
8. FAA. (2022). *Urban Air Mobility and Advance Air Mobility*. Retrieved from https://www.faa.gov/uas/advanced_operations/urban_air_mobility
9. Gates Corporation. (2010). *Heavy Duty V-Belt Drive Design Manual* . Gates Corportation.
10. Hartzell Propeller. (2022). *115N Propeller Owner's Manual and Logbook* . Hartzell Propeller .
11. InvenSense. (2013). *MPU-6000 and MPU-6050 Product Specification.* InvenSense.
12. Jack D. Mattingly, K. M. (2016). *Elements of Propulsion: Gas Turbines and Rockets 2nd Edition* . AIAA Education .
13. Jansen, R. (2017). *Overview of NASA Electrified Aircraft Propulsion Activites.* Retrieved from NASA Glenn Research Center : https://ntrs.nasa.gov/api/citations/20180000593/downloads/20180000593.pdf
14. Joshua Johnsen, T. R. (2021). Integration of a 7-kW Turboelectric Power System in a Vertical Take-off and

15. Landing Unmanned Aircraft. *AIAA Propulsiona and Energy Forum* .

16. Manuel A. Rendon, C. D. (2021). Aircraft Hybrid-Electric Propulsion: Development Trends, Challenges, and Oppurtunities . *Journal of Control, Automation and Electrical Systems* .

17. Mark, R. (2019, April 22). *Turbine Engine Upgrades* . Retrieved from Flying : https://www.flyingmag.com/turbine-engine-upgrades/

18. MathWorks. (n.d.). *Estimate Orientation with a Complementary Filter and IMU Data*. Retrieved from MathWorks : https://www.mathworks.com/help/fusion/ug/estimate-orientation-with-a-complementary-filter-and-imu-data.html

19. Millett, P. (2022). *Brushless Vs Brushed DC Motors: When and Why to Choose One Over the Other*. Retrieved from Monolithic Power: https://www.monolithicpower.com/en/brushless-vs-brushed-dc-motors

20. Mitsuboshi. (2014). *Design Manual V-Belt DIN.* Mitsuboshi.

21. Muwanika Jdiobe, K. R. (2022). Validation of a Wind Tunnel Propeller Dynamometer for Group 2 Unmanned Aircraft. *MDPI*.

22. Off the Grid Sun. (n.d.). *50KW 154120154BRUSHLESS OUT RUNNER MOTOR 35-80KV LARGE AIR CRAFT*. Retrieved from Off the Grid Sun: https://offthegridsun.com/Brushless-Motor/50KW-154120154Brushless-Out-Runner-Motor-35-80kv-Large-Air-Craft

23. PBS Aerospace . (2014). *PP-36 Operation Manual TP100 Turboprop Engine* . PBS Aerospace .

24. PBS Aerospace . (2015). *PP-63 Basic Technical Information Turboprop Engine TP100.* PBS Aerospace.

25. PBS Aerospace . (2017). *PP-79 AUXILIARY ALTERNATOR INSTALLATION MANUAL*. PBS Aerospace .

26. PBS Aerospace . (2017). *PP-91 Turboprop Engine TP100 Propeller Selection Guide* . PBS Aerospace .

27. PBS Aerospace. (2014). *PBS TP100 Turboprop Engine.* Retrieved from https://www.pbsaerospace.com/aerospace-products/engines/turboprop-engines/ts-100-turboshaft-engine

28. PBS Aerospace. (2014). *PP-48 Installation Manual Turboprop Engine TP100.* PBS Aerospace .

29. Raj Ghelani, I. R. (2022). DESIGN METHODOLOGY AND MISSION ASSESSMENT OF PARALLEL HYBRID ELECTRIC PROPULSION SYSTEMS. *ASME Turbo Expo* .

30. Smruti Sahoo, M. D. (2022). SYSTEM-LEVEL ASSESSMENT OF A PARTIALLY DISTRIBUTED HYBRID ELECTRIC PROPULSION SYSTEM. *ASME Turbo Expo*.

APPENDICES

Flight controls are typical of a general aviation class aircraft with a yoke that rotates and translates about the centerline of the aircraft. As the yoke moves into the dashboard the nose is pushed down while when the yoke is pulled back the nose goes up. When spun to the right the aircraft rolls to the right and vice versa for the left. Rudder control is executed by use of two-foot pedals in the foot well of the aircraft. The right pedal effects a nose right yaw and opposite yaw for the left pedal. The pedals also control braking through use of toe brakes. A toe brake works by pivoting the ankle forward, this rotates the peddle and pushes the top, where the toes are, down compressing a brake cylinder. One braking cylinder system per peddle with the left peddle controlling the left main wheel brake and the right peddle controlling the right main brake. Aileron, elevator, and rudder control forces are transferred through tensioned cables that are routed through numerous pulleys. The aileron control cable system is a complete loop. From the control yoke a cable moves through the belly of the aircraft, up a piler immediately aft of the cabin doors. Then the cables span outboard to the front of the aileron bell crank. Then a new cable extends from the back of the bell crank to the opposite aileron bell crank, then the front cable on the bell crank returns to the control yoke. Once tensioned this system allows for both ailerons to be controlled simultaneously, though in opposite directions. It also allows the yoke to be rotated and left at position without a restorative force. A diagram of the aileron control scheme can be found below in figure 77.

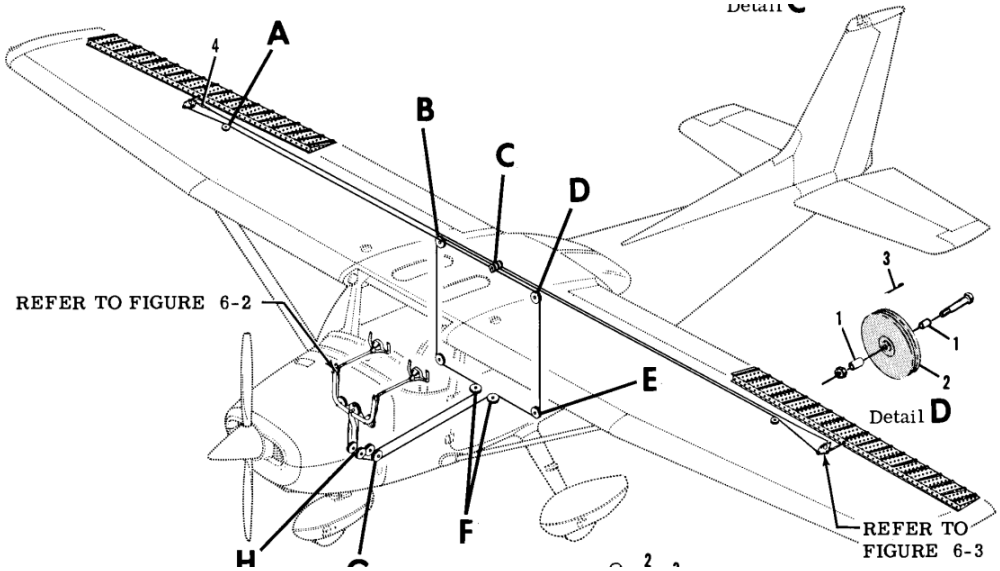

Figure 77. Aileron Control Scheme (Cessna Aircraft Company, 1985).

The elevator is similar, the control yoke assembly pivots at the bottom, where it is mounted, and this pivoting manipulates a push rod that pivots a bell crank. The push rod and bell crank are in the belly immediately below the pilot and copilot. As this bell crank pivots one end pulls a cable forward while the other allows for a cable to move aft. These cables extend from the bell crank straight to the elevators in the tail where they are bolted to another bell crank in the centerline of the aircraft. The pivoting of the forward bell crank forces this aft bell crank to rotate up and down turning the elevators up and down. A schematic of the elevator control scheme can be found below in figure 78.

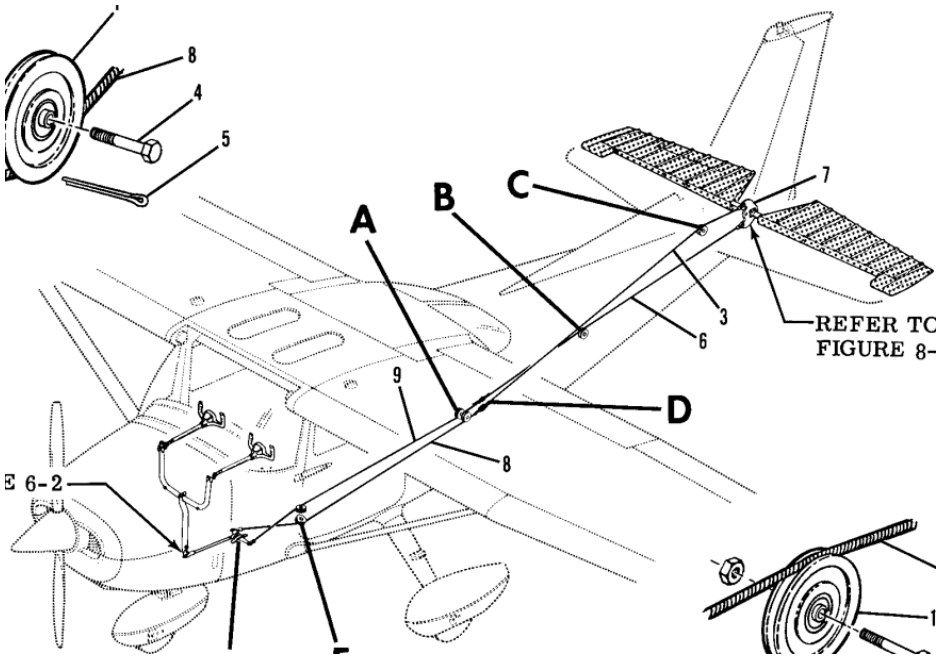

Figure 78. Elevator Control Scheme (Cessna Aircraft Company, 1985).

Finally, the rudders are controlled by a significantly simpler system. Two cables stretch from the rudder pedal assembly straight to the rudder and attaching to either side of the rudder. However, these cables are attached to the rudder pedal assembly with springs. These springs keep the rudder cables tensioned while also ensuring that the rudder is kept neutral. The springs also serve a third function, a buffer between the rotation of the nose wheel ensuring that the rudder is not deflected past its limits. A diagram of the rudder control system is shown below in figure 79.

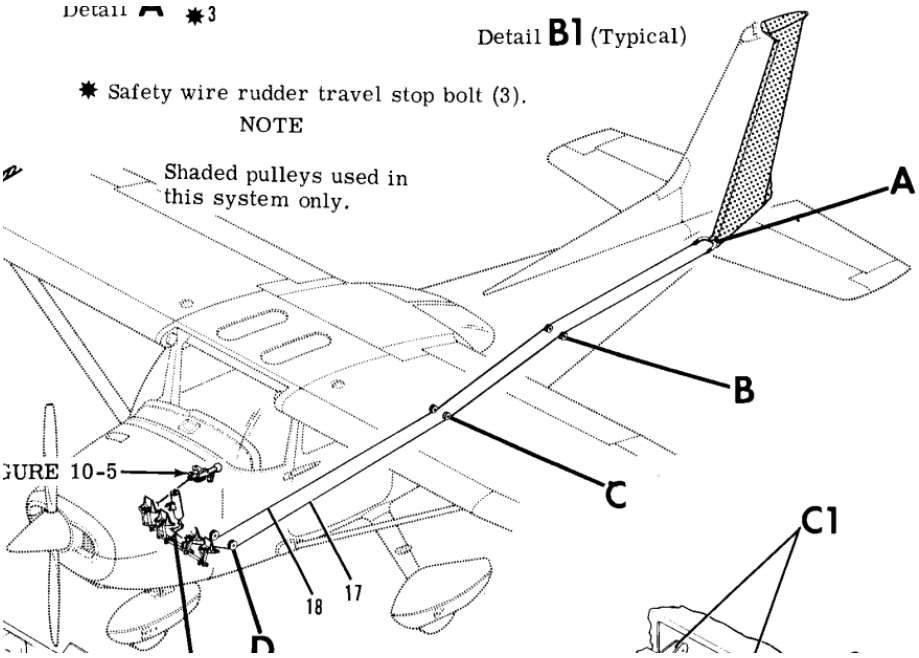

Figure 79. Rudder Control Scheme (Cessna Aircraft Company, 1985).

VITA

Joshua Melvin

Candidate for the Degree of

Master of Science

Thesis: INTEGRATION AND EVALUATION OF A 180-KW TURBOPROP ENGINE WITH A TURBOELECTRIC GROUND TEST RIG

Major Field: Mechanical and Aerospace Engineering

Biographical:

Education:

Completed the requirements for the Master of Science in Mechanical and Aerospace Engineering at Oklahoma State University, Stillwater, Oklahoma, in May, 2023.

Completed the requirements for the Bachelor of Science in Aerospace Engineering at Oklahoma State University, Stillwater, Oklahoma in 2021.

Completed the requirements for the Bachelor of Science in Mechanical Engineering at Oklahoma State University, Stillwater, Oklahoma in 2021.

Experience:

Graduate Research Assistant, Undergraduate Research Assistant, Aircraft Mechanic Apprentice.

Professional Memberships:

AIAA and ASME